Do mutations in *gyrA* cause incompatibility between DNA gyrase and certain Qnr variants, resulting in deleterious fitness cost in *Escherichia coli*?

Julie Røkke Osen

Master thesis in Molecular Biology and Biochemistry
60 credits

Department of Biosciences
Faculty of Mathematics and Natural Sciences

UNIVERSITY OF OSLO

May 2021

2021

Do mutations in *gyrA* cause incompatibility between DNA gyrase and certain Qnr variants, resulting in deleterious fitness cost in *Escherichia coli*?

Julie Røkke Osen

http://www.duo.uio.no/

Print: Reprosentralen, Universitetet i Oslo

Acknowledgements

This study was performed at the Institute of Oral Biology, University of Oslo.

First, I´d like to thank my primary supervisor Roger Simm for providing me with the opportunity to work with this interesting topic. Thank you for the good discussions, guidance and for always being helpful throughout this master thesis. I´d also like to thank my co-supervisor Dirk Linke for providing good advice and for always being available.

I´d like to thank the whole Simm-group for all the advice during this project. And a special thanks to Krystyna Anna Liskiewicz, for making the days in the laboratory fun. I´d also like to thank the people at the Institute of Oral Biology for making me feel welcome and for always being available.

Thanks to Bjørn Dalhus and Rune Forstrøm Johansen at structure biology for guidance and advice related to the interaction studies.

Lastly, I would like to thank my family and friends for all the support and for making my student years perfect.

Abstract

Antibiotic resistance is an emerging concern in modern society. Serious infections are becoming harder to treat, leading to higher treatment cost, longer hospital stays and higher mortality rates. Quinolones are an important class of antibiotics that target DNA Gyrase and Topoisomerase IV in bacteria. Resistance against quinolones can occur through plasmid-mediated and chromosome-mediated resistance. The presence of both types of resistance has been shown to cause clinically resistant strains. To prevent the emerge of quinolone-resistant bacteria it is important with correct diagnosis. In order to facilitate this in future sequence-based diagnostics, knowledge about the interplay between different resistance mechanisms is necessary.

This study aims to increase the knowledge about the interplay between plasmid-mediated and chromosome-mediated resistance. Specifically, the interplay between Gyrase A, WT and S83L mutated, and the three plasmids encoded Qnr proteins, QnrS1, QnrS2 and QnrB19. In this thesis, all five proteins were expressed in *Escherichia coli* (*E.coli*) BL21 (DE3) and purified by immobilized metal affinity chromatography. The interaction between the proteins was studied, utilizing the methods microscale thermophoresis and surface plasmon resonance. Quinolone susceptibility of *E.coli* strains expressing different Qnr proteins in the presence of wildtype or mutated Gyrase A was determined by broth microdilution assays. The bacterial fitness of the *E.coli* strains was tested in growth assays.

The results showed that expression of Qnr proteins causes resistance to ciprofloxacin, and when expressed together with S83L mutated Gyrase A, the strains become clinically resistant. The following growth assays showed that there was no disadvantage of expressing Qnr proteins. However, a fitness advantage was found for the clinically resistant strains expressing S83L mutated Gyrase A and QnrS1 or QnrS2. The data obtained in the interaction studies were not reliable enough to determine if any of the Qnr variants interact differently with the two Gyrase A variants. Later analysis revealed that the protein was not in the expected dimer-form, which could explain the uncertainty of the data.

Abbreviations

ADP	Adenosine diphosphate
ATP	Adenosine triphosphate
ATPase	Adenosine triphosphatase
BLAST	Basic local alignment search tool
Bp	Base pairs
BSA	Bovine serum albumin
CTD	C-terminus domain of Gyrase A
C-terminus	Carboxyl-terminus
ddH20	Double distilled water
DNA	Deoxyribonucleic acid
DNase	Deoxyribonuclease
dNTP	Deoxynulceotide triphosphate
DTT	Dithiothreitol
E.coli	*Escherichia coli*
EDTA	Etylendiamintetraacetat
HGT	Horizontal gene transfer
His-tag	Polyhistidine-tag (6x)
gDNA	Genomic DNA
GE	General Electric
G-segment	Gate-segment
GyrA	Gyrase A
GyrB	Gyrase B
IMAC	Immobilized metal affinity chromatography
IPTG	Isopropyl β-d-1 thiogalactopyranoside
IR	Infrared
Kb	Kilobases
K_d	Equilibrium dissociation constant

LB	Lysogeny broth
mAU	Milli absorption unit
MCS	Multiple cloning site
MFS	Major facilitator superfamily
MIC	Minimum inhibitory concentration
Min	Minutes
MST	Microscale thermophoresis
NEB	New England Biolabs
Ni-NTA	Nickel-nitrilotriacetic acid
N-terminus	Amino-terminus
OD	Optical density
ParC	DNA topoisomerase IV subunit A
ParE	DNA topoisomerase IV subunit B
PBS	Phosphate buffer saline
PBS-P+	Phosphate buffer saline with Tween-20
PCR	Polymerase chain reaction
PDB	Protein databank
Pi	Inorganic phosphate
QRDR	Quinolone resistance determining region
QREC	Quinolone resistant *Escherichia coli*
RND	Resistance nodulation division
RNA	Ribonucleic acid
ROS	Reactive oxygen species
PMQR	Plasmid mediated quinolone resistance
PRP	Pentapeptide repeat protein
PVDF	Polyvinylidene fluoride
RBS	Ribosome binding site
RT	Room temperature
s	Seconds

SDS-PAGE	Sodium dodecyl sulphate polyacrylamide gel electrophoresis
SEC	Size-exclusion chromatography
SPR	Surface plasmon resonance
TAE	Tris acetate etylendiamintetraacetat
TBS-T	Tris buffer with Tween-20
Tris	Tris (hydroxymethyl) aminomethane
T-segment	Transferring-segment
UV	Ultraviolet
WT	Wildtype

Table of content

1 Introduction

1.1 Antibiotics

Antibiotics are strictly defined as antimicrobial substances with antibacterial activity that are produced by microorganisms. For simplicity, in this thesis, the term will be used in reference to all substances with antibacterial activity and include synthetic and semi-synthetic antibacterial drugs.

Antibiotics are used to treat infections caused by bacteria. These drugs are very important in modern medicine because they are also used to prevent infections during cancer therapy, organ transplant, animal bites and open heart surgery (Calhoun et al., 2020; Hutchings et al., 2019). The use of antimicrobial substances started many thousand years ago, with natural remedies like herbs, honey and moldy bread (Gould, 2016). However, antibiotics were not introduced before the 20th century and the extensive search for new antibiotics started in the 1940s (Gould, 2016; Hutchings et al., 2019). Today there are several classes of antibiotics, either naturally produced by bacteria and fungi or made synthetically in the laboratory (Pankey & Sabath, 2004). The different types either kill or prevent bacterial growth, by targeting important cellular processes (Figure 1) (Calhoun et al., 2020; Hutchings et al., 2019). Antibiotics that kill bacteria are called bactericidal, and usually target DNA/RNA synthesis, folate synthesis or cell wall synthesis. Antibiotics that target protein synthesis usually inhibit bacterial growth and are called bacteriostatic (Kohanski et al., 2010b; Leekha et al., 2011). In contemporary medical research, few antibiotics are introduced to clinical use. At the same time, bacteria are developing resistance to the already existing antibiotics (Ventola, 2015).

1.2 Antibiotic resistance

Antibiotic resistance occurs when bacteria have the ability to resist the effects of antibiotics (Folkehelseinstituttet, 2017). Even before the extensive use of antibiotics, antibiotic resistance against penicillin was reported (Abraham & Chain, 1940). Today, many types of antibiotic resistance mechanisms are known. Some mechanisms can target several types of antibiotics, but bacteria can also express several mechanisms causing resistance against one or more classes of antibiotics (Munita & Arias, 2016).

There is a multiplicity of way in which resistance against antibiotics may occur. One way is by expressing enzymes, which inactivates the antibiotics (Figure 1). This can be achieved by adding chemical moieties or degrading the drug, preventing the drug from interacting with its target molecule (Abraham & Chain, 1940; Crossman et al., 2008; Oteo et al., 2006; Yigit et al., 2001). Other mechanisms resulting in resistance are by protecting the target molecule from the activity of the antibiotic (Figure 1). This may occur by enzymatic alterations or target mutations, in the binding site of the target molecule, leading to reduced affinity for the antibiotic (Heep et al., 2000; Toh et al., 2007; Vedantam et al., 1998). This protection can also be by other molecules, which either prevent binding of the antibiotics or removing the bound antibiotics (Dönhöfer et al., 2012; Tran et al., 2005a). The target can also be protected by replacement of the target with a molecule with similar function, but that does not bind the antibiotics. Additionally, the target can be bypassed though overexpression of it. This way the target can continue with its cellular function even if some molecules are inhibited by antibiotics (Cetinkaya et al., 2000; Eliopoulos & Huovinen, 2001; Pinho et al., 2001). Bacteria is also able to resist the activity of antibiotics by decreasing the intracellular concentration of the drug (Figure 1). Efflux pumps can pump antibiotics out of the cell decreasing the concentration and binding of antibiotics to the target. Mutations occurring in the regulatory genes of these efflux pumps can also lead to higher resistance due to overexpression of the efflux pumps (Poole, 2005). The intracellular concentration can also be affected by changing the membrane permeability (Figure 1). In gram-negative bacteria, antibiotics cross the outer membrane through channels called porins. Downregulation of the porins would lead to decreased uptake of the antibiotics, and less antibiotics reaching their targets. Alterations in the porins could also affect the transport through the porins, potentially affecting the intracellular concentration (Choi & Lee, 2019; Pagès et al., 2008).

The resistance mechanisms can be either intrinsic, meaning that the resistance is caused by a trait that is naturally occurring in the bacterial species, or it can be acquired. The acquired resistance is caused by changes in the genetic material through horizontal gene transfer (HGT) or chromosomal mutations (Reygaert, 2018). In HGT, bacteria can take up free DNA from the environment (transformation), or the DNA could be transferred from one bacteria to another through a virus (transduction), or directly transferred between two bacterial cells (conjugation) (Madigan et al., 2015). In some cases, antibiotic resistance has been shown to influence the fitness of the bacteria. This means that it affects the ability of bacteria to grow (Madigan et al., 2015). Since many of the resistance mechanisms interfere with important cellular functions,

like target mutation or modification of enzymes, it is not hard to believe that it affects the fitness of the bacteria (Melnyk et al., 2015). The effect on fitness will vary between bacterial species and depends on the resistance mechanisms, but mutations compensating for the fitness cost caused by the resistance mechanism can occur (MacLean et al., 2010; Melnyk et al., 2015)

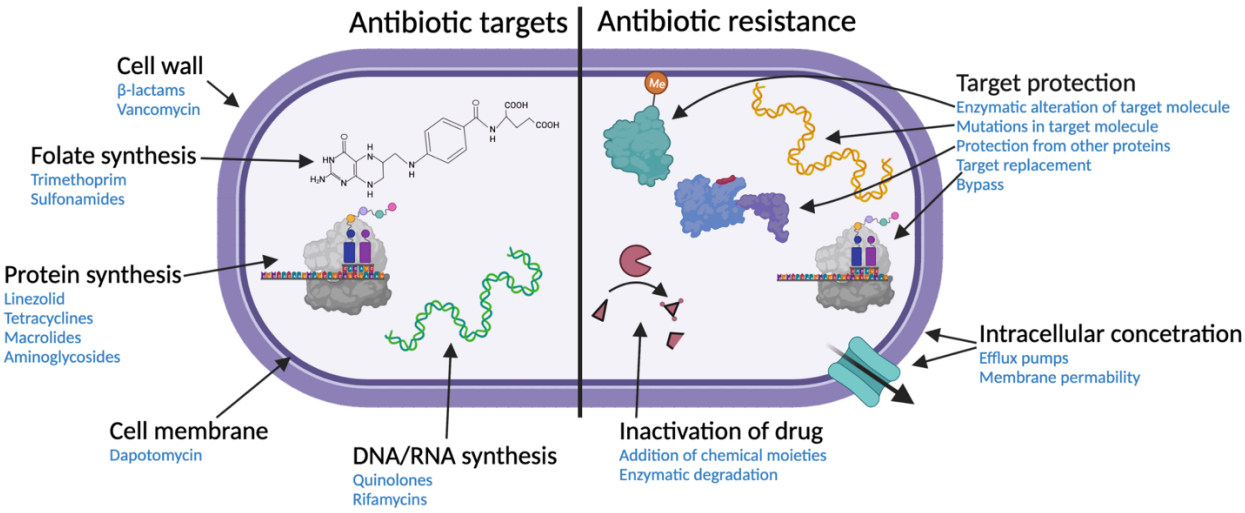

Figure 1: Antibiotic targets and resistance mechanisms. Examples of antibiotics are listed under the target (Wright, 2010). The figure was made in BioRender.

1.3 Topoisomerase

Topoisomerases are enzymes that play an important role in relieving torsional stress in the DNA and packing of the chromosome (Lodish, 2016). Torsional stress occurs in the DNA due to the unwinding of the DNA, to get access to the nucleotide sequence information (Vos et al., 2011). To alter the DNA topology, topoisomerase creates a transient break in the DNA. There are two classes of topoisomerase, type I topoisomerase and type II topoisomerase, which are present in both eukaryotes, prokaryotes and archaea. Type I topoisomerase makes a single-strand cut in the DNA and passes the unbroken strand through the break before the strand is re-ligated (Cox & Nelson, 2013).

1.3.1 Type II topoisomerase

Type II topoisomerase act by creating a transient double-strand break in the DNA and passes another part of the DNA strand through this break, with the use of adenosine triphosphate (ATP) as a energy source for the strand passage (Vos et al., 2011; J. C. Wang, 1998). In bacteria,

there are two types of type II topoisomerase: DNA Gyrase and Topoisomerase IV. Topoisomerase IV consists of two subunits of DNA topoisomerase IV subunit A (ParC) and two subunits of DNA topoisomerase IV subunit B (ParE), making up a heterotetrameric complex (Laponogov et al., 2009). The enzyme is localized behind the replication fork and transcription complex on the DNA. Here it can resolve both negative and positive supercoils to reveal torsional stress. The enzyme is also important for the unlinking of catenates in the DNA (Cebrián et al., 2015; Neuman et al., 2009; Postow et al., 2001).

1.3.2 DNA Gyrase

The other type II topoisomerase in bacteria is DNA Gyrase (later referred to just Gyrase). Gyrase is a heterotetramer composed of two subunits of Gyrase B (~90 kDa) (GyrB) and two subunits of Gyrase A (~97 kDa) (GyrA) (Figure 2) (Consortium, 2021). It is localized in front of the replication fork and transcription complex, relieving torsional stress made during DNA replication and transcription (Postow et al., 2001). Unlike other topoisomerases, Gyrase can introduce negative supercoils into the DNA, which is an important feature for the packing of the chromosome in the cell (Gubaev & Klostermeier, 2014; Peter et al., 1998; Reyes-Domínguez et al., 2003). The heterotetrameric enzyme complex forms three gates to enable cut, strand passage and re-ligation of the DNA (Figure 3A). The DNA-gate is made up of the N-termini of the two GyrA subunits, and the C-termini topoisomerase primase (TOPRIM) domains of the two GyrB subunits (Figure 2 and 3A). The N-gate is made up of the N-termini of two GyrB subunits, which contain the ATPase domain, while the C-gate is made by the coiled-coils of the two GyrA subunits (Vanden Broeck et al., 2019). Gyrase functions by wrapping DNA around the GyrA C-termini domains (CTD), placing on part of the DNA strand called the Gate-segment (G-segment) in the DNA-gate, and another part of the DNA strand called the Transferring-segment (T-segment) in and N-gate of the enzyme (Lanz et al., 2014; Stelljes et al., 2018) (Figure 3B). When one ATP molecule binds to each of the GyrB subunits, there is a conformational change, bringing the two GyrB subunits in contact with each other, trapping the T-segment (Gubaev & Klostermeier, 2014) (Figure 3C). The two nucleophilic tyrosine residues in position 122 on each GyrA subunit (*Escherichia coli* (*E.coli*) numbering) reacts with the 5´phosphordiester backbone of the G-segment localized in DNA-gate. This reaction forms a covalent bond between the Gyrase and the DNA, creating a double-strand break (D S Horowitz & J C Wang, 1987; Vanden Broeck et al., 2019). Next, ATP is hydrolyzed,

and the T-segment is translocated through the double-strand break and to the C-gate (Figure 3D). This is followed by closing of the DNA-gate and re-ligation of the DNA strand. The T-segment of the DNA strand exits through the C-gate (Figure 3E) (Roca & Wang, 1992; J. C. Wang, 1998). The exact timing of ATP hydrolysis is not known, but the first hydrolysis is proposed to open the DNA-gate while the second hydrolysis opens the C-gate (Hartmann et al., 2017; Soczek et al., 2018). When adenosine diphosphate (ADP) + inorganic phosphate (Pi) leaves the enzyme it is reset for another round of strand passage (Figure 3A and E) (Bush et al., 2020; Soczek et al., 2018).

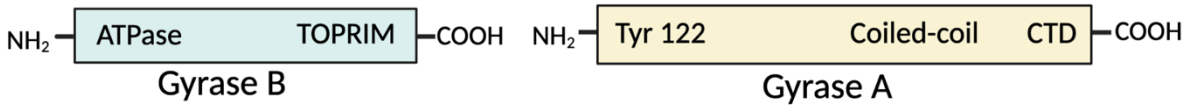

Figure 2. The two gyrase subunits. GyrB has the ATP binding site at the N-terminus and TOPRIM domain, which is a part of the DNA-gate, at the C-terminus. The C-terminus region (CTD) of GyrA wraps the DNA placing it in the DNA- and N-gate, while the N-terminus has the nucleophilic tyrosine important for cleavage of DNA. The coiled-coil makes up the C-gate which the DNA exits through after passing through the double strand break. The figure was made in BioRender.

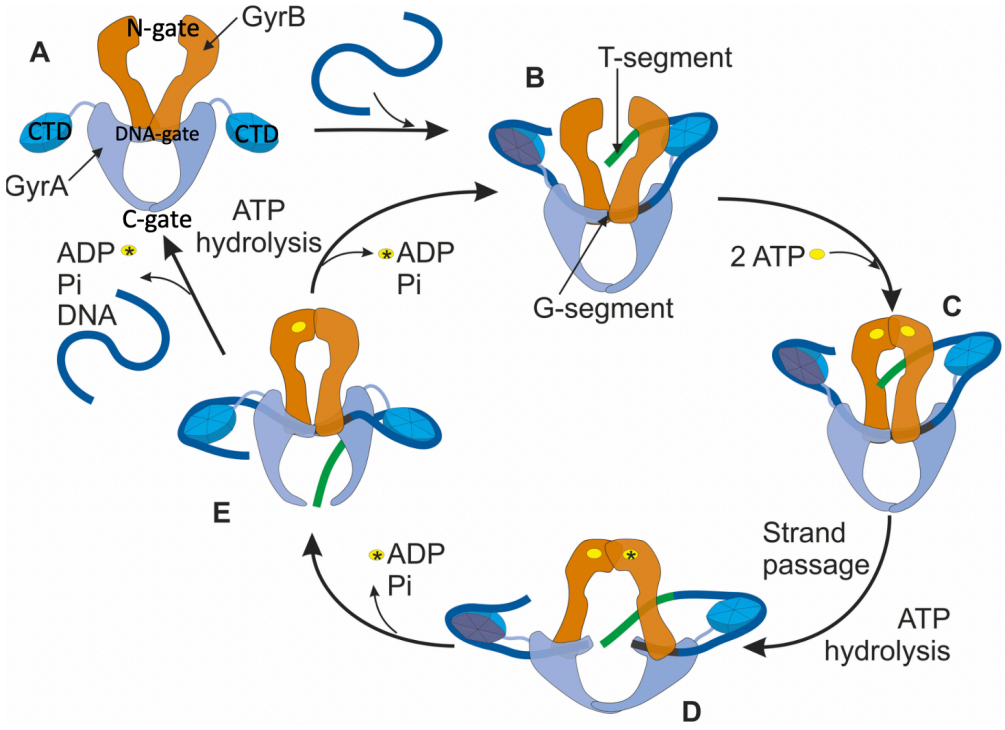

Figure 3. The catalytic mechanism of Gyrase. **A)** Structure of the Gyrase complex. **B)** CTD of GyrA bind to the DNA placing it in the DNA-gate and N-gate. **C)** ATP binds, leading to dimerization of the GyrB subunits. **D)** G-segment of the DNA strand is cleaved, and T-segment passes from the N-gate through the double-strand break. **E)** T-segment exits through the C-gate followed by dissociation of DNA and ADP + Pi. The hydrolysis of ATP in the figure is where the ATP is proposed to hydrolyze. Figure from (Monochamus Sutor, 2018) used with permission under the common creative license Attribution-ShareAlike 4.0 International (CC BY-SA 4.0). Changes to the figure were made by adding text to figure 3A.

1.4 Quinolones

Quinolones are a synthetic class of antibiotics, derived from 1,8-naphthyridine, used for treating infections caused by gram-negative and gram-positive bacteria (Hooper & Strahilevitz, 2015) (Figure 4). The first quinolone, nalidixic acid, was discovered in the 1960s and was used to treat urinary tract infections (Lesher et al., 1962). In the 1980s fluoroquinolones (later referred to as just quinolones) were discovered. These compounds are similar to regular quinolones, but the addition of fluorine at position 6 and a piperazinyl at position 7 showed greater activity of the drug (Stein, 1988). New improvements have been made over the years and today quinolones are used for treating many types of infections like respiratory tract infections, urinary tract infections, bone and joint infections, skin and soft tissue infections and sexually transmitted diseases (Pham et al., 2019; Rubinstein & Lagacé-Wiens, 2017) (Figure 4).

Quinolones interfere with the process of bacterial DNA and RNA synthesis through the inhibition of type II topoisomerases (Piddock et al., 1990). When type II topoisomerases have made the double-strand cut in the DNA, quinolones bind and stabilize the topoisomerase-DNA complex. Two quinolone molecules stack between the double-strand break and inhibit the free 3´hydroxyls to attack the phosphotyrosine, which would result in DNA re-ligation (Bax et al., 2010; Laponogov et al., 2009). Quinolones bind to type II topoisomerases through a water-metal ion bridge. The keto acid on position C3/C4 on quinolones chelates an Mg^{2+}-ion, stabilized by four water molecules (Figure 4). Two of these water molecules will form hydrogen bonds to a serine and an acidic residue on GyrA and/or ParC subunits, as seen with Ser83 and Asp87 in *E.coli* GyrA (Aldred, McPherson, et al., 2013; Blower et al., 2016; Wohlkonig et al., 2010). The human type II topoisomerase lacks these two amino acid residues and quinolones can therefore not target the human topoisomerase, which makes them specifically for use against bacterial topoisomerase (Aldred, Schwanz, et al., 2013). The stabilized topoisomerase-DNA complex, called the cleavage complex, will eventually be lethal to the cell.

At low quinolone concentrations, the bacterial growth is inhibited because RNA and DNA synthesis are blocked due to quinolone binding to type II topoisomerase. This will slowly over time kill the bacteria (Drlica et al., 2009). At higher quinolone concentrations, bacteria are killed due to fragmentation of the chromosome. The fragmentation occurs when the topoisomerase is removed from the DNA, either by another enzyme or by dissociation, leading to permanent chromosome break (Aedo & Tse-Dinh, 2013; Malik et al., 2006; Shea & Hiasa, 2003). With

many double-strand breaks in the chromosome, the DNA repair machinery will be overwhelmed and eventually lead to cell death (Malik et al., 2006; Tamayo et al., 2009). Quinolone action is also associated with the accumulation of intracellular reactive oxygen species (ROS). ROS are thought to accumulate as a response to the double-strand break and are important for the bactericidal function of quinolones (Dwyer et al., 2007, 2015; Hong et al., 2020).

Like some types of antibiotics, sublethal concentrations of quinolones increases the mutation rate in bacteria (Bell et al., 2014; de Lastours et al., 2014; Kiffer et al., 2011; Kohanski et al., 2010a; López et al., 2007; Terahara & Nishiura, 2019). The double-strand DNA break created in the chromosome due to quinolone activity, activates stress responses in the bacteria. These stress responses induced DNA repair, which also includes error-prone DNA repair pathways that can introduce mutations in the bacterial chromosome (Kohanski et al., 2010a; Kreuzer, 2013; López et al., 2007; López & Blázquez, 2009).

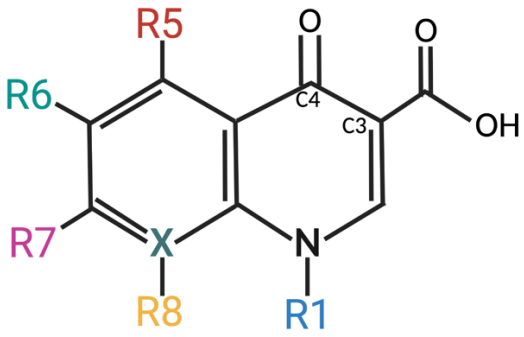

Figure 4. The general structure of quinolones. The keto acid group at position C3/C4 is involved in the water metal-ion bridge binding to the target. Position R1, R5, R6, R7, R8 and X have different modifications between different types of quinolones which affect the activity of the drug. R1: Increases the potency, meaning lower concentrations of the drug are needed for a response. R5: Increases the activity against gram-positive bacteria. R6: Fluorine in fluoroquinolones. Increases activity against the bacteria and increases potency R7: Effects the potency and pharmacokinetics. Pharmacokinetics is how the organism affects the drug. X and R8: Increased activity against anaerobe bacteria and effect the pharmacokinetics (Andersson, 2003; Pham et al., 2019). The figure was made in BioRender and inspired by Pham et al., 2019.

1.5 Quinolone resistance

Quinolone resistance was first reported in the 1970s. It was reported that chromosomal mutations caused resistance against nalidixic acid (Stamey, 1976). Over the years, several resistance mechanisms have been identified. Today both resistance mechanisms encoded on plasmids and the chromosome are known. All the resistance mechanisms can be transferred

vertically, meaning that it will be passed on to the daughter cells, but only plasmid-mediated resistance can be transferred horizontally (Aldred et al., 2014).

Chromosome-mediated resistance is caused by mutations in genes or transcriptional regulators encoded on the bacterial chromosome. Mutations in the gene encoding type II topoisomerase can lead to a decreased affinity for quinolones (Barnard & Maxwell, 2001; Blower et al., 2016) (Figure 5-1A). Most resistance-causing mutations occur in the quinolone resistance determining region (QRDR) of GyrA, GyrB, ParC and/or ParE. The mutations are usually found in the QRDR of GyrA (residues 67-106) and/or ParC (residues 63-102) (*E.coli* numbering) which is located close to the quinolone binding site (Bax et al., 2010; Wohlkonig et al., 2010; Yoo et al., 1997; Yoshida et al., 1990, 1991). This region also includes the amino acids important for the water metal-ion bridge binding of quinolones, the serine and acidic residue. These two amino acids are the ones usually found mutated in GyrA with reduced affinity to quinolones (Chien et al., 2016; Fu et al., 2013; Johnning et al., 2015; Singh et al., 2015; D. Zhu et al., 2019). Mutations in the GyrB and ParE have been shown to cause some level of resistance, but in general, the effect is lower compared to the GyrA and ParC mutations (Hopkins et al., 2005). Another type of chromosome-mediated resistance is mutations in genes encoding porins and/or regulators of porin expression. In gram-negative bacteria, quinolones enter the cell through porins. Both downregulation in the expression of porins and alteration of the porins can reduce membrane permeability, preventing quinolones from reaching their target (Fernández & Hancock, 2012) (Figure 5-1B). The intracellular concentration of quinolones can also be affected by the expression of efflux pumps. The most relevant efflux pump superfamilies for quinolone resistance, that are encoded on the chromosome, are the resistance-nodulation-division superfamily (RND) and the major facilitator superfamily (MFS). Mutations in regulatory genes of these efflux pumps can cause overexpression of the pumps leading to decreased intracellular concentrations (Li & Nikaido, 2009) (Figure 5-1C). Efflux pumps are also a type of plasmids-mediated quinolone resistance (PMQR).

PMQR are quinolone resistance mechanisms found on plasmids. The multidrug-resistance efflux pumps OqxAB and QepA are found on chromosome of some bacteria. However, is have been shown that the efflux pumps are expressed at higher levels when they are encoded on plasmids, leading to resistance against quinolones (Hansen et al., 2007; Périchon et al., 2007; Yamane et al., 2007). (Figure 5-2C). Another type of PMQR is the aac(6′)-Ib-cr protein, which is a type of aminoglycoside acetyltransferase (Robicsek et al., 2006). Aminoglycoside

acetyltransferases usually acetylate drugs like streptomycin, kanamycin, gentamicin and tobramycin, causing reduced binding of the antibiotics to their target (Krause et al., 2016; Sanz-García et al., 2019). Acetylation is associated with reduced affinity of the drug to the target because of the acetyl group. Due to the two specific mutations at positions W102R and D197Y in aac(6′)-Ib-cr this protein can acetylate the piperazinyl substituent localized on C7 (Figure 4) of some quinolones (Robicsek et al., 2006) (Figure 5-2B). The last type of PMQR is Qnr proteins which bind to the topoisomerase protecting it from the activity of quinolones (Tran et al., 2005a) (Figure 5-2A). These proteins will be described in more detail in section 1.6. The plasmids encoding these resistance mechanisms vary in size, copy number, expression level, transfer efficiency and other proteins encoded on the plasmids (Martínez-Martínez et al., 2008). Bearing the plasmids is also often associated with fitness cost, due to the energy used for replication and transcription of genes encoded on the plasmid (Dahlberg & Chao, 2003).

Both chromosome-mediated resistance and PMQR usually cause low levels of resistance, but strains can harbor several types of resistance mechanisms leading to higher quinolone resistance levels (Machuca et al., 2014, 2017). The level of resistance is also dependent on the type of quinolone being used and the targeted bacterial strain (Hooper & Jacoby, 2016).

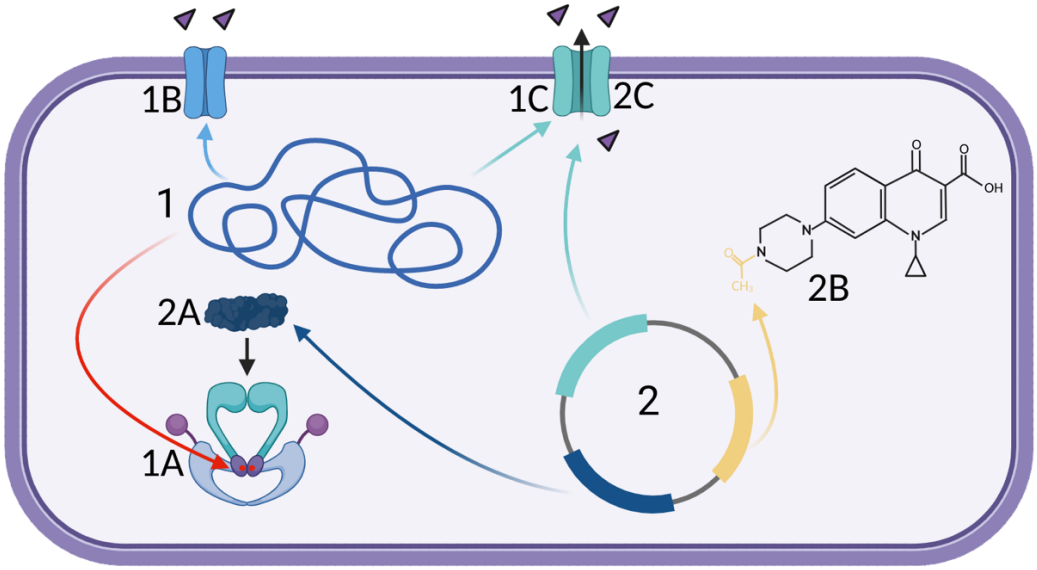

Figure 5. Quinolone resistance mechanisms. 1: Chromosome-mediated quinolone resistance. **1A:** Mutation in genes encoding type II topoisomerase can cause reduced drug binding. **1B:** Downregulation in the expression of porins and/or alteration in porins leading to reduced membrane permeability in gram-negative bacteria. **1C:** Upregulation in efflux pumps (RND and MFS) encoded on the chromosome due to mutations in regulatory genes. **2:** Plasmid-mediated quinolone resistance. **2A:** Qnr proteins bind to topoisomerase protecting it from quinolone activity. **2B:** Aac(6′)-Ib-cr can acetylate ciprofloxacin leading to decreased affinity to type II topoisomerase of the drug. **2C:** Expression of OqxAB and QepA efflux pumps leads to decreased in intracellular concentration of quinolones. The figure was made in BioRender and is inspired by Aldred et al., 2014.

1.6 Qnr proteins

The first PMQR, discovered in 1998, was the Qnr proteins (Martínez-Martínez et al., 1998). Qnr protects type II topoisomerases against quinolone activity (Tran et al., 2005a). The *qnr* gene is associated with plasmids, but can also be found on the chromosome of some bacteria (Poirel, Liard, et al., 2005; Poirel, Rodriguez-Martinez, et al., 2005; Velasco et al., 2010). The Qnr protein family consists of several paralogs, QnrA, QnrB, QnrC, QnrD, QnrS and QnrVC, which share 35% sequence identity or more. For each paralog, there are different allele variants with 90% sequence identity or more (G. Jacoby et al., 2008; G. A. Jacoby et al., 2014). Qnr proteins belong to the pentapeptide repeat protein family (PRP), which is present in both gram-negative and gram-positive bacteria (Rodríguez-Martínez et al., 2003, 2008; M. Wang et al., 2003, 2004).

Pentapeptide repeat proteins consist of pentapeptide tandem repeat sequences with the consensus (A/C/S/V/T/L/I) (D/N/S/K/E/I/R) (L/F) (S/T/R/E/Q/K/V/D) (G/D/E/N/R/Q/K) (Zhang et al., 2019). The structure has been solved for two Qnr proteins, QnrB1 and AhQnr (Vetting et al., 2011; Xiong et al., 2011). The proteins fold as right-handed quadrilateral β-helices, which dimerize through the C-terminal α-helices, and have two projecting loops (Vetting et al., 2011; Xiong et al., 2011) (Figure 6). The two loops, A and B, are important for the ability of Qnr to cause resistance. Loop A consists of 8 residues and plays a minor role in the resistance. Loop B consists of 12 residues and has a bigger impact on the resistance. Loop B is conserved (*XN*X(I/V)(S/T)*XXX*(W/F/Y)FC*X*) among Qnr proteins, and deletions in the loop can lead to loss of ability to cause resistance against quinolones (G. A. Jacoby et al., 2013; Kim et al., 2015; Tavío et al., 2014; Vetting et al., 2011; Xiong et al., 2011). Qnr proteins cause generally low level of resistance. However, placed under stronger promotors, which increase the expression of the protein, Qnr proteins can cause clinical resistance without any significant fitness cost (Garoff et al., 2018).

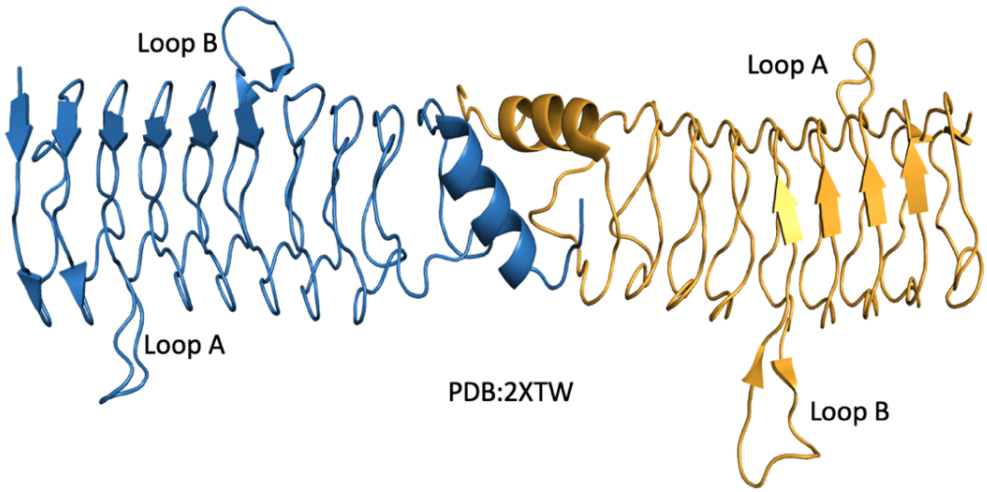

Figure 6. Structure of QnrB1 (PDB accession: 2XTW) (Vetting et al., 2011). The model was made in Pymol using the structure of QnrB1 found in PDB: 2XTW. The loops are marked in the figure, and each monomer is colored differently.

1.6.1 Gyrase-Qnr interaction

Qnr protects Gyrase from quinolone activity, but the interaction between the two proteins is not fully understood (Kim et al., 2015; Tran et al., 2005a; Vetting et al., 2011; Xiong et al., 2011). Due to the structure of the PRP resembling double-stranded DNA, one theory is that Qnr bind Gyrase in a similar matter. Here PRP competes with the G-segment of the DNA-strand for binding in the DNA-gate. This would inhibit the formation of the stabilized cleavage complex since no double-strand break is made in the DNA (Hegde et al., 2005; Xiong et al., 2011). This way of binding would also inhibit the supercoiling activity of Gyrase which some pentapeptide repeat proteins do (Hegde et al., 2011; Mérens et al., 2009). However, Qnr proteins only inhibit Gyrase at a concentration much higher than what is required for rescuing Gyrase from quinolone activity (G. A. Jacoby et al., 2006; Mazurek et al., 2021). It was therefore proposed that Qnr can interact with the stabilized cleavage complex and destabilize the complex, leading to loss of the quinolones instead (Vetting et al., 2011). This way supercoiling of DNA can continue after the removal of quinolones. The way this is proposed to occur is that Qnr interacts with Gyrase in a similar way as the T-segment. When Qnr binds to Gyrase, ATP binds and hydrolyses. The ATP hydrolysis is thought to cause a conformational change in the complex leading to the removal of the quinolone, either due to destabilization of the complex or by physically dislodge the quinolone from the complex. This is followed by re-ligation of DNA and release of the Qnr protein and ADP + Pi (Feng et al., 2021; Mazurek et al., 2021; Shah & Heddle, 2014; Vetting et al., 2011).

Qnr can interact with both Gyrase subunits separately, but for optimal binding, the whole complex is required (Kim et al., 2015; Mazurek et al., 2021). Of the two Gyrase subunits, GyrB has the highest affinity for Qnr . GyrB is thought to be more important of the initial binding of Qnr to the complex, while the interaction with the GyrA subunits is thought to be more important for the resistance activity (Kim et al., 2015; Mazurek et al., 2021). Here the two loops in the Qnr protein are thought to be involved in the positioning of Qnr in the complex, by interacting with the GyrA subunits. The correct positioning of Qnr is thought to be important for the removal of quinolones and re-ligation of the DNA (Mazurek et al., 2021).

1.7 Antibiotic resistance today

Over the many years of overuse and misuse of antibiotics, new antibiotic resistance mechanisms have emerged and have become a problem in modern medicine. Serious infections are becoming harder to treat, leading to longer hospital stays, higher treatment costs and higher mortality rates. If this continues we may end up with a situation where simple infections become fatal, which was common before the antibiotic era (World Health Organization, 2021). If action is not taken it is estimated that by 2050 there will be 10 million deaths related to antibiotic resistance (Jim O'Neill, 2016). The antibiotics on the market are becoming less effective and there are few new antibiotics in development (Jim O'Neill, 2016; Leekha et al., 2011). With better diagnostics, infection prevention, better surveillance and education of antibiotic prescribers, misuse and overuse of antibiotics and the rapid development of antibiotic resistance can be slowed. This way the effect of new and existing antibiotics can be maintained (Jim O'Neill, 2016; World Health Organization, 2021).

1.7.1 Quinolone resistance today

Quinolones are listed on the World Health Organization´s list of critically important antimicrobials for human medicine, as one out of five antibiotics. They are one of the few drugs which can be used for the treatment of serious *Salmonella* and *E.coli* infections (World Health Organization, 2019). At the same time, the prevalence of quinolone-resistant *E.coli* (QREC) in Europe has increased from 2013 to 2016 (European Centre for Disease Prevention and Control, 2017). The risk of being infected by QREC is related to demographic factors, other diseases,

present and prior treatments, and where the patient became infected. The risk of dying is also higher for patients infected with QREC compared to control patients (D.-M. Zhu et al., 2020).

1.8 Project background

Quinolone resistance is an increasing problem, and fast and precise diagnostics are important for minimizing overuse and misuse of quinolones. Traditionally culture-based methods have been used for diagnosis and resistance mechanism screening. A drawback of these methods is that they depend on the ability to grow the bacteria in the laboratory and that they are time-consuming. Hence, sequencing has arisen as the new method for diagnosis and screening for resistance. One of the limitations of using sequencing is that it reveals the genotype, but the phenotype depends on other factors as well. One of these factors is the interplay between the resistance mechanisms. Knowledge about the interplay between different quinolone resistance mechanisms is important for the correct diagnosis of infection, which in turn is crucial for the success of treatment. It is also important for the surveillance of quinolone resistance since it will enable interpretation of data for different genotypes.

In Norway, antibiotic resistance is monitored by NORM (Norsk overvåkningssystem for antibiotikaresistens hos mikrober) and NORM-VET (Norsk overvåkningssystem for antibiotikaresistens hos mikrober fra fôr, dyr og næringsmidler). The use of quinolones in Norway is low and has also decreased over the years (Norsk overvåkningssystem for antibiotika resistens hos mikrober & Norsk overvåkningssystem for antibiotika resistens hos mikrober fra fôr, dyr og næringsmidler 2019). Despite the low use of quinolones, screening of isolates from Norwegian livestock has shown low levels of resistance in a large proportion of the samples. Through the QREC-MaP (Quinolone resistance despite low antimicrobial usage – mechanisms and possible preventive measures) project, the questions: how, why, when and where these resistance mechanisms occurred in animal populations were studied. The project was a collaboration between the Norwegian University of Life Science, the Norwegian Institute of Public Health, Animalia and Felleskjøpet Forutvikling AS (Veterinærinsituttet, 2016).

Some of the results from QREC-MAP project are presented in the publication “Dissemination of quinolone-resistant *Escherichia coli* in the Norwegian broiler and pig production chain, and possible persistence in the broiler production environment” (Kaspersen et al., 2020). In the article, the authors showed that 58 of the analyzed isolates carried *qnr* genes. Eight of these

isolates also had a mutation in the QRDR of type II topoisomerases, where 7 isolates had the S83L mutation in GyrA. The *qnrS1* gene was found most frequently with the GyrA S83L mutation, with 6 out of 30 isolates carrying both resistance mechanisms. In isolates carrying the *qnrB19* gene, only 1 out of 20 had a GyrA S83L mutation. None of the isolates carrying the *qnrS2* gene had the S83L mutation. These results suggest that some *qnr* genes are found more often together with the S83L mutation in GyrA. This can have several explanations: 1) Qnr protein variants interact differently with Gyrase variants resulting in differences in quinolone susceptibility, 2) There is an altered fitness cost due to the expression of Qnr and/or the proteins interfering with the normal Gyrase activity, 3) There are differential fitness costs due to bearing the different plasmids encoding the Qnr proteins.

1.8.1 Proteins important for this project

Gyrase A S83L

The S83L mutation in Gyrase is the most common mutation in GyrA leading to quinolone resistance and is found in the QRDR of GyrA (*E.coli* numbering) (Figure 7) (Bhatnagar & Wong, 2019; Johnning et al., 2015; Mirzaii et al., 2018; Pourahmad Jaktaji & Mohiti, 2010). The hydroxyl group on the serine residue plays an important role in the hydrogen bond involved in the water-metal ion bridge binding to quinolones. Therefore, a mutation to a non-polar amino acid will lead to decreased affinity against quinolones (Barnard & Maxwell, 2001). Leucine is a hydrophobic amino acid and can therefore not bind to the water molecules in the water-metal ion bridge (Sigma Aldrich, n.d.). The mutation does not cause any reduced catalytic activity of gyrase in contrast to the other common mutation in the QRDR of GyrA at residue D87, which has been shown to reduce the activity of negative supercoiling (Aldred, McPherson, et al., 2013; Barnard & Maxwell, 2001).

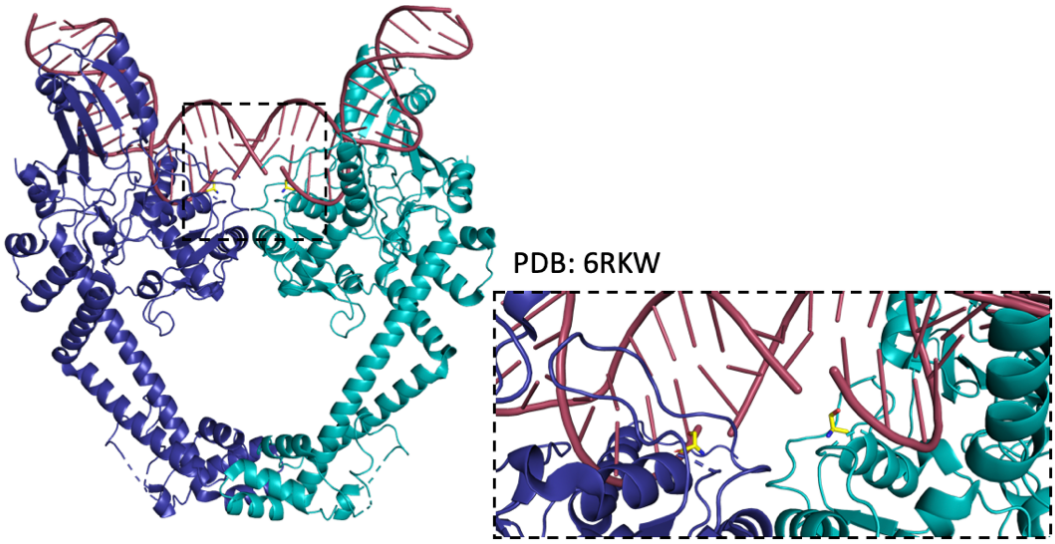

Figure 7. Structure of GyrA wildtype bound to DNA, CTD is not included in the structure (PDB accession: 6RKW) (Vanden Broeck et al., 2019). Each monomer is colored differently. Zoomed in: One quinolone molecule stack between each of the double-strand breaks. Ser83 residue is colored yellow and is positioned close to the double-strand break and the at were the quinolone is supposed to bind. The models were made in Pymol.

QnrS1, QnrS2 and QnrB19

QnrS1 is a protein that is 218 amino acids long and was first reported in Japan (Hata et al., 2005). The protein was discovered in *Shigella flexneri* 2b isolated from patients in 2003. Another allele variant of QnrS is the QnrS2 protein, which is 218 amino acids long as well. The first report of the protein was in the United States in non-Typhi *Salmonella* isolates (Gay et al., 2006). This protein has a 92 % sequence identity to QnrS1. QnrB19 belongs to another subfamily and has a 40 % sequence identity to QnrS1 and 42 % to QnrS2. The protein is 214 amino acids long and was first reported in an *E.coli* isolate from a patient in Colombia in 2002 (Cattoir et al., 2008)

1.9 Hypothesis and aims of the thesis

The hypothesis of this master thesis is based on the findings presented by Kaspersen et al., 2020, which suggested that some *qnr* genes are found more often together with the S83L mutation in GyrA. The hypothesis of the thesis is: Amino acid substitutions in the QRDR of DNA gyrase can affect the interaction between Qnr variants and the target protein, which in turn alters the fitness gain/cost of acquiring certain *qnr* genes.

The main aim of this thesis is to increase the knowledge of the interplay between chromosomal-mediated resistance and plasmid-mediated resistance. This study is limited to three Qnr proteins, QnrS1, QnrS2 and QnrB19, and two variants of GyrA, the WT protein and the mutated S83L version of the protein. To study the interplay between these proteins, the aim was divided into three objectives:

1) Identify if different Qnr proteins can interact differently with the two variants of GyrA.

2) Find out if there are any fitness cost related to expression of the different Qnr proteins.

3) Determine if the expression of different Qnr proteins result in different susceptibility to quinolones.

2 Materials and Methods

Strains are listed with origin in Appendix A. The complete list of all solutions, buffers and gels are found in Appendix D where they are listed with recipe and vendor.

2.1 Preparation of chemically competent *E.coli* cells

Competent *E.coli* DH5α cells (DH5α) (Appendix A, Table S1) were prepared for cloning due to their high insert stability and DNA yield of the isolated DNA. For protein expression, competent *E.coli* BL21 (DE3) (BL21) (Appendix A, Table S1) was prepared due to its lack of several proteases reducing the degradation of recombinant protein. It also expresses the T7 RNA polymerase which is necessary for protein expression from certain plasmids (Section 2.2.1). Competent *E.coli* 2015-01-5022 (GyrA-S83L-5022) (Appendix A, Table S1) and *E.coli* 2006-01-1085 (GyrA-WT-1085) (Appendix A, Table S1) cells were prepared for broth microdilution assays and growth assays. These strains are isolates from production animals obtained from the Norwegian veterinary institute (NVI). The strains harbor either the S83L mutated GyrA (GyrA S83L) or wild type GyrA (GyrA WT).

Cells were incubated overnight in lysogeny broth (LB) at 37 °C and 225 rpm. The overnight culture was diluted 1:100 before further incubation at 37 °C and 225 rpm until OD_{600} = 0.4 - 0.6 was reached. Cells were then harvested at 6000 xg for 5 minutes (min) at 4 °C (Eppendorf 5810). The pellet was resuspended in transformation and storage solution (1 mL/10 mL overnight culture) before 15 min incubation on ice. Fifty µL bacterial suspension was added to each tube and flash-frozen in liquid nitrogen. Competent cells were stored at - 80 °C.

2.2 Molecular cloning

There are several techniques used for cloning, in this study restriction enzymes were used to clone the genes of interest into the chosen vector. The restriction site for the enzymes was added to the gene of interest by PCR with specific primers. This made it possible to create overhangs in the PCR product by digesting the PCR product with restriction enzymes. These overhangs are complementary to the vector of choice digested with the same enzymes. The PCR product can then be ligated with the vector, creating recombinant DNA (Hoseini & Sauer, 2015).

2.2.1 Vectors

pET28a(+) vector

The pET28a(+) vector system is commonly used for expression of recombinant protein in *E.coli*, due to its high level of expression from the T7 promoter (Figure 8). Expression of the recombinant protein requires T7 RNA polymerase, which has to be encoded in the genome of the cells used. Expression is induced by isopropyl β-d-1 thiogalactopyranoside (IPTG) which binds to the lac repressor. This leads to a conformational change in the repressor reducing its ability to bind to its binding site on the DNA (lac operator). The lac operator is present in the vector and the bacterial genome. This way, expression from both the T7 RNA polymerase and the recombinant protein are repressed in the absence of IPTG (Dubendorf & Studier, 1991; William Studier et al., 1990). Amplicons of genes encoding GyrA S83L, GyrA WT, QnrS1, QnrS2 and QnrB19 were cloned into the multiple cloning site (MCS) in the pET28a(+) vector for protein overexpression and purification. The selective marker for the pET28a(+) vector is kanamycin and the working concentration used for kanamycin was 50 µg/mL. The vector is from Novagen.

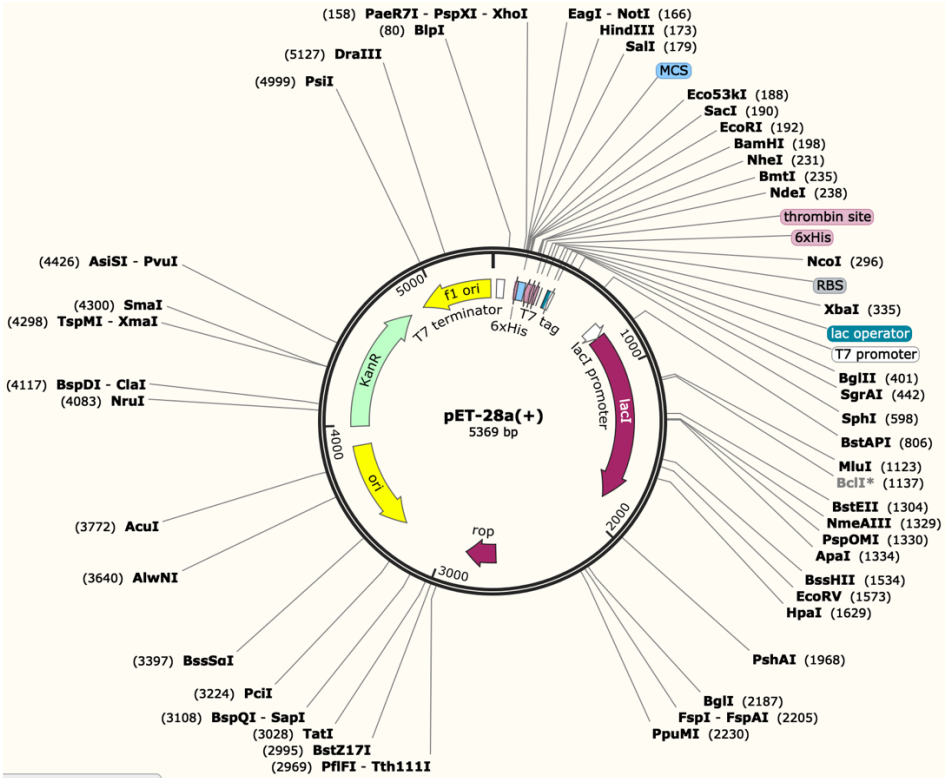

Figure 8. pET28a(+) vector. Genes were cloned into the MCS which is placed downstream of the T7 promotor. The figure was made in SnapGene Viewer using the pET28a(+) DNA sequence.

pBAD30

The genes encoding QnrS1, QnrS2 and QnrB19 were subcloned into pBAD30 for broth microdilution and growth assays (Figure 9). Since several of the strains used in these experiments do not express the T7 RNA polymerase, which are necessary for protein expression from the pET28a(+) vector, subcloning was performed. Expression from genes encoded in the MCS are controlled by the araBAD promoter. In the absence of L-arabinose, the regulatory AraC protein repress transcription from the promotor. The addition of L-arabinose causes a conformational change in AraC, leading to alternative biding to the DNA, allowing expression from the araBAD promoter (Guzman et al., 1995; Schleif, 2010). The selective marker for the pBAD30 vector is ampicillin and the working concentration used for ampicillin was 100 µg/mL. The vector is from Novagen.

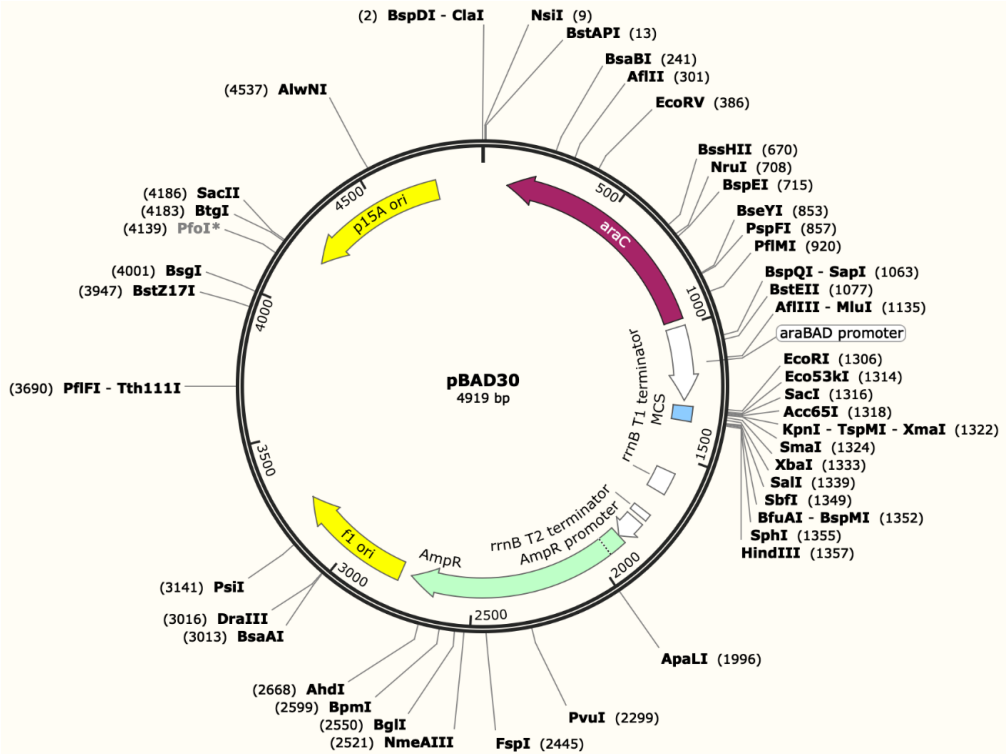

Figure 9. pBAD30 vector. Genes were subcloned into the MCS downstream of the araBAD promotor. The figure was made in SnapGene Viewer using the pBAD30 DNA sequence.

2.2.2 Primers

Primers made for cloning, colony PCR and sequencing were all ordered from Sigma Aldrich (Appendix A, Table S2). Restriction analysis was performed in SnapGene Viewer (GSL Biotech LLC), before making the primers. Equation 2.1 was used to calculate the melting temperature of the primers.

$$Tm(°C) = 4°C\,x(G + C) + 2°C\,x(A + T) \quad (2.1)$$

pET28a(+) primers

Forward primers were designed with a 5'restriction site for either XbaI or NcoI, while reverse primers were designed to give a 3'BamHI restriction site. A 5'hexa-nucleotide extension of the restriction site was included to ensure efficient digestion of the restriction site. Primers with XbaI restriction site were designed with a ribosome binding site (RBS), because the site would be cut out of the vector when digested with XbaI. A polyhistidine-tag (6x) (His-tag) was encoded in all reverse cloning primers. Primers designed for sequencing and colony PCR were designed to anneal about 100 base pairs (bp) from the gene of interest. Three extra sequencing primers for GyrA was designed to enable good sequencing of the entire gene.

pBAD30 primers

Primers used for colony PCR and sequencing of pBAD30 constructs were supplied by Krystyna Anna Liskiewicz. They anneal about 100 bp from the gene of interest.

2.2.3 Genomic DNA extraction and polymerase chain reaction (PCR)

PCR is a method that can be used for amplification of nucleotide sequences. The first step is denaturation of the double-stranded DNA. Primers anneal to the DNA template, and with the help of a heat-stable DNA polymerase, dNTPs are incorporated, producing a new DNA strand. DNA Phusion polymerase was used for the amplification of genes of interest for cloning purpose because of its high fidelity and speed (Dolgova & Stukolova, 2017).

Genomic DNA (gDNA) was extracted from GyrA-S83L-5022, GyrA-WT-1891, *E.coli*; 2016-17-292 (QnrS1-292), *E.coli*; 2016-01-725-2 (QnrS2-725) and *E.coli*; 2015-01-1826 (QnrB19-1826) (Appendix A, Table. S1). Approximately two colonies were resuspended in 180 µL enzyme buffer for genomic DNA extraction following Qiagen DNeasy DNA extraction

protocol for bacterial cultures, gram-positive bacteria. The gram-positive protocol was followed due to the low concentration of extracted DNA when the gram-negative extraction protocol. The low concentration was due to human errors, and the gram-negative protocol could probably been used in the second extraction without any problems. DNA concentration was measured using a spectrophotometer at wavelength 260 nm (Thermo scientific Nanodrop 2000/2000c).

Genes of interest in the extracted gDNA was amplified using the protocol for Phusion® High-Fidelity DNA Polymerase (New England Biolabs (NEB)) (Appendix B, Table S4). As template 1 µL gDNA extracted from GyrA-S83L-5022 (170 ng/µL), GyrA-WT-1891 (78 ng/µL), QnrS1-292 (102 ng/µL), QnrS2-725 (112 ng/µL) or QnrB19-1826 (106 ng/µL) was used for a 50 µL PCR reaction together with specific cloning primers (Appendix A, Table S2). Thermo-cycling conditions for the PCR are described in Appendix B, Table S5. PCR products were analyzed on a 1 % agarose gel (section 2.2.4) and purified by the Thermo Scientific Gene JET gel extraction kit.

2.2.4 Agarose gel electrophoresis

Agarose gels can be used to separate DNA mainly based on size, by applying electricity. DNA will migrate toward the positive end (anode) due to the negative charge of the phosphate backbone. The DNA will migrate through pores made by the agarose, where small DNA fragments will migrate faster that bigger DNA fragments (Lee et al., 2012).

A 1 % (w/v) agarose gel was made by dissolving agarose in 1x TAE buffer by heating in a microwave. After the solution had cooled down to approximately 50 °C, SYBR safe (1 µL/10 mL agarose) (Invitrogen) was added to enable visualization of DNA by UV light. The gel was allowed to solidify at room temperature (RT) for 30 min before it was transferred to an electrophoresis chamber (Bio-rad) with 1x TAE buffer. DNA samples were mixed with 6x loading dye (final concentration 1x) (Thermo scientific) before they were loaded on the gel. As size marker, DNA Thermo scientific gene ruler 1 kb DNA ladder was used (Appendix D, Figure S14A) (Thermo Fisher). The gels were run for 45 min at 75 volts with 1x TAE buffer as running buffer. DNA was visualized under UV light using a Syngene G-box.

2.2.5 Digestion

pET28a(+)

The pET28a(+) vector (Figure 8) was isolated from an overnight culture of *E.coli* TOP10 cells using Thermo scientific GeneJET Plasmid miniprep kit. Vector and PCR products encoding GyrA-S83L, GyrA-WT and QnrB19 were digested with XbaI (Thermo scientific) and BamHI (Thermo scientific), following Thermo Fisher fast digest of DNA protocol with modifications. Three µL of 10x fast digest buffer, 1 µL of each restriction enzyme and 500 ng DNA was added to nuclease-free water to a total volume of 30 µL. Digestion reactions were incubated at 37 °C for 20 min. The same procedure was followed for pET28a(+) vector and PCR products encoding QnrS1 and QnrS2, but with NcoI (Thermo scientific) and BamHI (Thermo scientific) restriction enzymes. Digestion reactions were run on a 1 % agarose gel (section 2.2.4) with PCR products and vector digested with one and zero enzymes as controls. DNA was purified using Thermo scientific GeneJET gel extraction kit before the concentration was measured on a spectrophotometer (Thermo scientific Nanodrop 2000/2000c).

Subcloning into pBAD30

The pBAD30 vector was provided by Krystyna Anna Liskiewicz (Figure 9). The genes encoding QnrS2 and QnrB19 were subcloned into the pBAD30 vector by digesting pBAD30, pET28a-QnrS2 and pET28a-QnrB19 with XbaI (Thermo scientific) and SalI (Thermo scientific). For subcloning of *qnrS1*, pET28a-QnrS1 and pBAD30 were digested with XbaI (Thermo scientific) and HindIII (Thermo scientific). Digestion was performed as described for the pET28a digestion (section 2.2.5), but with 1200 ng DNA instead of 500 ng. Inserts were purified from the agarose gel using Thermo scientific Gene Jet gel extraction kit. The concentration of purified DNA was measured with a spectrophotometer (Thermo scientific nanodrop 2000/2000c).

2.2.6 Ligation

pET28a(+) and pBAD30

For the ligation, a 3:1 molar excess of insert over vector was used. The amount of insert needed was found using NEB ligation calculator. Ligation was performed following the Rapid DNA ligation protocol from Thermo Fisher with modifications. A ligation reaction of 20 µL with 25-

50 ng digested vector, 3:1 molar excess of insert over vector, 1 µL T4 DNA ligase (5 u/µL) (Thermo scientific), 4 µL 5x Rapid Ligation buffer (Thermo scientific) and nuclease-free water was incubated for 20 min at 22 °C. Digested vector incubated in the absence of insert was used as a control for frequency of vector re-ligation. The ligation reactions, including control reactions, were transformed into DH5α cells (section 2.2.7).

2.2.7 Transformation of chemically competent *E.coli* cells

One to 5 µL of the ligation reaction or 20 ng-100 ng of purified plasmid was mixed with 50 µL competent cells (section 2.1) and incubated for 10 min on ice. Cells were heat-shocked at 42 °C for 40 seconds (s), before 2 min incubation on ice while 1 mL LB medium was added. Samples were incubated at 37 °C for 1 h and 15 min while shaking, to allow recovery and expression of resistance genes. Bacteria were thereafter harvested by centrifugation at 6000 xg (mikro 120 Hettich Zentrifugen) for 2 min. The supernatant was removed, except 100 µL which the bacterial pellet was resuspended in. Resuspended cells were plated on agar plates with ampicillin or kanamycin and incubated overnight at 37 °C. Untransformed cells were used as a control for growth of cells not expressing the selective marker.

2.2.8 Colony PCR

Colony PCR is a method used for screening for positive transformants. These are bacteria harboring the recombinant DNA of interest. Under the PCR cycling program, DNA is released when the cells are lysed during the denaturation step. This way primers specific for the vector can anneal to the vector backbone around 100 bp from insert and amplify the DNA sequence. If the colony harbors the recombinant DNA of interest, the amplified DNA will have a size corresponding to the gene of interest + 200 bp. This can be visualized on an agarose gel for quantitative identification (Walch et al., 2016).

Colony PCR master mix was made following Taq DNA polymerase protocol (NEB) (Appendix B, Table S6). Twenty µL of the colony PCR master mix was added to each PCR tube. Colonies were picked and streaked on an agar plate with an appropriate selective marker to prepare bacterial stocks (Section 2.2.10). The remaining bacteria were resuspended in the 20 µL PCR reaction mix in the PCR tube. The thermo-cycling program, described in Appendix B Table S7,

was followed for the PCR reaction. To verify positive transformants, PCR products were run on a 1 % agarose gel (section 2.2.4). As a positive control for the PCR reaction, 50 - 100 ng pET28a-PDE1-N-His or pBAD30- PDE1-N-His were used (supplied by Krystyna Anna Liskiewicz).

2.2.9 Sequencing

Ten mL LB medium with kanamycin or ampicillin was inoculated with positive transformants and incubated overnight at 37 °C, 200 rpm. Plasmid DNA was isolated with Thermo scientific Gene JET Plasmid miniprep. PCR products sent for sequencing were amplified with DNA Phusion polymerase (section 2.2.3) and purified with Thermo scientific Gene Jet gel extraction kit. Qualitative validation of plasmid inserts, and PCR products was done by LIGHTRUN tube sequencing at GATC Eurofins genomics. Seven µL plasmid DNA (65-100 ng/µL) or PCR product (12 ng/µL) and 5 µL primer (5 µM) were added to the samples sent for Sanger sequencing. Concentration of the DNA sent for sequencing was measured on a spectrophotometer at 260 nm (Thermo scientific Nanodrop 2000/2000c).

2.2.10 Preparation of bacterial glycerol stocks

Bacterial stocks were made of bacterial strains transformed with plasmids validated by sequencing. Approximately two colonies were resuspended in LB medium with 20 % glycerol and stored at -80 °C. An overview of bacterial stocks can be seen in Appendix A, Table S3.

2.3 Broth microdilution assay

Broth microdilution assay is a method used to test the bacterial susceptibility to antibiotics and can be used to determine the minimum inhibitory concentration (MIC). The MIC value is the lowest concentration of antibiotics needed to inhibit growth and was determined following European Committee on Antimicrobial Susceptibility Testing (EUCAST) reading guide for broth microdilution (The European Committee on Antimicrobial Susceptibility Testing, 2021c). The MIC values was used to determine if the strain was resistant based on the EUCAST epidemiological cut-off values (ECOFFs) (The European Committee on Antimicrobial Susceptibility Testing, 2021a). ECOFF is the highest MIC a WT strain is expected to have. For

E.coli, strains with MIC over 0.06 μg/mL for ciprofloxacin and 16 μg/mL for nalidixic acid is considered resistant (The European Committee on Antimicrobial Susceptibility Testing, 2021a). This must not be confused with the clinical breakpoint for resistance. A clinically resistant strain displays a MIC over 0.5 μg/mL for ciprofloxacin. When the microorganism is categorized as clinically resistant there is a high chance for therapeutic failure, even with increased exposure to the antibiotic (The European Committee on Antimicrobial Susceptibility Testing, 2021b). The clinical breakpoint for nalidixic acid has been removed because it cannot detect PMQR (Leclercq et al., 2013). This is because PMQR only have a small or no effect on nalidixic acid and strains can therefore be determined as susceptible to nalidixic acid, even if the strains causes resistance against other types of quinolones (Humphries et al., 2019).

Approximately two colonies of DHα, BL21, GyrA-S83L-5022 and GyrA-WT-1085 transformed with pBAD30-QnrS1, pBAD30-QnrS2, pBAD30-QnrB19 or pBAD30 (section 2.2.7) were resuspended in Mueller-Hinton broth (MHB). The bacterial suspension was diluted to an OD_{600} of 0.001 in MHB supplied with ampicillin and arabinose (0 %, 0.001 %, 0.01 % or 0.1 %). The bacterial suspension was added to a 96-well plate with 98 μL bacterial suspension in each well. Ciprofloxacin or nalidixic acid solutions prepared in two-fold dilution series were added to a final volume of 100 μL. The plate was incubated for 22 h and 30 min at 37 °C. Growth control of each bacterial suspension and sterile control of medium was included on the plate. The experiment was repeated at least three times for each strain.

2.4 Growth assay

The growth assay is a method that can be used to study the growth of bacterial cells. By measuring the OD_{600} over time, a growth curve for the strains can be obtained. The growth curve was used to find the generation time in the exponential growth phase and maximum OD_{600}. Generation time is the time a bacterial population uses to double its population, while the maximum OD_{600} is how high the density the bacterial culture can reach (Madigan et al., 2015). The growth curves were used to determine if there is a fitness cost related to expressing different Qnr variants.

To determine if there are any differences in the generation time between the different strains, the Kruskal-Wallis test with significant level $\alpha = 0.05$, followed by the Dunn test, was performed in GraphPad Prism v.9. Since the dataset does not have enough observations, the

dataset can't be assumed to be normal, and therefore the Kruskal-Wallis test was chosen. The test is a non-parametric method used to determine if there is a significant difference between the groups. The Dunn test is a non-parametric multiple comparison method which is often used after the Kruskal-Wallis test to locate where the differences between the groups are.

2.4.1 Growth assay in the absence of quinolones

A 96-well plate was set up with 90 µL LB medium supplemented with different arabinose concentration, 0%, 0.001%, 0.01% or 0.1%. Approximately two colonies of GyrA-S83L-5022 and GyrA-WT-1085 transformed with pBAD30-QnrS1, pBAD30-QnrS2, pBAD30-QnrB19 or pBAD30 was resuspended in LB medium. Ten µL bacterial suspension was added to each well of the 96-well plate to a final OD_{600} of 0.01. Growth assays were performed on a Cytation3 imaging reader from Biotek at 37 °C for 20 h. OD_{600} was measured every 5 min with 15 s shaking before every measurement. This plate setup was performed with and without the supplementation of ampicillin in the LB medium.

2.4.2 Growth assay in the presence of quinolones

For the GyrA-S83L-5022 strain transformed with pBAD30-QnrS1, pBAD30-QnrS2, pBAD30-QnrB19 or pBAD30 the growth assay was performed in the presence of nalidixic acid. This was to determine if the bacterial growth would be affected in the presence of a quinolone that Qnr do not cause resistance to.

A 96-well plate was set up with 90 µL LB medium supplemented with different arabinose concentrations (0 %, 0.001 %, 0.01 % or 0.1 %.), ampicillin and 64 µg/mL nalidixic acid (4-fold dilution of MIC (Table 4)). Approximately two colonies of GyrA-S83L-5022 transformed with pBAD30-QnrS1, pBAD30-QnrS2, pBAD30-QnrB19 or pBAD30 were resuspended in LB medium. Ten µL bacterial suspension was added to each well of the 96-well plate to a final OD_{600} of 0.01. Growth assay was performed as described in section 2.4.1

2.5 Protein expression

BL21 cells were transformed with pET28a(+) constructs for protein expression. LB medium with kanamycin was inoculated with one transformed colony and incubated overnight at 37 °C, 200 rpm.

Expression of GyrA S83L, GyrA WT and QnrB19

Overnight cultures with BL21 cells expressing GyrA S83L or GyrA WT were diluted 1:100 in 1.2 L LB medium with kanamycin. Overnight culture of BL21 cells expressing QnrB19 was diluted 1:100 in 2.4 L LB medium with kanamycin. The cultures were prepared in Erlenmeyer flasks with the size 5x larger than the volume of expression culture, so that the growth would not be limited by low oxygen concentration. Cultures were incubated at 37 °C and 200 rpm, until mid-exponential phase. At OD_{600} 0.4 - 0.6, protein expression was induced with 1 mM IPTG. The expression of protein was induced at mid-exponential phase because this is when the majority of bacteria are metabolically active and dividing. Cultures was incubated at 37 °C, 200 rpm for 3 h after induction to allow expression of the protein. Bacteria were harvested after 3 h by centrifugation at 6000 xg (Eppendorf 5810R) for 10 min at 4 °C. The bacterial pellet was frozen at -20 °C in falcon tubes.

Expression of QnrS1 and QnrS2

Overnight cultures with BL21 cells expressing QnrS1 or QnrS2 were diluted 1:100 in 4 L LB medium with kanamycin and 1 % glucose. The cultures were prepared in Erlenmeyer flasks with the size of 5x larger than the volume of the culture. Bacteria cultures were incubated at 37 °C, 200 rpm until mid-exponential phase. At OD_{600} 0.4 - 0.6, 0.1 mM IPTG was added to the cultures to induce protein expression. Cultures were incubated overnight at 16 °C, 200 rpm for protein expression. The following day the bacteria was harvested at 6000 xg in an Eppendorf 5810R centrifuge for 10 min at 4 °C. Pellet was frozen at -20 °C in falcon tubes.

BL21 cells transformed with empty pET28a(+) vector were used as a control to simplify observation of protein expression. Controls without IPTG were included to check for leakage in the promoter.

For the expression of soluble QnrS1 and QnrS2, the following conditions were tested for optimization of soluble protein expression:

1) Temperatures: 37 °C, 25 °C and 16 °C
2) Concentration of IPTG : 1 mM, 0.5 mM, 0.1 mM, 0 mM
3) Presence and absence of 1 % glucose in the liquid medium
4) Presence of 15 % glycerol the in liquid medium
5) Absence and presence of ciprofloxacin (0.007 mg/mL)
6) Cooling down the culture before induction with IPTG.

2.6 Protein isolation and purification

A 30 µL sample from each step of protein isolation and purification was collected for SDS-PAGE (section 2.7.2).

2.6.1 Isolation of soluble protein

For the isolation of soluble protein is it necessary to break the bacterial cell wall to release cytosolic protein. The frozen bacterial pellet was first thawed as the first step of cell lysis. Ice crystals formed will puncture the cells when the pellet is thawed. Cells were further lysed by sonication, which uses ultrasonic waves. The ultrasonic waves will create small vacuum bubbles that will become larger and disrupt the cell membrane when they collapse. To help with the degradation of the cell wall lysozyme was added, while DNase was added to break down DNA, reducing the viscosity. To inhibit the breakdown of the recombinant protein, protease inhibitor was added.

GyrA S83L and GyrA WT

The frozen bacterial pellets were thawed on ice and resuspended in 15 mL equilibration buffer-PBS with 0.1 mg/mL Lysozyme, 10 µg/mL DNase, 100 mM $MgCl_2$ and 1x Protestase inhibitor (Sigma). Cells were lysed by sonication on ice for 30 s with 30 s breaks, repeated 10 times. The

lysates were centrifuged (Eppendorf 5810R) at 10000 xg for 10 min at 4 °C to separate the soluble protein from the cell debris and inclusion bodies.

QnrS1, QnrS2 and QnrB19

The frozen bacterial pellets were thawed on ice and resuspended in 15 mL equilibration buffer-Tris with 0.1 mg/mL Lysozyme, 10 μg/mL DNase and 1x Protestase inhibitor (Sigma). Cells were lysed by sonication for 30 s with 30 s breaks, repeated 10 times on ice. The cell lysates were centrifuged (Eppendorf 5810R) at 12000 xg at 4 °C for 15 min to separate soluble protein from the cell debris and inclusion bodies. The supernatant from the first round of centrifugation was centrifuged an additional time at the same program, for better separation of supernatant and pellet.

Due to poor production of soluble protein, different lysis buffers were tested for isolation of soluble QnrS1 and QnrS2:

1) Glycerol concentration: 0 %, 10 %, 20 % and 30 %
2) pH 7.4 and 8.0
3) Salt concentration: 100 mM and 200 mM
4) Addition of 0.5 % Triton X-100

Incubation of bacteria in lysis buffer overnight at 4 °C was also tested (Tavío et al., 2014).

2.6.2 Immobilized metal affinity chromatography

The recombinant proteins were expressed with a C-terminal His-tag. This tag can be used for purification by immobilized metal affinity chromatography (IMAC). The metal, here Ni^{2+}, in stationary phase binds to proteins with a highly repeated sequence of histidine's. Untagged protein can therefore easily be removed since they do not bind to the stationary phase, but flow through instead. The his-tagged proteins can be eluted with high imidazole concentration, which outcompetes the protein and binds to the Ni^{2+} instead (Bornhorst & Falke, 2000; Spriestersbach et al., 2015).

General purification procedure: Ethanol was removed from the 2 mL Nickel- nitrilotriacetic acid resin (Ni-NTA resin) ethanol slurry (Thermo fisher). For equilibration, Ni-NTA resin was washed with 2x 4 mL equilibration buffer (equilibration buffer-PBS (GyrA) or equilibration buffer-Tris (Qnr)). Supernatant from protein isolation (section 2.6.1) was applied to the equilibrated Ni-NTA resin, this was incubated on an end over end rotator for 30 min at 4 °C. Untagged proteins were washed away using 4 mL wash buffer with an increasing concentration of imidazole. The protein of interest was eluted with 2 mL elution buffer containing 250 mM imidazole. Absorbance at 280 nm of each elution fraction was measured using a spectrophotometer. Elution stopped when absorbance was close to zero or stabilized. All pure fractions were pooled and dialyzed using Snakeskin dialysis tubing (3.5K MWCO, 35mm dry, Thermo scientific) overnight, followed by 7 h in fresh buffer at 4 °C. The dialyzed protein was concentrated using a Amicon ultra-15 (3k, Millipore) centrifugal filter unit at 5000 xg (Eppendorf 5810R), 4 °C. Concentrated protein was aliquoted in 200 µL fractions and stored at -20 °C

After use, Ni^{2+} is bound to imidazole and needs to be regenerated before the next round of purification. Ni^{2+} was detached from the Ni-NTA resin by adding 2x 5 mL stripping buffer followed by a 10 mL ddH_2O wash. Ni^{2+} was attached to the resin using 4 mL nickel loading buffer followed by 10 mL ddH_2O wash. The loaded resin was stored in 20 % ethanol at 4 °C.

GyrA S83L and GyrA WT

GyrA S83L and GyrA WT were purified using wash buffer 1-PBS (25 mM imidazole) and wash buffer 2-PBS (50 mM imidazole). To each elution fraction 20 % glycerol was added and the fractions were stored at -20 °C until dialysis. The proteins were dialyzed against storage buffer-PBS before concentration and storage.

QnrS1, QnrS2 and QnrB19

QnrS1, QnrS2 and QnrB19 were purified with wash buffer 1-Tris (25 mM imidazole), wash buffer 2-Tris (50 mM imidazole), and wash buffer 3-Tris (100 mM imidazole). Elution fractions were stored at -20 °C until dialysis. QnrB19 was dialyzed against storage buffer 2-Tris before the protein was concentrated. The protein was thawed after 3 weeks and dialyzed against storage buffer-Tris for the interaction studies. QnrS1 and QnrS2 were dialyzed directly against storage buffer-Tris followed by concentration and storage.

Additional storage buffers tested for QnrS1 and QnrS2:

1) 50 mM Tris, pH 8.0, 200 mM NaCl and 10 % glycerol
2) 50 mM Tris, pH 8.0, 200 mM NaCl, 10 % glycerol and 0.05 % Tween-20

Additional storage buffer tested for GyrA S83L, GyrA WT and QnrB19:

1) 50 mM Tris, pH 7.4 and 100 mM NaCl

2.6.3 Size exclusion chromatography

In size exclusion chromatography (SEC), also called gel filtration, proteins are separated depending on their size. The resin in the column makes a pours matrix which the protein migrates through. Here the larger proteins will be eluted first because they are not able to penetrate the pores like the smaller proteins which results in fewer interactions with the matrix (Lodish, 2016). SEC was also used as an analytic method in this study.

SEC was performed using a Superrose^{TM} 6 Increase 10/300 GL (General electric (GE) Healthcare) column installed on an Äkta Pure system (GE Healthcare) equilibrated with running buffer. Volumes of samples applied ranged from 100 µL - 500 µL. Flow-rate was set to 0.5 mL/min and proteins were eluted with 1.2 column volumes of running buffer. Absorbance was measured at 280 nm (Unicorn 7.1 GE healthcare). Elution fractions were collected in 1 mL aliquots. Fractions with absorbance above background level were run on an SDS-PAGE gel (section 2.7.3). To determine the size of the eluted proteins, protein markers from Gel filtration markers kit 12-2000 kDa (Sigma Aldrich) was diluted in running buffer and applied to the column as described in the accompanying manual. The elution volume and size of the standard proteins was used to make a standard curve to determine the size of the proteins of interest.

2.7 Protein analyses

2.7.1 Protein concentration measurements

Protein concentration was measured using Biorad protein assay: DC protein assay, a colorimetric assay. Five µL sample with protein was mixed with 25 µL of reagent A (alkaline copper tartrate solution). Two hundred µL reagent B (Folin dilution) was added before incubation for 15 min at RT. Absorbance was measured at 750 nm in a plate reader (Cytation 3, imaging reader, Biotek). A standard curve using different concentrations (1.5 mg/mL, 1.2 mg/mL, 0.8 mg/mL, 0.4 mg/mL and 0.2 mg/mL) of bovine serum albumin (BSA) was made to determine the unknown protein concentration. All samples were measured in triplicate.

In the interaction studies protein concentration was measured at 280 nm on a spectrophotometer (Nanodrop One, Thermo scientific) using the theoretical molar extinction coefficient and Beer-Lambert law for calculating the concentration (Equation 2.2). ExPASy ProtParam tool (Gasteiger et al., 2005) was used to calculate the extinction coefficient based on the amino acids sequence. All samples were measured in triplicate.

$$A = \varepsilon l c \qquad 2.2$$

A = Absorbance, ε = Molar extinction coefficient ($M^{-1}cm^{-1}$), c = Molar concentration (M), l = Optical path length (cm)

2.7.2 Sodium Dodecyl Sulphate Polyacrylamide Gel Electrophoresis

Sodium Dodecyl Sulphate Polyacrylamide Gel Electrophoresis (SDS-PAGE) is a method used for separating proteins based on their size. Acrylamide and bis-acrylamide (N,N'-methylenebisacrylamide) polymerizes and make up a gel matrix with pores that proteins migrate through. SDS binds to the proteins in a constant molar ratio (1.4:1), leading to a negative charge and partially unfolded protein. This will lead to migration of protein almost only based on molecular weight, where the smallest proteins will migrate fastest against the anode (positive terminal) when an electric current is applied (Cox & Nelson, 2013).

Samples were mixed in a 50:50 ratio with 2x SDS sample buffer and heated at 99 °C for 10 min. The samples were spun down at 6000 xg for 1 min (mikro 120 Hettich Zentrifugen), before

loaded on the 12 % SDS-PAGE gel. Gels were run in a Bio-rad mini cell on constant 33 milliampere per gel for approximately 30 min with 1x SDS-PAGE running buffer. To determine the protein size, PageRuler Plus Stained Protein Ladder (Thermo Fisher) (Appendix D, Figure S14B), Precision Plus Protein™ Kaleidoscope™ Prestained Protein Standard (Bio-rad) (Appendix D, Figure S14C), or Precision Plus Protein™ All Blue Prestained Protein Standard (Bio-rad) (Appendix D, Figure S14D) was used as ladder. SDS-PAGE gels were stained with Coomassie staining solution and destained with destaining solution until there was a contrast between background and protein bands.

2.7.3 Western blotting

Western blotting is a method to detect proteins of interest with the use of specific antibodies. Proteins separated by gel electrophoresis are transferred to a membrane by applying an electric current. The negatively charges proteins will migrate from the SDS-PAGE gel to the membrane as they move toward the anode. The membrane with bound proteins is incubated with primary antibody followed by incubation with secondary antibody. Primary antibody binds to the protein of interest. The secondary antibody binds to the primary and enables visualization of the protein by different methods, depending on what the secondary antibody is conjugated to (Cox & Nelson, 2013; Lodish, 2016).

An SDS-PAGE with separated proteins (section 2.7.2), a 0.45 µm PVDF membrane (Immobilon-E, Merck Millipore) with size corresponding to the SDS-PAGE gel and four filter papers (Bio-Rad) were incubated in 1x transfer buffer, before the assembly of the blotting sandwich. On the top of two filter papers the SDS-PAGE gel was placed followed by the PVDF membrane and two filter papers. Air bubbles was removed by rolling a glass tube on top of the filter papers. One western blot sponge was placed on each side of the sandwich, before it was transferred to a mini blot cell (Bio-Rad) with the SDS-PAGE gel facing the cathode. An ice block was placed in the mini blot cell before it was filled with 1x transfer buffer. Transfer of was run at 100 volts, 360 milliampere (constant) for 1 h in RT. SDS-PAGE gel was stained and destained after transfer as described in section 2.7.2.

After transfer, the PVDF membrane was incubated with 10 mL blocking buffer for 1 h, at RT or overnight at 4 °C to avoid unspecific binding of the antibody to the membrane. After blocking, the membrane was washed 3x 10 min with 10 mL TBS-T. His-tag specific primary

antibody (Appendix D, Table S8) (Invitrogen) was diluted 1:4000 in 10 mL blocking buffer and incubated with the membrane for 1 h in RT or overnight at 4 °C. Before incubation with secondary antibody, the TBST-T washing step was repeated. Secondary antibody (Appendix D, Table S8) (Invitrogen) was diluted 1:10000 in 10 mL blocking buffer and incubated with the membrane for 1 h in RT. The membrane was washed 3x 10 min with 10 mL TBST-T, before 0,125 mL/cm^2 chemiluminescence reagent (Pierce ECL Western, blotting substrate, Thermo scientific) was applied to the membrane followed by incubation for 1 min at RT. The two chemiluminescence reagents were mixed before applied to the membrane. Picture of the membrane was taken using an iBright 1500 system (Invitrogen, Thermo Fisher Scientific) with chemiluminescence detection.

2.8 Bioinformatics - Homology modelling

To model the structure of the three Qnr proteins of interest several bioinformatics tools were used. This was performed to reveal any potentially structural differences between QnrS1, QnrS2 and QnrB19. A protein search using Basic Local Alignment Search Tool (BLAST) (Altschul et al., 1990) was performed with the amino acid sequence of each of the Qnr proteins of interest as query. The searches were performed against the protein data bank (PDB) database (Berman et al., 2000), with default settings. In a BLAST search, the query sequence, here the Qnr sequences, will be used to find other sequences with local similarities in the chosen database, and calculate the statistical significance of the matches. The PDB database was used because it contains proteins with available structures. Matches taken into further analyses were based on sequence identity, query cover and e-value (parameter describing the chance of the hit being random). The results from the BLAST search were confirmed by a homology search using the HHpred server (Zimmermann et al., 2018). Secondary structure prediction using the Predictprotein server (Bernhofer et al., 2021) was performed on the best hits from HHpred and BLAST and for the three Qnr proteins of interest, QnrS1, QnrS2 and QnrB19. The hits were also aligned against the three Qnr proteins of interest using Muscle (Edgar, 2004) with defaults in Jalview (Waterhouse et al., 2009) to determine if consensus regions typical for pentapeptide repeat proteins were present. Homology modeling was performed in both Phyre^2 (Kelley et al., 2015) and SWISS-model (Guex & Peitsch, 1997) to determine if the predicted structures of QnrS1, QnrS2 and QnrB19 would display any differences that could explain any differences in interaction with GyrA. Illustrations of the predicted structures for use in this theses were

prepared in Pymol (Schrödinger LLC, 2015) based on the predicted structures from SWISS-model.

2.9 Interaction studies

To study the interaction between the two variants of GyrA and the three variants of Qnr, two methods was used: Microscale thermophoresis (MST) and surface plasmon resonance (SPR). Using these methods, the equilibrium dissociation constant (K_d) for each interaction can be obtained. K_d is the ligand concentration where half of the ligand binding sites on the protein is occupied. The smaller K_d, the higher affinity is it between the protein and ligand (Cox & Nelson, 2013). The K_d for each of the interaction can therefore be used to determine if the different Qnr variants interacts differently with the two GyrA variants.

2.9.1 Microscale thermophoresis

MST is a method used to study biomolecular interactions. The method measures the movement of molecules along a temperature gradient (generated by an IR laser), which is called thermophoresis (Jerabek-Willemsen et al., 2011; NanoTemper Technologies, 2021). The thermophoresis depends on the solvation shell, size, conformation and charge of the molecules, which changes upon binding to another molecule. The thermophoresis is monitored by labeling one of the molecules with a fluorescent dye enabling measurement of the fluorescence excited by UV-light. When the fluorophore labelled molecule binds to the non-fluorescent ligand, the thermophoretic movement out of the heated area changes compared to the unbound molecule (Figure 10A). To make a binding curve, the ligand is titrated against a constant concentration of the fluorescent molecule to observe the change in thermophoresis at different ligand concentrations (Figure 10B) (Jerabek-Willemsen et al., 2011, 2014).

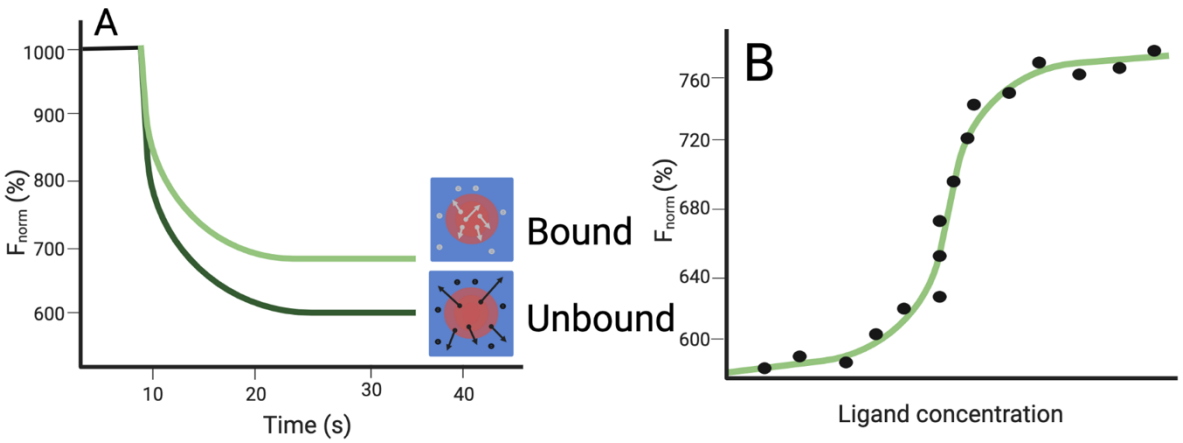

Figure 10.A) When the fluorescent protein binds to the non-fluorescent ligand the movement of the molecule changes out of the heated area changes compared to the unbound molecule. F_{norm} is the normalized fluorescence (F_{hot}/F_{cold}), F_{hot} is the fluorescence in the red area while F_{cold} is the fluorescent in the blue area shown in the figure. **B)** The gradual change in fluorescence observed due to change in thermophoresis at different ligand concentrations can be used to make a binding curve. This curve can be used to obtain binding constants. The figures were made in BioRender and is inspired by Nanotemper Technologies, 2021.

MST experiments were conducted together with Dr. Bjørn Dalhus (Department of medical biochemistry, Oslo University Hospital). Lysines on GyrA S83L and GyrA WT were labeled with NT-647-NHS fluorescent dye following the Monolith NT^{TM} Protein Labeling Kit RED-NHS protocol. Twelve µM GyrA S83L and 15 µM GyrA WT was mixed with NT647 dye in a 1:2.5 concentration ratio. The reaction was incubated in the dark at RT for 30 min. A NAP-5 gel filtration column was used to remove free dye. Labeled GyrA was eluted from the column with 600 µL storage buffer-PBS in 100 µL fractions.

A two-fold-dilution series of each Qnr protein starting with the highest possible concentration was prepared in sixteen PCR tubes. The protein was diluted in storage buffer-Tris, to keep the buffer constant. To each PCR tube 10 µL labeled GyrA S83L or GyrA WT was added to a final concentration of 60 nM. Concentration of Qnr protein in the first PCR tube after addition of GyrA was 7.5 µM for QnrS1, 10 µM for QnrS2 and 31 µM for QnrB19. The reaction was incubated in RT for 5 min before approximately 4 µL of each sample was loaded into standard capillaries (Monolith NT.115 Capillaries). Capillaries were put onto the sample loader and loaded into a Monolith NT.115 instrument (Nanotemper Technologies). The MST experiments were executed at 25 °C with three different MST powers (IR laser), 20 %, 40 % and 80 %. Light power (UV light) was set to 50 %. MO.Affinity analysis software was used for analyzing the data. All experiments were repeated two times.

2.9.2 Surface plasmon resonance

SPR is an optical method that can be used for interaction studies. In SPR the ligand is immobilized on a sensor surface and the analyte is flowing over the ligand in the mobile phase (Patching, 2014) (Figure 11A). On the opposite side of the sensor chip, light is reflected and monitored by a detector. Upon binding of the analyte to the ligand, the refractive index close to the sensor chip changes, leading a change in the angle of the reflected light. This is observed as an increase in resonance units (RU) in the sensorgram (Douzi, 2017; Patching, 2014) (Figure 11B).

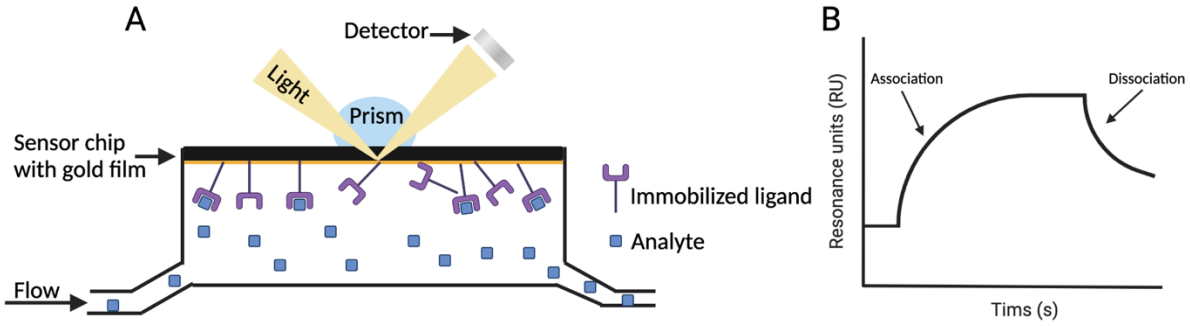

Figure 11. A) Ligand immobilized on the sensor chip with analyte flowing over in mobile phase. The angle of the reflected light changes upon analyte binding which is measured by the detector. **B)** Analyte binding is observed as an increase in RU. When buffer is injected in the flow cell, dissociation of the analyte is observed as a decrease in RU. The figures were made in BioRender.

R_{max} is the theoretically maximum response, in RU, expected for the interaction between the analyte and ligand, if all binding sites are available for interaction. The value was used to determine the level of ligand that should be immobilized to achieve the desired response from analyte binding. R_{max} for a 1:1 interaction was calculated using equation 2.3.

$$R_{max} = \frac{MW_{analyte}}{MW_{ligand}} x\ immobilized\ ligand(RU) \qquad (2.3)$$

The SPR experiments were conducted on a Biacore S2000 (GE Healthcare), followed by curve fitting and calculations in Biacore S200 Evaluation Software Version 1.1 (GE Healthcare) together with Rune Johansen Forstrøm (Engineer at Oslo University Hospital, Oslo). All SPR experiments were performed at 20 °C.

Immobilization of GyrA

A GM5 chip (GE healthcare), which contains 4 channels, was placed in the Biacore S200 (GE healthcare) and normalized with BIAnormalizing solution (GE healthcare). The channels were

washed with 1 M NaCl and 100 mM NaCl followed by 1x PBS-P+ wash. Channel 2 and 4 were activated with 75 µL 1-ethyl-3-(3-dimethylaminopropyl)carbodiimide and 75 µL N-hydroxysuccinimide. This will create a reactive succinimide ester bound to the dextran which will react with the amine group on the lysine. GyrA S83L in 10 mM acetate buffer, pH 4.0 (GE healthcare) was immobilized in channel 2 with flowrate 10 µL/min. Immobilization of GyrA WT in channel 4 was performed in the same way. The channels were deactivated with 1 M ethanolamine-HCl pH 8.5 (GE healthcare) to deactivate the reactive succinimide esters to prevent immobilization of the analyte. Channel 1 and 3 were used as reference channels.

A two-fold dilution series of the QnrS1, QnrS2 and QnrB19 (analyte) in 1xPBS-P+ was made (125 nM - 2 µM) and run over the channels (30 µL /min for 60 s). A duplicate was prepared of the 1 µM sample to secure reproducible results in each experiment. Regeneration with 1 M NaCl was performed between each analyte injection, to remove bound analyte, followed by 1x PBS-P+ wash before the next analyte injection. This was performed two times.

Immobilization of Qnr

GyrA S83L and GyrA WT were dialyzed against the running buffer used (SPR-buffer) at 4 °C for 2x 2 h and overnight using Snakeskin dialysis tubing (3.5K MWCO, 35mm dry, Thermo scientific). A GM5 chip was normalized as described for the immobilization of GyrA followed by SPR-buffer wash. Activation, immobilization and deactivation were performed as described for GyrA. QnrS1 was immobilized in channel 2, QnrS2 in channel 3 and QnrB19 in channel 4. Channel 1 was used as a reference. A two-fold dilution series of GyrA S83L and GyrA WT in SPR-buffer (125 nM - 2 µM, 2x 1 µM) was flowed over the immobilized proteins (30 µL /min for 60 s). For regeneration 1 M NaCl was used, followed by SPR-buffer wash before next analyte injection. The same experiment was repeated with a two-fold dilution series of GyrA S83L and GyrA WT with concentrations 62.5 nM-16 µM, 2x 8 µM.

In the experiments all curves were double blank subtracted. The response caused by unspecific analyte binding in the empty reference channel, and the response from a buffer injection in channel with immobilized ligand was subtracted from the curves. This was to remove the background signal.

3 Results and discussion

3.1 Cloning

Plasmid constructs were designed containing the genes of interest with a C-terminal His-tag, that could be used for purification with IMAC and quantitative identification by western blotting. The His-tag is a small and flexible tag and is thought to have little impact on the protein structure (Carson et al., 2007). Also, both GyrA and certain Qnr proteins have been shown to be active with a C-terminal His-tag (Matrat et al., 2007; Pan & Fisher, 1999; Tran et al., 2005b; Tran & Jacoby, 2002; Xiong et al., 2011). Therefore, no cleavage site for removing the His-tag was included in the construct. The "native" ribosome binding site (RBS) was removed from the pET28a(+) digested with XbaI (Figure 8). Amplicons encoding GyrA S83L, GyrA WT and QnrB19 were therefore constructed with an RBS, starting 13 bp upstream from the start codon. This was to ensure binding of the ribosome, which is necessary for protein synthesis.

3.1.1 pET28a(+) constructs

The genes encoding GyrA S83L, GyrA WT, QnrS1, QnrS2 and QnrB19 were successfully amplified using gene-specific cloning primers (Figure 12). All bands were of the expected theoretical size, which is approximately 2700 bp for GyrA (lane 1, 2 and 3) and 650 bp for Qnr (lane 4, 5 and 6). Weak bands in the lower part of lanes 1, 2, 3 and 4 are probably primer dimers. The PCR products were successfully cloned into pET28a(+) expression vector. Positive transformants were identified with colony PCR and sent for Sanger sequencing. Sequencing confirmed that constructs harbored the gene of interest, without any mutations, and with a C-terminal His-tag. Plasmids encoding GyrA S83L, GyrA WT and QnrB19 also harbored the optimized RBS (Appendix C, Figure S1-S4).

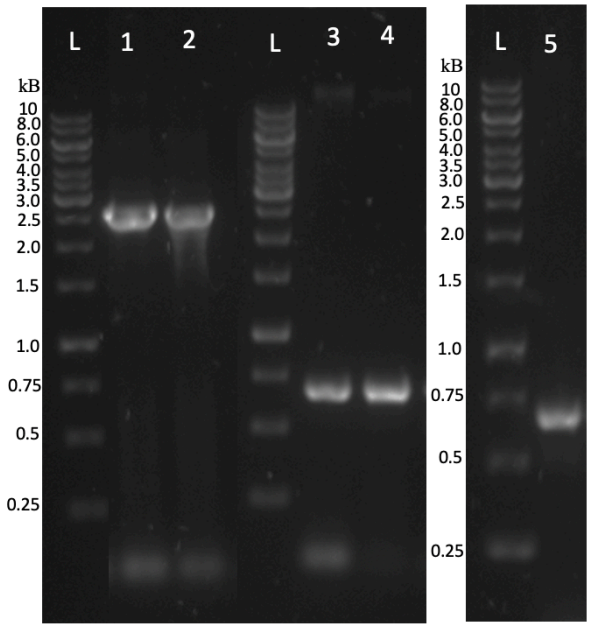

Figure 12. Amplification of GyrA S83L, GyrA WT, QnrS1, QnrS2 and QnrB19 with cloning primers on a 1 % agarose gel. DNA sequences was cloned into pET28a(+) expression vector. **L** refers to 4 µL Thermo scientific gene ruler 1 kb DNA ladder. **1** refers to amplified *gyrA* S83L ~2671 bp with RBS and His-tag. **2** is the amplified *gyrA* WT ~2671 bp with RBS and His-tag. **3** represents amplified *qnrB19* ~688 bp with RBS and His-tag. **4** is the amplified *qnrS2* ~687 bp with His-tag and **5** refers to amplified *qnrS1* ~687 bp with His-tag.

3.1.2 pBAD30 constructs

The genes encoding QnrS1, QnrS2 and QnrB19 were cut out of the corresponding pET28a(+) constructs (Appendix C, Figure S2-S4) using appropriate restriction enzymes (Figure 13) and subcloned into the pBAD30 vector, digested with the same enzymes (Appendix C, Figure S5-S7). The pBAD30 constructs contained the RBS, gene of interest and the C-terminal His-tag. Sequencing confirmed that all genes were sub-cloned without any mutation.

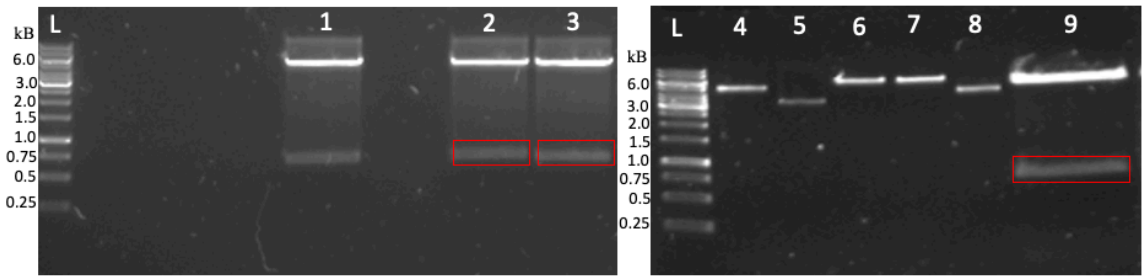

Figure 13. 1 % agarose gel with digested pET28a-Qnr constructs. L refers to 4 µL Thermo scientific gene ruler 1 kb DNA ladder. **1** is pET28a-QnrS1 digested with XbaI and SalI. **2** is pET28a-QnrS2 digested with XbaI and SalI, insert in red (745 bp). **3** represents pET28a-QnrB19 digested with XbaI and SalI, insert in red (707 bp). **4** is the pBAD30 vector digested with XbaI and HindIII. **5** refers to undigested pBAD30. **6** refers to pET28a-QnrS1 digested with XbaI**. 7** is pET28a-QnrS1 digested with HindIII. **8** refers to undigested pET28a-QnrS1. **9** is pET28a-QnrS1 digested with XbaI and HindIII, insert in red (751 bp).

3.2 Protein expression

BL21 cells were transformed with the pET28a(+) constructs for protein expression. GyrA S83L, GyrA WT, QnrS1, QnrS2 and QnrB19 were expressed to obtain protein for purification and subsequent protein-protein interaction studies.

Protein expression was first tested in a small-scale experiment to see if there would be any protein expression from the constructs, and if so to determine if the proteins were of expected size. The whole cell lysates were loaded on the SDS-PAGE gel, therefore it was not possible to distinguish between insoluble and soluble proteins. Figure 14 shows that there was overexpression of one protein in each expression culture with corresponding size to the protein of interest (GyrA: 97 kDa, QnrS1 and S2: 24.7 kDa, QnrB19:23.8 kDa). There was no overexpression of proteins observed for the BL21 cells transformed with an empty pET28a(+) vector. The expression test also showed that there was protein expression in the absence of IPTG, indicating leaky expression from the pET28a(+) vector.

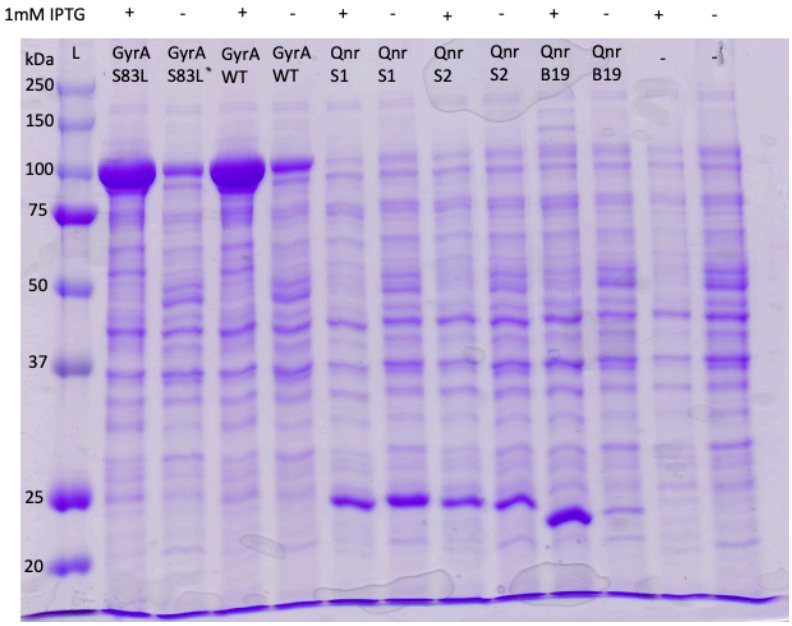

Figure 14. Coomassie stained 12 % SDS-PAGE gel displaying protein bands in whole cell lysate from a small scale expression test. BL21 cells were transformed with pET28a(+) constructs. IPTG (1 mM) was added (+) or not (-) in mid-exponential phase followed by incubation at 37 °C and 200 rpm for 3 h. **L** represents 5 µL Precision Plus Protein™ Kaleidoscope Prestained™ Protein Standards. Lanes marked: **–** represents whole cell lysate of BL21 cells with empty vector.

Expression of GyrA S83L, GyrA WT and QnrB19 was performed at 37 °C for 3 h with the addition of 1 mM IPTG in mid-exponential phase, which gave soluble protein (Figure 16, 17 and 18). For QnrS1 and QnrS2, the proteins were in inclusion bodies when the protocol used for GyrA S83L, GyrA WT and QnrB19 was followed, and therefore more optimalization was needed (Figure 15A and B). Inclusion bodies are large aggregations of protein, typically consisting of the overexpressed protein. Many different strategies can be tested to optimize the yield of soluble protein during overexpression. This includes different culture parameters, bacterial strains used for expression, vectors and co-expression of chaperones (Francis & Page, 2010). Here the focus was first set to change the culture parameters to slow down protein synthesis, which has been shown to give a higher yield of soluble protein (Arya et al., 2015; Rizkia et al., 2015). The highest yield of soluble QnrS1 and QnrS2 was obtained by expressing at 16 °C and induce the expression with 0.1 mM IPTG. LB medium was also supplemented with 1 % glucose to repress expression of recombinant proteins from the leaky promotor before induction with IPTG (Figure 19 and 20).

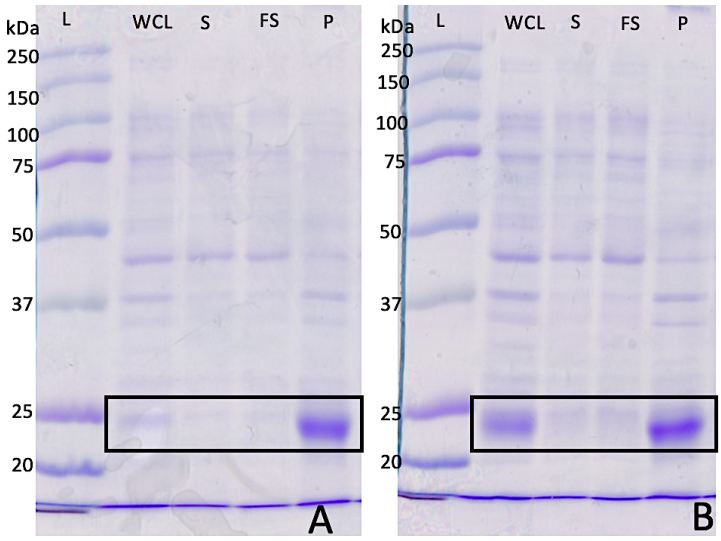

Figure 15. Coomassie stained 12 % SDS-PAGE gels displaying expression of QnrS1 and QnrS2. A) BL21 cells transformed with pET28a-QnrS1 induced 1 mM IPTG in mid-exponential phase and incubated for 3 h at 37 °C and 200 rpm. **B)** BL21 cells transformed with pET28a-QnrS2 induced 1 mM IPTG in mid-exponential phase and incubated for 3 h at 37 °C and 200 rpm. **L** represents 5 µL Precision Plus Protein™ Kaleidoscope Prestained™ Protein Standards, **WCL** is the whole cell lysate with both soluble and insoluble protein, **S** refers to supernatant with soluble protein, **FS** corresponds to filtrated supernatant with soluble protein and **P** refers to pellet with insoluble protein. QnrS1 and QnrS2 is approximately 25 kD.

3.3 Protein purification by immobilized metal affinity chromatography

To obtain pure protein for interaction studies all five proteins were purified by IMAC. The Ni-NTA Resin was washed with increasing imidazole concentration, removing untagged proteins yielding pure protein which was eluted with an imidazole concentration of 250 mM.

All five proteins of interest in this thesis were expressed and purified in two separate rounds. In the first round of expression and purification, proteins were purified by IMAC followed by SEC. After this round of expression and purification, the purified proteins were lost due to precipitation. There could be several reasons for this, for example storage conditions, storage time, buffer composition, or too high protein concentration, but most likely a combination of all of them. In the second round, the proteins were expressed in the same way as in round one, but only purified by IMAC and not SEC as in the initial round. SEC was not performed to avoid concentrating the proteins two times, since problems with precipitation and potential multimerization seemed to occur in this step. To avoid multimerization and precipitation as observed in the first round, the proteins were aliquoted and stored at -20°C. The proteins were also stored for a shorter period before the interaction studies. Attempts were also made to optimize the buffers to avoid non-specific protein-interactions and increase the stability of the proteins.

GyrA S83L

Figure 16A shows the first round of purification of GyrA S83L. GyrA S83L is approximately 100 kDa which probably corresponds to the prominent band found in all fractions. The SDS-PAGE gel shows that a large amount of GyrA S83L did not bind to the Ni-NTA resin after 30 min incubation (Eq). In the washing steps, untagged protein is eluted so these proteins seem to have bound unspecific to the Ni-NTA resin instead of the tagged recombinant protein. GyrA S83L was also eluted during the washing steps (25-50 mM imidazole). Although much protein being lost during purification, there was still a large amount of protein in the elution fractions. Elution fractions 1, 2 and 3 showed some contaminants and were therefore diluted to an imidazole concentration of 25 mM for another round, in which less Ni-NTA resin was used to increase specificity. Figure 16B shows the second round of purification where some of the contaminants at low molecular weight were removed in some of the elution fractions.

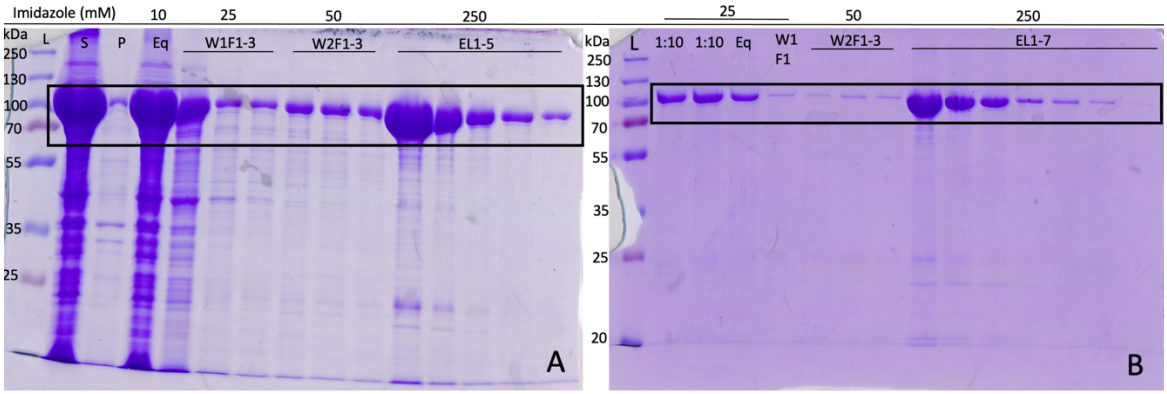

Figure 16. Purification of GyrA S83L by IMAC. Fractions from each purification step were loaded on a 12 % SDS-PAGE gel **A)** First stage of IMAC purification, **B)** Second stage of IMAC purification following 10-fold dilution of fractions from A containing relative pure GyrA S83L. **L** refers to 3 µL PageRuler Plus Stained Protein Ladder, **S** refers to the supernatant with soluble protein, **P** is the pellet containing cell debris and insoluble protein, **Eq** is the flow through containing protein not binding to the Ni-NTA resin after 30 min incubation. **W1Fx** refers to the fraction containing protein eluted by wash buffer 1 (25 mM imidazole), **W2Fx** is the protein eluted by wash buffer 2 (50 mM imidazole), **EL** refers to the fraction containing proteins eluted by elution buffer. GyrA S83L is approximately 97 kDa.

GyrA WT

As observed for the purification of GyrA S83L, a prominent band at approximately 100 kDa was present in all the lanes, most likely corresponding to GyrA WT (Figure 17A). Problems with initial binding and early elution were observed as described earlier, like for GyrA S83L. A large amount of pure protein was observed in the elution fractions, but for elution fraction 1 and 2 an additional round of purification was performed to get rid of impurities. The fractions were diluted to an imidazole concentration of 25 mM and purified by IMAC (Figure 17B), which removed most of the impurities.

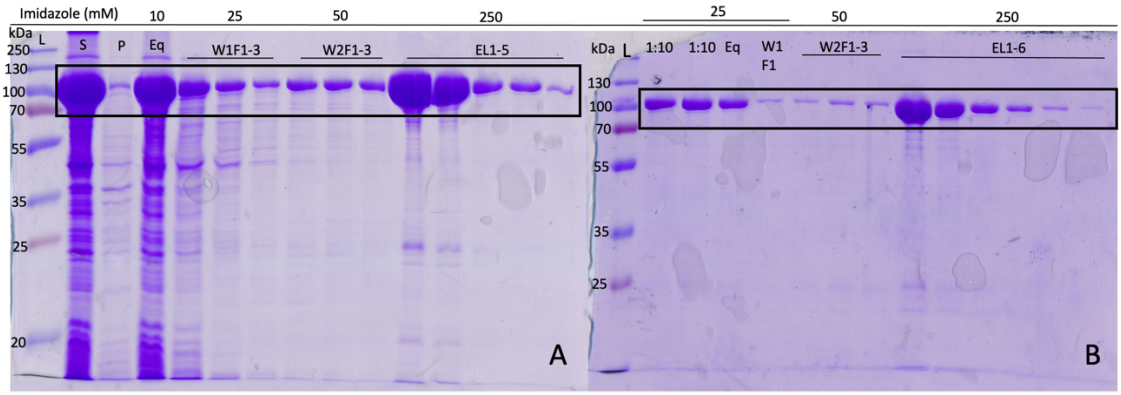

Figure 17. Purification of GyrA WT by IMAC. Fractions from each purification step were loaded on a 12 % SDS-PAGE gel **A)** First stage of IMAC purification. **B)** Second stage of IMAC purification following 10-fold dilution of fractions from A containing relative pure GyrA WT. **L** refers to 3 µL PageRuler Plus Stained Protein Ladder, **S** refers to the supernatant with soluble protein, **P** is the pellet containing cell debris and insoluble protein, **Eq** is the flow through containing protein not binding to the Ni-NTA resin after 30 min incubation. **W1Fx** refers to the fraction containing protein eluted by wash buffer 1 (25 mM imidazole), **W2Fx** is the protein eluted by wash buffer 2 (50 mM imidazole), **EL** refers to the fraction containing proteins eluted by elution buffer. GyrA WT is approximately 97 kDa.

In the lysis of cells expressing QnrS1 and QnrS2, different lysis buffers were tested to obtain highest yield of soluble protein. The buffer of choice resembles one used in previous study to purify QnrS1 (Tavío et al., 2014). Instead of $(NH_4)_2SO_4$, NaCl was used and the glycerol concentration was changed from 10 % to 30 % to increase the stability of the protein (Leibly et al., 2012; Vagenende et al., 2009). The buffer used for lysis and purification of QnrB19 in the first round of purification was a tris buffer with 50 mM tris, pH 7.4 and 100 mM NaCl. But the buffer was changed to the one used for QnrS1 and QnrS2 in the second round of purification to increase the stability of the protein.

QnrB19

QnrB19 was expressed the same way as the GyrA proteins but in bigger volumes. Due to a higher number of bacterial cells and poor binding of both GyrA proteins to the Ni-NTA resin, the QnrB19 expression culture was divided in two for the purification. In Figure 18A and B there is a prominent band at about 24 kDa, likely corresponding to QnrB19 ~23.8 kDa. In the pellet fraction there was a significant amount of protein due to inclusion bodies and/or insufficient lysis. There was some problem with early elution during the washing steps (25-100 mM imidazole), but most of the protein of interest was eluted at 250 mM imidazole. Some of the elution fractions were contaminated with unknown proteins of about 70 kDa. These fractions were diluted to an imidazole concentration of 25 mM and purified in an additional

round of IMAC (Figure 18C). In this round of purification, most of the contaminants at 70 kDa were removed.

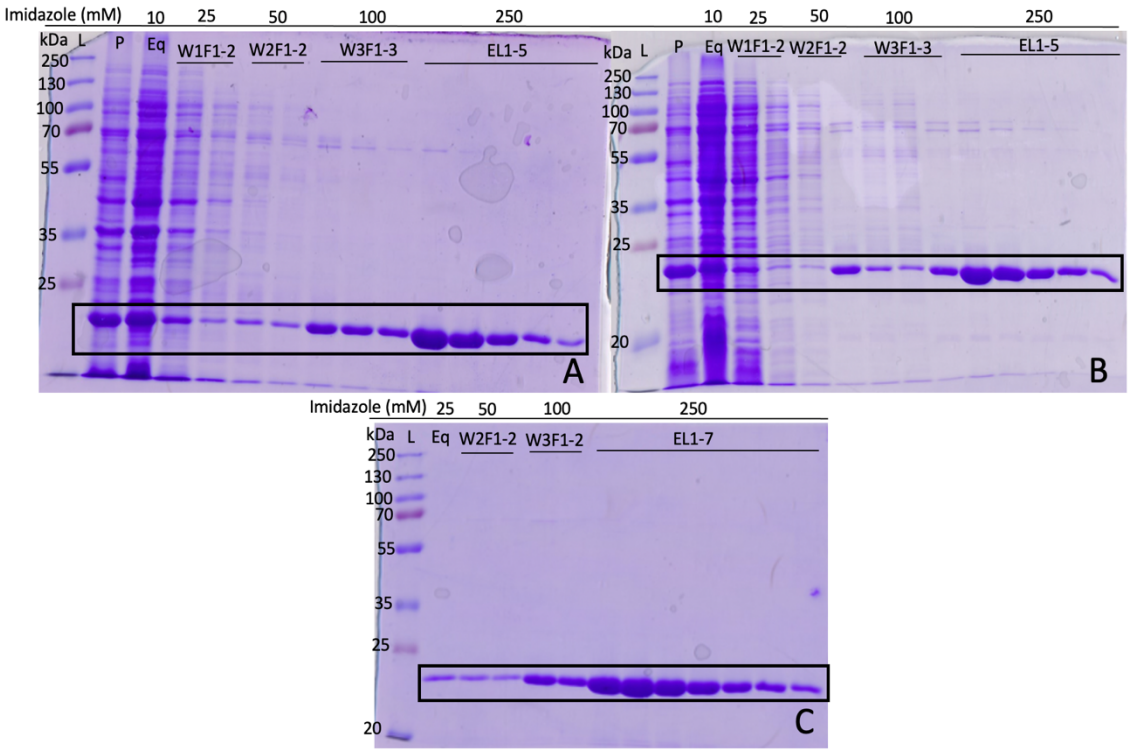

Figure 18. Purification of QnrB19 by IMAC. Fractions retrieved during purification were loaded on 12 % SDS-PAGE gels **A** and **B)** first stage of IMAC purification, and **C)** second stage of IMAC purification following 10-fold dilution of fractions from A containing relatively pure QnrB19. **L** refers to 3 µL PageRuler Plus Stained Protein Ladder, **S** refers to the supernatant with soluble protein, **P** is the pellet containing cell debris and insoluble protein, **Eq** is the flow through containing protein not binding to the Ni-NTA resin after 30 min incubation. **W1Fx** refers to the fraction containing protein eluted by wash buffer 1 (25 mM imidazole)**, W2Fx** is the protein eluted by wash buffer 2 (50 mM imidazole), **W3Fx** corresponds to proteins eluted in wash buffer 3 (100 mM imidazole), **EL** refers to the fraction containing proteins eluted by elution buffer. QnrB19 is approximately 24 kDa.

QnrS1

A large amount of the expressed QnrS1 proteins (~24.8 kDa) seemed to be present in inclusion bodies in the pellet fraction (Figure 19A and B). Most contaminants were washed out before elution at 250 mM imidazole, but there was still a visible contaminant at approximately 70 kDa in the elution fractions. Because the amount of pure protein was low, elution fraction with contaminants, wash buffer 3 fractions, and the Eq fractions were diluted to 25 mM imidazole for a new round of IMAC purification (Figure 19C). This removed most of the contaminants.

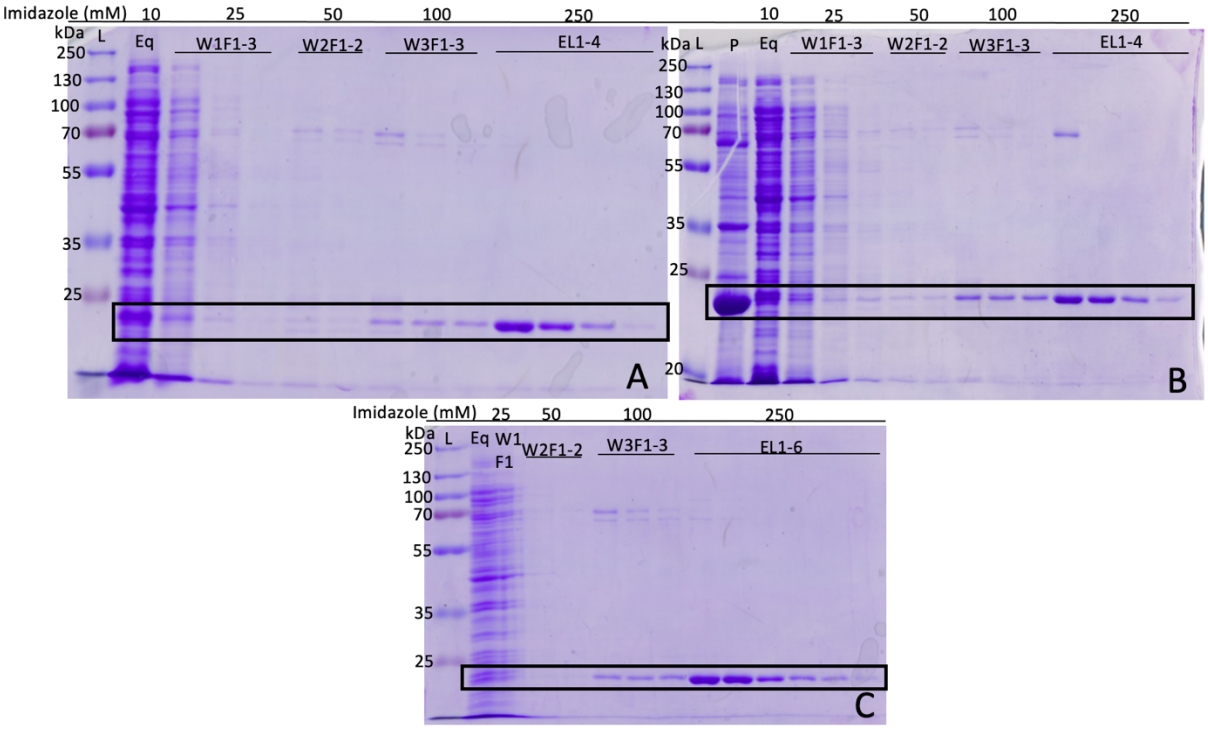

Figure 19. Purification of QnrS1 by IMAC. Fractions retrieved during purification were loaded on 12 % SDS-PAGE gels **A** and **B**) first stage of IMAC purification, and **C**) second stage of IMAC purification of elution fraction with contaminants, Eq fractions, wash buffer 3 fractions from A. **L** refers to 3 µL PageRuler Plus Stained Protein Ladder, **S** refers to the supernatant with soluble protein, **P** is the pellet containing cell debris and insoluble protein, **Eq** is the flow through containing protein not binding to the Ni-NTA resin after 30 min incubation. **W1Fx** refers to the fraction containing protein eluted by wash buffer 1 (25 mM imidazole), **W2Fx** is the protein eluted by wash buffer 2 (50 mM imidazole), **W3Fx** corresponds to proteins eluted in wash buffer 3 (100 mM imidazole), **EL** refers to the fraction containing proteins eluted by elution buffer. QnrS1 is approximately 25 kDa.

QnrS2

QnrS2 is approximately 25 kDa which is the size of the prominent band seen on the SDS-PAGE gel from QnrS2 purifications (Figure 20A and B). A large amount of the expressed protein was found in inclusion bodies in the pellet. As described earlier for the purification of QnrB19 and QnrS1, problems with tagged protein not binding to resin and the contamination at approximately 70 kDa were observed for QnrS2 as well. Most of the contamination was washed away, but some weak bands were still observed in the elution fractions. Due to low amount of pure protein, elution fractions with contaminations were pooled with wash buffer 3 fractions in Figure 20B and both Eq fractions. The imidazole concentration was diluted to 25 mM before the second round of purification (Figure 20C), which resulted in more pure protein.

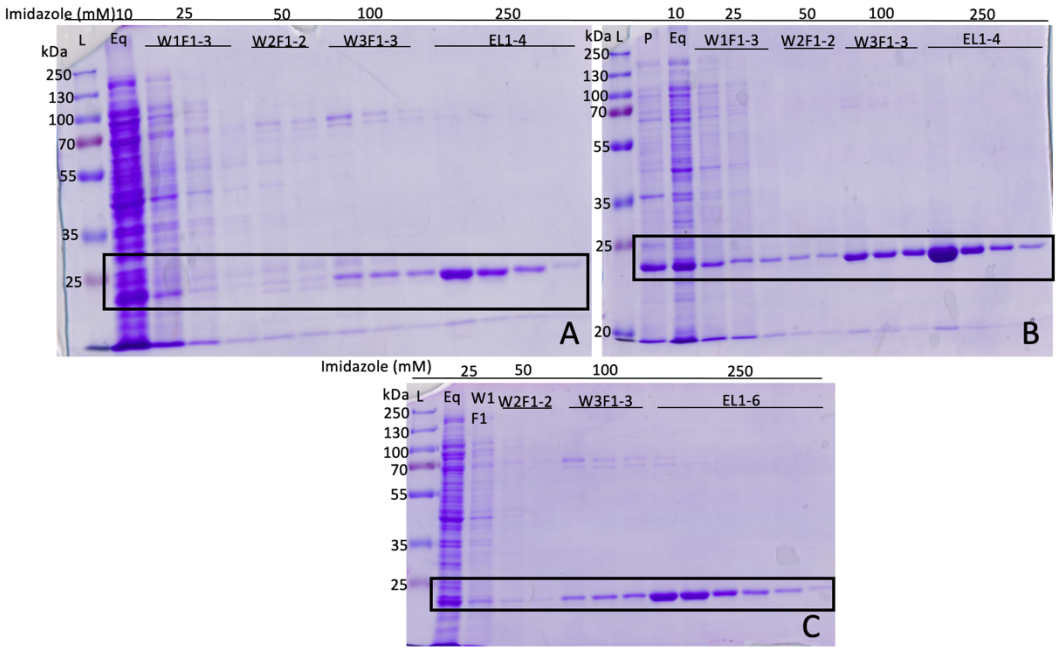

Figure 20. Purification of QnrS2 by IMAC. Fractions retrieved during purification were loaded on 12 % SDS-PAGE gels **A** and **B**) first stage of IMAC purification, and **C**) second stage of IMAC purification of elution fractions with contaminants, wash buffer 3 fractions from B and the Eq fractions. **L** refers to 3 µL PageRuler Plus Stained Protein Ladder, **S** refers to the supernatant with soluble protein**, P** is the pellet containing cell debris and insoluble protein**, Eq** is the flow through containing protein not binding to the Ni-NTA resin after 30 min incubation**. W1Fx** refers to the fraction containing protein eluted by wash buffer 1 (25 mM imidazole)**, W2Fx** is the protein eluted by wash buffer 2 (50 mM imidazole)**, W3Fx** corresponds to proteins eluted in wash buffer 3 (100 mM imidazole)**, EL** refers to the fraction containing proteins eluted by elution buffer. QnrS2 is approximately 25 kDa.

For QnrS1 and QnrS2 buffer optimalization was necessary to avoid precipitation when the proteins were concentrated. The buffer which yielded the highest protein concentration was 20 mM Tris, pH 8.0, 50 mM arginine and 10 % glycerol. This buffer has been used in other studies for purified Qnr proteins and has yielded high concentrations of the proteins (Tavío et al., 2014; Vetting et al., 2011). However, the protein concentration obtained here was lower compared to these studies. One explanation could be the position of the His-tag, since Tavío et al. and Vetting et al. used an N-terminal His-tag. Changing to an N-terminal His-tag or removing the C-terminal His-tag could increase the concentration. However, this was not attempted in this study since it was possible that the achieved concentration could have been high enough for the interaction studies.

Overall, the IMAC purifications was very effective for protein purification, but some loss of protein due to poor binding to Ni-NTA resin and early elution was a problem for all five recombinant proteins. Initial binding of recombinant protein can be affected by the accessibility of the C-terminal His-tag. The GyrA C-terminus binds to DNA and even if DNase was used in

the lysis step there could still be DNA binding and interfere with resin binding (Vanden Broeck et al., 2019). For Qnr proteins, the C-terminus could be less accessible due to dimerization of the protein via the C-terminal α-helix (G. A. Jacoby et al., 2013; Vetting et al., 2011). Changing the Qnr His-tag position to the N-terminus could possibly be a good idea, for both binding and solubility as discussed earlier. If the proteins are in aggregates or multimers this would also affect its ability to bind to the Ni-NTA resin due to less accessible His-tag. Additionally, all five proteins are expected to form dimers in solution. There could be a possibility that one monomer of the dimer is lost, because only one of the monomers binds to the Ni-NTA resin. To try increasing the initial protein binding to the resin, the amount of resin and incubation time was increased. However, this did not increase the initial binding, rather an increase in unspecific binding was observed when the amount of resin was increased. For future purification attempts, buffers with higher salt concentration and addition of detergents should be tried out to avoid non-specific interactions. This can increase the elution of untagged protein at lower imidazole concentrations and would also prevent some of the early elution of recombinant protein, because the imidazole concentration is reduced (Bornhorst & Falke, 2000; Spriestersbach et al., 2015). The imidazole concentration of the equilibration buffer can also be increased to avoid weak histidine interaction from untagged proteins in the initial binding. (Bornhorst & Falke, 2000).

This should be especially tried for the Qnr proteins, were a stronger wash buffer with 100 mM imidazole was used to remove contaminants at approximately 70 kDa (Figure 18-20). One possibility is that the band correspond to a trimer (~75 kDa) of Qnr, but can also be histidine rich present in *E.coli* (Andersen et al., 2013). Another possible contamination is DnaK, the bacterial homolog of heat shock protein 70 (Hsp70). This protein is a chaperone which is involved in folding of proteins, and is often observed during purification of proteins expressed in *E.coli* (Morales et al., 2019; Ratelade et al., 2009). The protein band was not further analyzed so this will only be speculations. However, if the contamination is DnaK, buffer with ATP and another substrate for chaperone (denatured protein or protein with DnaK binding site) has been shown to remove this kind of contamination (Morales et al., 2019; Rial & Ceccarelli, 2002).

3.3.1 Protein concentration and quantitative identification

The concentration of the proteins was measured using Bio-rad protein assay: DC protein assay with BSA as standard (Table 1). The concentration of GyrA S83L and GyrA WT was determined again after being dialyzed to a new buffer used for SPR experiments. The concentration was determined by measuring the absorbance at 280 nm on a spectrophotometer, using the theoretical extinction coefficient 52510 M^{-1} cm^{-1} (Table 1).

Table 1. Concentration of recombinant protein in mg/mL and μM.

Protein	Bio-Rad DC protein assay[1]		Spectrophotometer (A280)[2]	
	mg/mL	μM	mg/mL	μM
GyrA S83L	1.2	12.5	1.6	16.6
GyrA WT	1.5	15.1	2.1	21.8
QnrS1	0.4	15.6	-	-
QnrS2	0.5	20.2	-	-
QnrB19	1.5	62.5	-	-

1) Concentration was measured using Bio-rad protein assay: DC protein assay. BSA was used for making standard curve for determination of the concentration.

2) Concentration was measured using a spectrophotometer at 280 nm and theoretical extinction coefficient for GyrA: 52510 M^{-1} cm^{-1}

Purified and concentrated GyrA (200 ng) and Qnr (800 ng) proteins in storage buffer were loaded on an SDS-PAGE gel (Figure 21A). This was to determine the purity and confirm the concentration determination of the proteins. GyrA S83L and GyrA WT showed a prominent band of expected size, but there were also additional bands of larger size. This can be multimers of GyrA, since the bands appeared after the samples were concentrated and were not visible in the purification step. The relative intensity of the band compared to the expected GyrA band suggest that it should have been visible during purification. An attempt to remove the potential multimers by centrifugation at 12000 xg failed, suggesting that they are not part of larger insoluble aggregates. SEC could be used to remove the larger proteins, but this would require an additional step of concentration of the protein, where multimerization appears to have occurred in the first place. It was decided to continue with the interaction studies using the available samples. QnrS1, QnrS2 and QnrB19 all show one very clear band at the expected size. For QnrS1 and QnrS2 there were two very weak bands at 70 kDa and 20 kDa, but since these contaminants constituted a minor proportion of the protein, the samples were deemed pure enough for the interaction studies.

To confirm the results of the Coomassie stained gels, a western blot with the same amount of protein used for the Coomassie staining was performed (Figure 21B). The bands on the western blot were as expected at about 100 kDa (GyrA) and 25 kDa (Qnr). This indicates that the bands of expected sizes observed on the Coomassie stained gel are the recombinant proteins of interest. The signals for GyrA S83L and GyrA WT are very weak, possibly due the low amount of protein loaded on the gel. Coomassie stain binds at several sites on the protein, leading to a stronger band for GyrA compared to Qnr, if the same amount of protein was loaded. However, this is not the case for western blot because the antibody binds to the His-tag, which there is only one of in each protein molecule. The bands observed at higher molecular weight for GyrA S83L and GyrA WT was not observed on the western blot. This could mean that the bands are either contaminants or the concentration of the GyrA multimers are too low, similar to what was observed for the bands at the expected size. The accessibility of the His-tag can also be a problem if the proteins are in multimers. The two bands (70 kDa and 20 kDa) observed in the lanes with QnrS1 and QnrS2 was not visible in the western blot, indicating that they are contaminations. BL21 cells transformed with the pET28a(+) vector in lane 6 served as a negative control to check if there was any expression of a histidine rich proteins at approximately 100 or 25 kDa. A weak band at approximately 35 kDa was observed, most likely only a histidine-rich protein in *E.coli.*

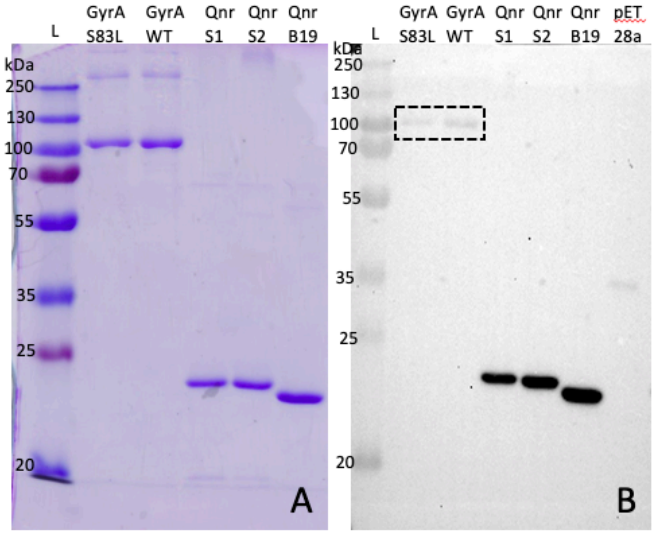

Figure 21. Purified and concentrated proteins. L represents 5 µL PageRuler Plus Stained Protein Ladder. **A)** 12 % SDS-PAGE gel with 200 ng GyrA ~97 kDa and 800 ng Qnr ~24 kDa, **B)** Proteins on SDS-gel in figure A transferred to an PVDF membrane and incubated with His-tag specific antibody for 1 h at RT. GyrA marked due to low signal.

3.4 Bioinformatics – Homology modelling

A structural model of the three Qnr proteins, QnrS1, QnrS2 and QnrB19 was modeled using homology modeling in SWISS-model based on the coordinates of the QnrB1 structure (PDB accession: 2XTW) (Vetting et al., 2011). The BLAST search of Qnr sequences showed that QnrB1 has a sequence identity of over 40 % compared to all three proteins and can therefore be used for homology modeling (Table 2). QnrB1 was isolated from *Klebsiella pneumonia* and is 217 amino acids long and 23.8 kDa.

Table 2. Comparison of QnrS1, QnrS2 and QnrB19 with QnrB1[1]

	Percentage identity	Query cover	E-value
QnrS1	44.97%	86%	$2e^{-52}$
QnrS2	47.09%	86%	$8e^{-56}$
QnrB19	97.20%	100%	$3e^{-155}$

1) Blast searches were performed against PBD database using the amino acid sequences of QnrS1, QnrS2 and QnrB19 as query sequences. Shown are parameters to the best hit (QnrB1).

Alignment of the three query sequences (QnrS1, QnrS2 and QnrB19) and QnrB1 displayed conservation of the B-loop (*XN*X(I/V)(S/T)*XXX*(W/F/Y)FCX), which is important for resistance (G. A. Jacoby et al., 2013; Tavío et al., 2014; Vetting et al., 2011; Xiong et al., 2011) (Figure 22). The four sequences also have the repeating pentapeptide tandem repeats (A/C/S/V/T/L/I) (D/N/S/K/E/I/R) (L/F) (S/T/R/E/Q/K/V/D) (G/D/E/N/R/Q/K) (Zhang et al., 2019).

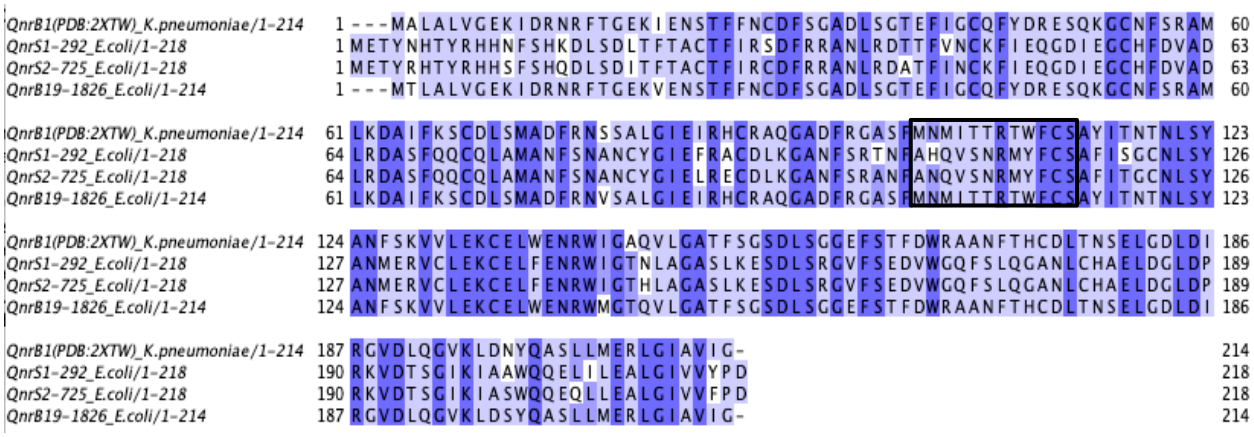

Figure 22. Alignment in Jalview. QnrS1, QnrS2, QnrB19 and QnrB1 aligned using muscle with default in Jalview. Marked with black square is loop B (12 aa).

The structures modeled in SWISS-MODEL and Phyre[2] based on the QnrB1 structure showed almost three identical models (Figure 23). All three structures folds into a right-handed quadrilateral β-helix with two loops that dimerize through the C-terminal α-helix. The only difference was that one of the N-terminal β-strands in QnrS2 was predicted to be longer than in the structures of QnrS1 and QnrB19.

Some parts of QnrS1 and QnrS2, especially the loops and both termini, were modeled with high uncertainty. While these programs are very good at determining the overall structure of a model, manual modelling of loop and side chain should be performed. This should be followed by refinements were the energy of the model is minimalized, and unfavorable conformations are removed to get a more reliable structure (personal communication: Dr Jon K. Lærdahl). With a better understanding of the interaction between GyrA and Qnr, this type of modelling could be useful to analyze differences between the amino acids involved in the GyrA-Qnr interaction. This is an important advancement required for future sequence based diagnostics, and surveillance of resistant bacteria.

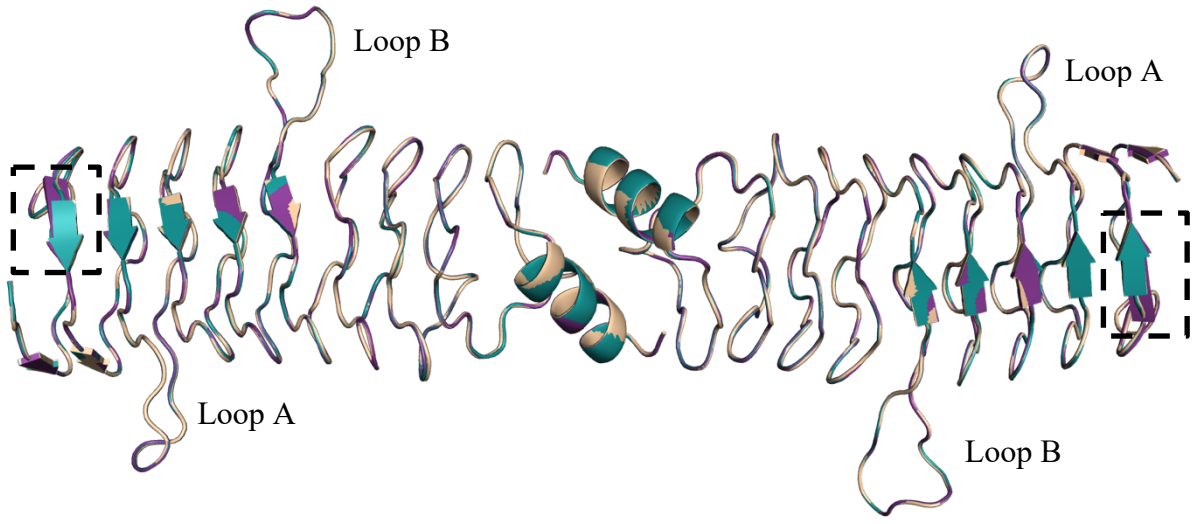

Figure 23. Modeled structures of QnrS1, QnrS2 and QnrB19. The three Qnr proteins were modeled using the coordinates of QnrB1 in SWISS-MODEL. QnrS1 is shown in green, QnrS2 in purple and QnrB19 in yellow. Both loops are marked in the figure. The black dotted squares show the beta strand that is different between QnrS2 compared to QnrS2 and QnrB19. The model was made in Pymol.

Protein interaction studies

The interaction between the two GyrA variants (S83L and WT) and the three different Qnr variants (QnrS1, QnrS2 and QnrB19) was studied to see if the S83L mutation in GyrA could affect the interaction to certain Qnr proteins. We chose to limit our study to the interaction between Qnr and the GyrA subunits since previous studies has demonstrated Qnr-GyrA interaction in the absence of GyrB subunits (Kim et al., 2015; Mazurek et al., 2021; Tran et al., 2005a).

3.4.1 Microscale thermophoresis

To be able to track GyrA S83L and GyrA WT during the experiments, the proteins were labeled with a fluorescent dye (NT647). The labeling efficiently was 1 μM dye per 6 μM protein. The different Qnr proteins were titrated against one of the fluorescently labelled GyrA variants. As start concentration for the Qnr protein (ligand), a concentration of 20x K_d is recommended. K_ds of the relevant interactions are unknown, therefore the highest possible concentration achievable for each Qnr variant was chosen as start concentration; QnrS1: 7.5 μM, QnrS2: 10 μM, QnrB19: 31 μM. The experiments were performed with different MST power (IR laser) and light power (UV-light), where 20 % MST power and 50 % UV light gave the best results.

Interaction between GyrA and QnrS1

Figure 24 shows the average binding curves from two experiments with GyrA S83L-QnrS1 (green) and with GyrA-WT-QnrS1 (red). Due to an unlikely high change in relative fluorescent, causing uncertainty to the model, one outlier (one sample with 974 nM QnrS1 in GyrA-WT-QnrS1) was removed before proceeding with calculations. The K_d obtained from the experiments were 15.06 ± 2.47 μM GyrA WT-QnrS1 and 10.97 ± 1.76 μM for GyrA S83L-QnrS1 interaction. However, it was not possible to determine if the S83L mutation in GyrA will affect the binding of QnrS1 because of the variability of the K_d values. In addition, the binding between QnrS1 and GyrA was not saturated, and the curves were manually fitted to the data points. This causes high uncertainty regarding the K_d values and the values are probably higher than displayed in the calculation. These data cannot be used to determine the affinity for any of the GyrA-QnrS1 interaction.

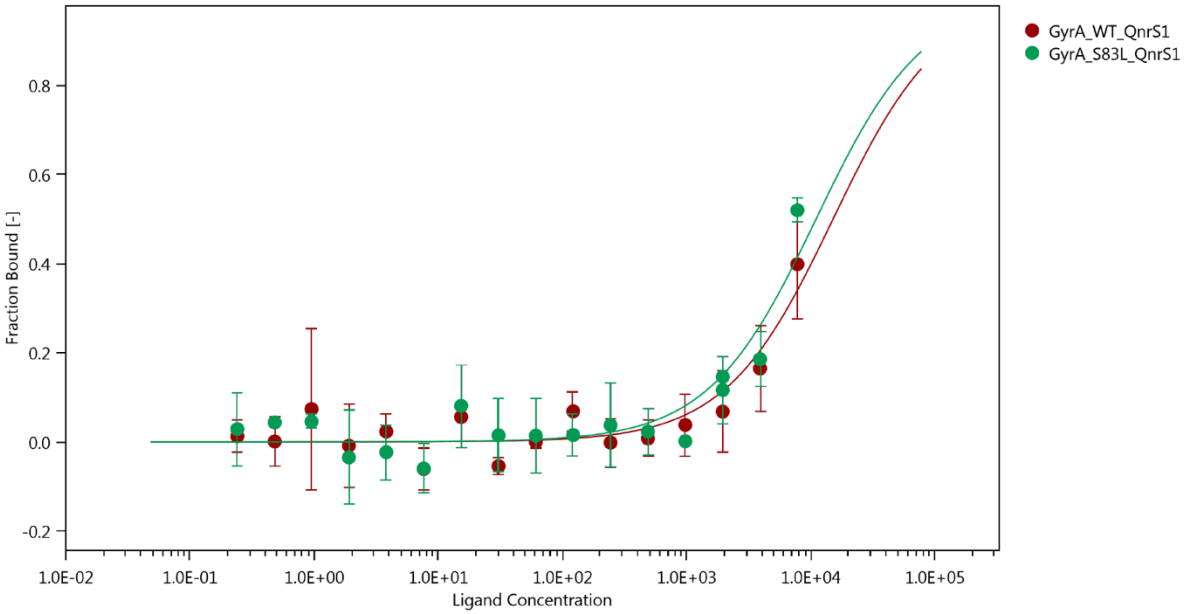

Figure 24. Binding curve of GyrA-QnrS1 interaction. Binding curves shows changes in the fraction of bound molecule at different ligand concentration. Data was obtained using 20 % MST power, 50 % light power at 25 °C. Data points are averages of two experiments, while the error bars show original placement of data points. The highest concentration of QnrS1 was 7.5 µM. Curves were made using MO.Affinty analysis software.

Interaction between GyrA and QnrS2

Based on the binding curves of GyrA S83L and QnrS2 (green), and GyrA WT and QnrS2 (red) in Figure 25, and the K_d obtained from these curves, it is not possible to determine if QnrS2 has a higher affinity for GyrA S83L or GyrA WT. The K_d obtained for GyrA WT-QnrS2 was 14.70 ± 13.46 µM and for GyrA S83L-QnrS2 it was 12.84 ± 1.96 µM. One outlier was removed (one sample with 621 nM QnrS2 in GyrA WT-QnrS2) for better fitting of the curve. The concentration of QnrS2 was too low to obtain any saturation of the interaction. For GyrA WT-QnrS2 interaction, the software was able to fit a binding curve, but for GyrA S83L-QnrS2, the binding curves was manually fitted. The variability of the K_d for the manually fitted GyrA S83L-QnrS2 is much lower compared to GyrA WT-QnrS2. This reflects the problem mentioned earlier where the variability of K_d for manually fitted data decreases, even though it possibly brings even more uncertainty to the data. The data obtained for these interactions are of too high uncertainty to determine any differences in interaction.

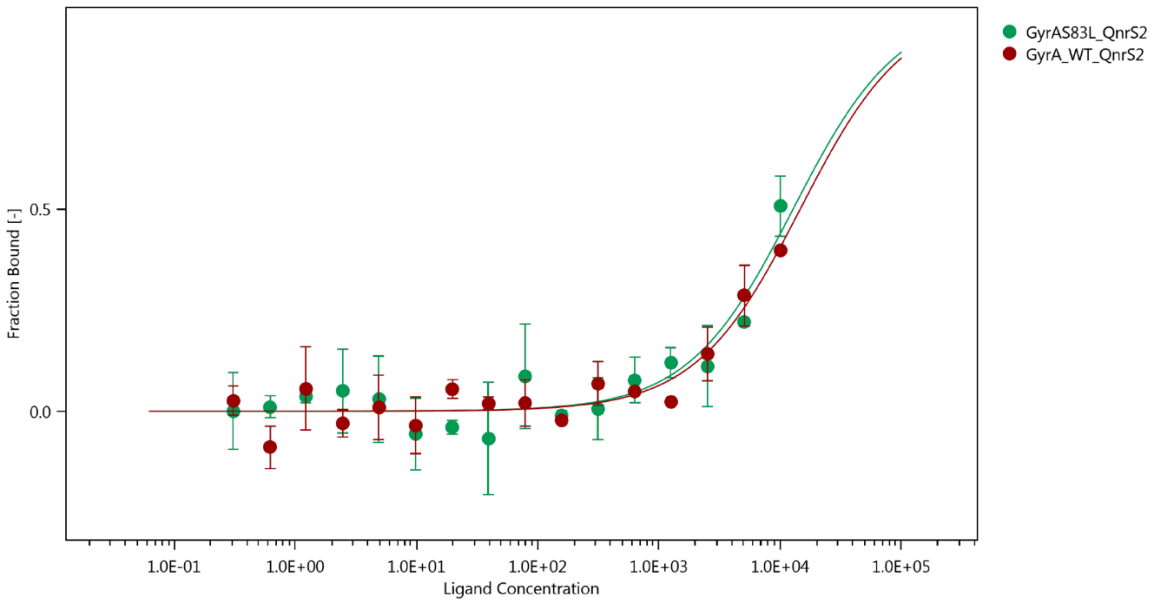

Figure 25. Binding curve of GyrA-QnrS2 interaction. Binding curves show changes in the fraction of bound molecule at different ligand concentration. Data was obtained using 20 % MST power, 50 % light power at 25 °C. Data points are averages of two experiments, while the error bars show original placement of data points. The highest concentration of QnrS2 was 10 µM. Curves were made using MO.Affinty analysis software.

Interaction between GyrA and QnrB19

The most reliable MST results obtained were for GyrA S83L-QnrB19 (green) and GyrA WT-QnrB19 (red) (Figure 26). One outlier (one sample with 1952 nM QnrB19 in GyrA WT-QnrB19) was removed. The K_d values were calculated to be 5.15 ± 1.56 µM for GyrA WT-QnrB19 and 14.66 ± 6.59 µM for GyrA S83L-QnrB19. Based on these data, QnrB19 have higher affinity for GyrA WT, meaning that the S83L mutation has a negative effect on the interaction with QnrB19. However, these results need to be confirmed with more reliable results, because the uncertainty of the K_d values is still high due to the lack of saturation of the binding.

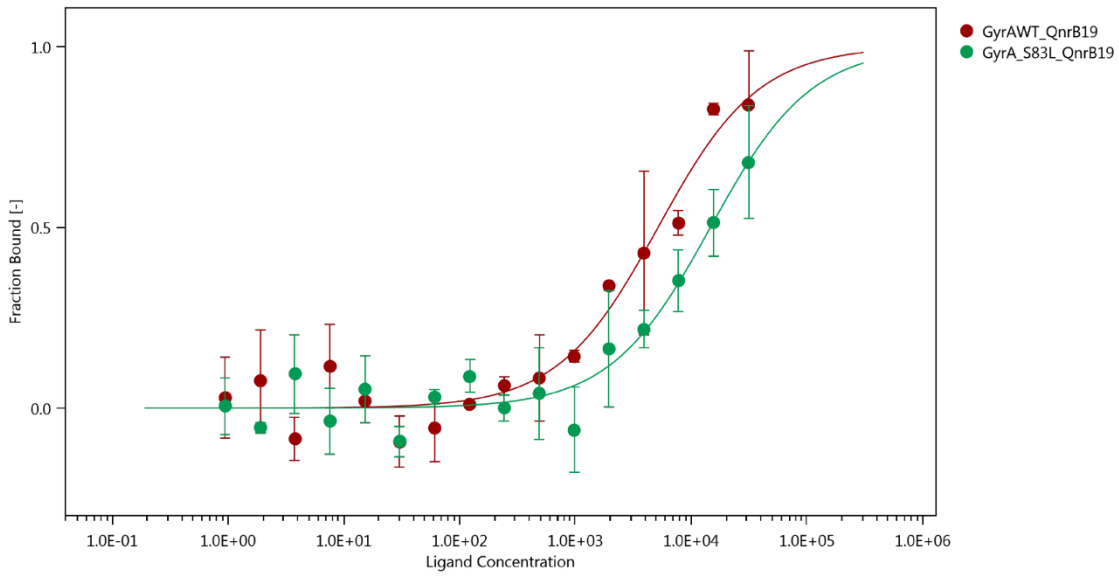

Figure 26. Binding curve of GyrA-QnrB19 interaction. Binding curves shows changes in the fraction of bound molecule at different ligand concentration. Data was obtained using 20 % MST power, 50 % light power at 25 °C. Data points are averages of two experiments, while the error bars show original placement of data points. The highest concentration of QnrB19 was 31 µM. Curves were made using MO.Affinty analysis software.

Based on the increase in fraction of bound molecule with increasing ligand concentration observed for all the MST experiments, both GyrA variants alone were able to interact with the Qnr proteins of interest. However, MST is not optimal for studying interactions of medium affinity. A big limitation in this method is the high concentration of ligand required for optimal results (20x K_d). To get one extra data point in the binding curve the concentration of the ligand must be doubled. Looking at the binding curves, especially for QnrS1 and QnrS2, several data points are needed to reach saturation. Considering the difficulties with protein precipitation during sample concentration, it was not attempted to increase the concentration of the proteins further.

Conditions like buffer, temperature and incubation time before measurements could also affect the interaction. The fluorophore used in the labeling could also interfere with binding, depending on the positioning of the lysines. Ideally, docking studies should be done to look for possible interference, but there is not enough information about the interaction between GyrA and Qnr. However, the main problem here was thought to be the low concentration of the Qnr proteins. The method was therefore changed to SPR which is more sensitive and requires a lower concentration of both proteins. Since the proteins are present in multimers or protein aggregates (Figures 30-34), it is possible that the absolute protein concentration is within limits, but the concentration of available interaction surfaces may be relatively low.

3.4.2 Surface plasmon resonance

The SPR experiments were performed by immobilizing a ligand on a CM5 sensor chip (GE healthcare) and the analyte was passed over it in mobile phase. First GyrA S83L and GyrA WT were immobilized on one chip with QnrS1, QnrS2 and QnrB19 in the mobile phase. The opposite was also tried with QnrS1, QnrS2 and QnrB19 immobilized on a new chip with GyrA S83L and GyrA WT in the mobile phase.

Immobilized GyrA

In channel 2, Gyr A S83L was immobilized to 1750 RU, while GyrA WT was immobilized to 1850 RU in channel 4. This gives a theoretical R_{max} of approximately 440 RU for each Qnr protein. Channel 1 and 3 were empty and used as reference channels. The response in RU observed when the analyte was injected suggests that there was no protein-protein interaction for any of the Qnr variants tested (Appendix C, Figure S8-S13). The minor response observed can come from changes in buffer composition and small differences between the reference channels and binding channels. Even though all the graphs are blank-subtracted with signal from both an empty reference channel and a buffer injection there will still be some differential response due to this. The analyte-buffer could be changed to reduce this potential problem, but this was not done since the signals indicated that there was no protein-protein interaction worth optimizing.

Since there was no protein-protein interaction observed under these conditions it was decided to immobilize the three Qnr proteins on a new chip.

Immobilized Qnr

In channel 2, QnrS1 was immobilized to 208 RU, QnrS2 in channel 3 to 158 RU and QnrB19 in channel 4 to 103 RU. Channel 1 was empty and was used as a reference channel. The running buffer was changed to SPR-buffer, which resembles a buffer commonly used in gyrase activity assays (Maxwell et al., 2006). Both GyrA WT and GyrAS83L were dialyzed against it to avoid an increase in signal due to changes in buffer composition. The graphs from the first experiment with analyte concentrations ranging from 125 nM - 2 μM displayed several artifacts and a very low increase in RU. The analyte concentration was therefore increased to potentially get a significant increase in RU. The results from these experiments are shown here because these graphs displayed a protein-protein interaction.

Immobilized QnrS1 interacting with GyrA WT and GyrA S83L

The expected theoretical R_{max} for both of the interactions was calculated to be about 830 RU. The observed increase in RU was significantly lower for both QnrS1-GyrA WT and QnrS1-GyrA S83L (Figure 27A and B). The interaction between QnrS1 and GyrA WT seemed to reach saturation at approximately 2 µM, while for QnrS1 and GyrA S83L saturation seemed to be reached at 1 µM. However, there is still no significant increase in RU which would be expected at saturation of the interaction. K_d values were calculated to be 476 nM for QnrS1-GyrA WT and 527 nM for QnrS1-GyrA S83L, but the curves used for calculations (black lines in the sensorgrams) does not fit the observed data. Also, the replicate samples (8 µM) for QnrS1-GyrA S83L, which was meant to ensure reproducibility, do not show similar traces.

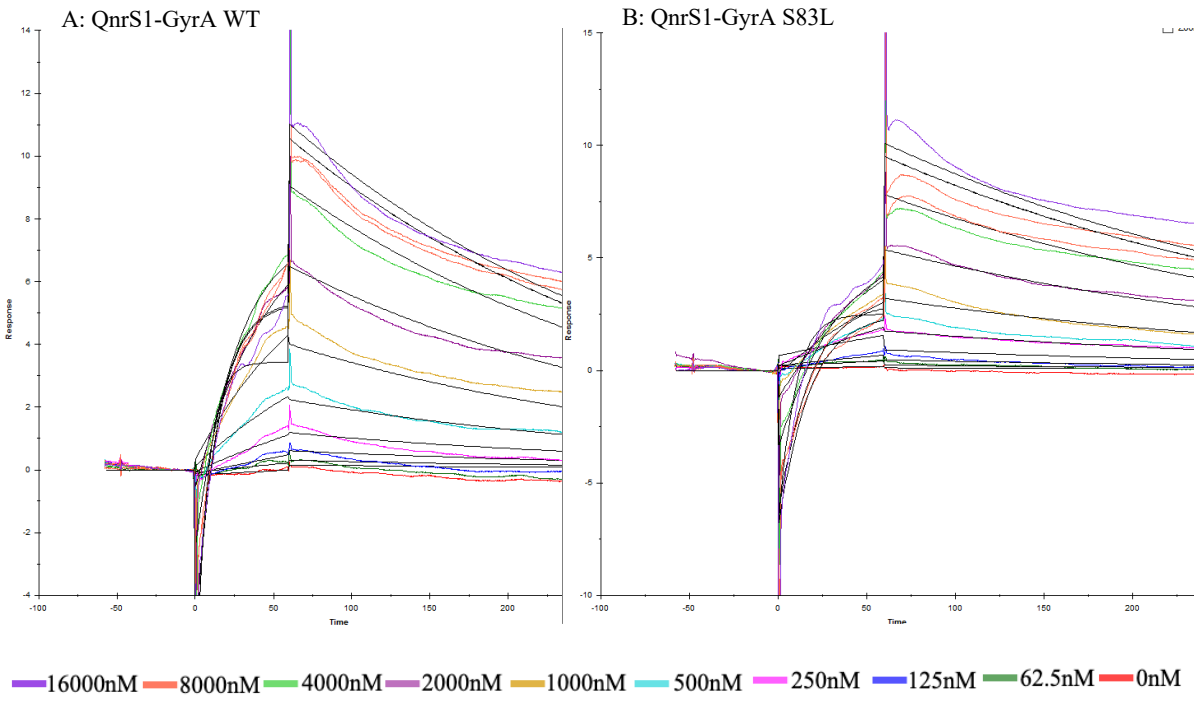

Figure 27. Blank subtracted sensorgrams of QnrS1-GyrA WT and QnrS1-GyrA S83L interactions Black curves were fitted by the software (Biacore S200 Evaluation Software Version 1.1) and were used for calculations of the K_d. **A)** GyrA WT (62.5 nM- 16000 nM) interacting with QnrS1 (208 RU immobilized) in channel 2, flowrate 30 µL/min. **B)** GyrA S83L (62.5 nM- 16000 nM) interacting with QnrS1 (208 RU immobilized) in channel 2, flowrate 30 µL/min.

Immobilized QnrS2 interacting with GyrA WT and GyrA S83L

The increase in RU reached for QnrS2-GyrA WT and QnrS2-GyrA S83L was very low compared to the expected theoretical R_{max} at 630 RU (Figure 28 A and B). The curve for analyte sample with 16 µM for QnrS2-GyrA WT and one of the replicate samples at 8 µM, for both QnrS2-GyrA WT and GyrA S83L, were removed to enable fitting of the data. For QnrS2-GyrA WT, the K_d was calculated to be 746 nM, while for QnrS2-GyrA S83L it was calculated to be 566 nM. However, the curves used for the calculation do not fit the actual data. The replicates at 8 µM for both experiments did not show similar traces, so the data were not reproducible.

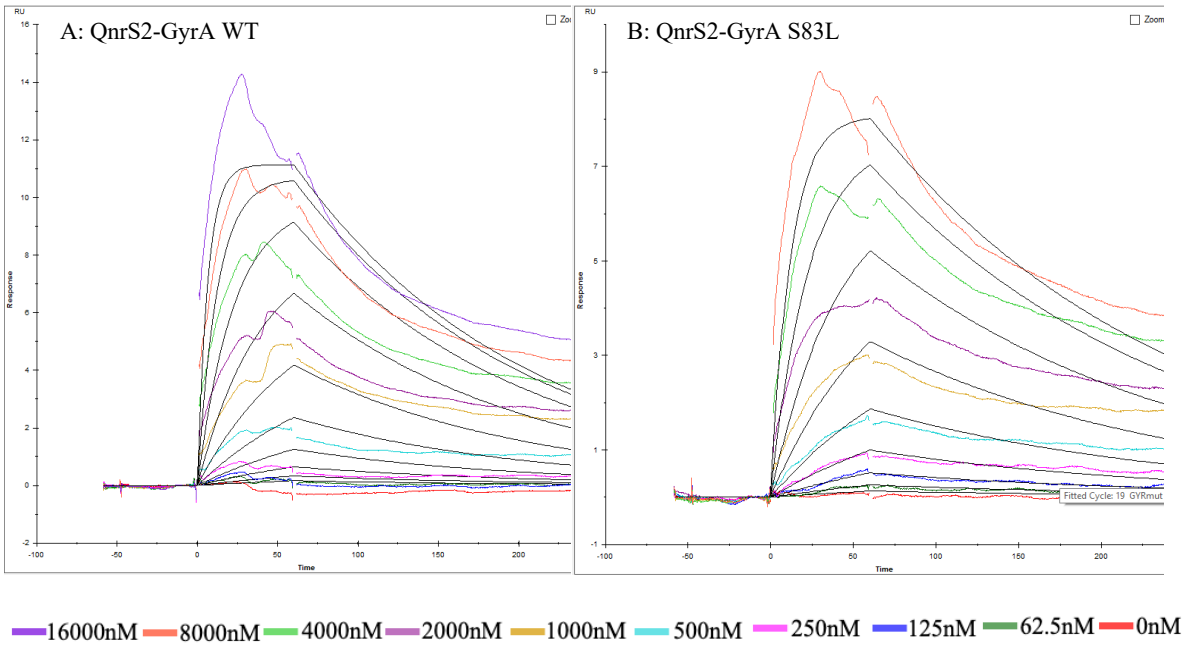

Figure 28. Blank subtracted sensorgrams of QnrS2-GyrA WT and QnrS2-GyrA S83L interactions Black curves were fitted by the software (Biacore S200 Evaluation Software Version 1.1) and were used for calculations of the K_d. **A)** GyrA WT (62.5 nM- 16000 nM) interacting with QnrS2 (158 RU immobilized) in channel 2, flowrate 30 µL/min. **B)** GyrA S83L (62.5 nM- 16000 nM) interacting with QnrS2 (158 RU immobilized) in channel 2, flowrate 30 µL/min.

Immobilized QnrB19 interacting with GyrA WT and GyrA S83L

The increase in RU observed was also very low compared to the theoretically expected R_{max} at 415 RU, for both QnrB19-GyrA WT and QnrB19-GyrA S83L (Figure 29A and B). The K_d obtained from the interaction between QnrB19 and GyrA WT was 513 µM and for QnrB19-GyrA S83L interaction it was 30 µM. Curves representing GyrA concentrations lower than 2 µM were removed to enable calculations. The fitted curves used for the calculations of the K_d do not fit the actual data properly, the signal of analyte binding is very low and there are artifacts

in the curves. The traces of the replicated analyte sample (8 µM) are different for both QnrB19-GyrA WT and QnrB19-GyrA S83L.

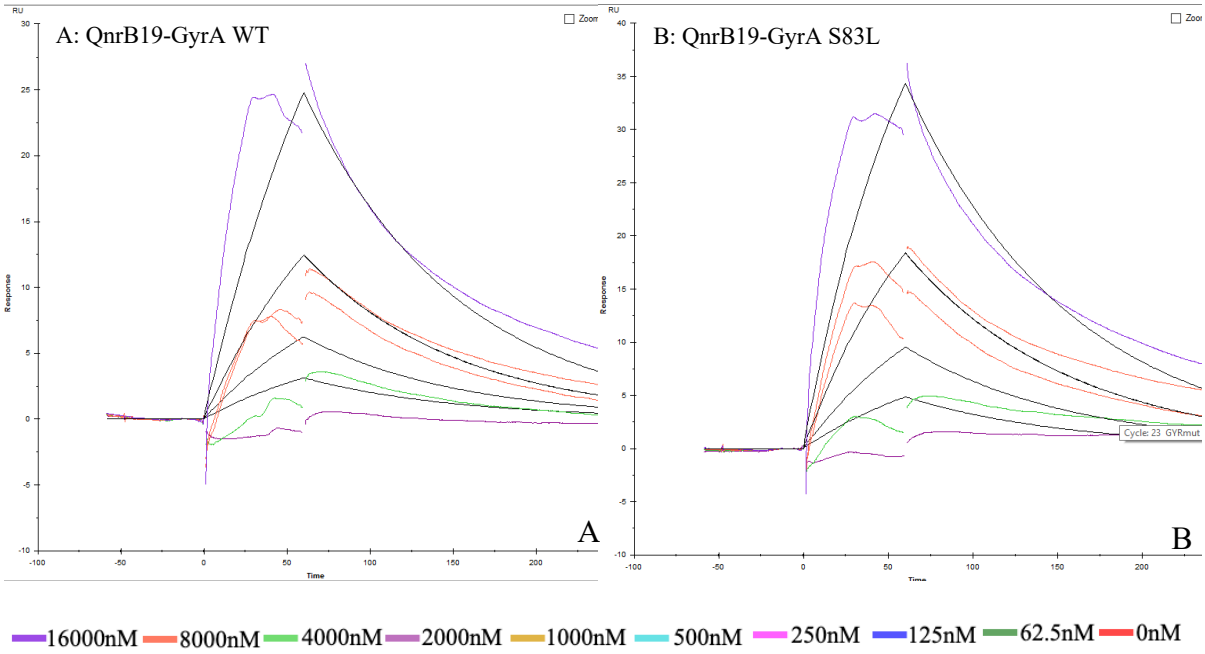

Figure 29. Blank subtracted sensorgrams of QnrB19-GyrA WT and QnrB19-GyrA S83L interactions Black curves were fitted by the software (Biacore S200 Evaluation Software Version 1.1) and were used for calculations of the K_d. **A)** GyrA WT (62.5 nM- 16000 nM) interacting with QnrB19 (103 RU immobilized) in channel 2, flowrate 30 µL/min. **B)** GyrA S83L (62.5 nM- 16000 nM) interacting with QnrB19 (103 RU immobilized) in channel 2, flowrate 30 µL/min.

The data obtained from the SPR experiments are of high uncertainty because of low RU signal, artifacts and poor fitting of the curves used for the calculation of the K_d values. Also, the duplicate injection, which was used to check that the data was reproducible, showed different traces in most of the experiments. Even though it is not expected for the signal of analyte-binding to reach theoretically calculated R_{max}, the increase in signal seen for all the above SPR experiments is very low compared to what is expected for these protein-protein interactions. The protein-protein interaction must therefore be between two molecules where one or both are in low concentration. SEC analyses revealed that GyrA WT, GyrA S83L, QnrS1 and QnrS2 are mostly in multimers or protein aggregates and not in the expected dimer-form (Figure 30-34). QnrB19 was mostly in the dimer-form, but a high concentration was also in multimers. This could explain the low responses observed, since the concentration of protein with available interaction surfaces in the mobile phase and/or immobilized on the sensor chip is low. However, even if some of the analyte is in the functional form, several factors could reduce the ability of the immobilized ligand to interact with the analyte. The ligand could have been inactivated when the ligand was immobilized. The acetate buffer at pH 4.0 used for the immobilization, the

1M ethanolamine-HCl solution at pH 8.5 used to inactivate the reactive succinimide esters and the 1M NaCl used for regeneration, could all affect the functionality of the immobilized ligand. Also, the ligand could be immobilized in a way that makes it inaccessible for the analyte, which could result in small responses (Personal communication: Rune Johansen Forstrøm). The buffer and temperature used during the experiments could also affect the interaction.

On the Coomassie stained SDS-PAGE gel, a low concentration of two contaminants was seen for QnrS1 and QnrS2. The SEC also showed a peak at low molecular weight for all five proteins which was not visible on an agarose gel or Coomassie stained SDS-PAGE-gel. The possibility of that the protein-protein interactions observed is between a contamination and GyrA or Qnr is not very likely because GyrA and Qnr are known to interact, but it cannot be ruled out as a possibility.

There could be many reasons for the results obtained in the SPR experiments, alone or combined. However, before optimizing the parameter for the interaction experiments, all proteins need to be in the right form. Multimerization and aggregation could have occurred in several of the steps back to the expression of the protein and in each step from that. For the optimization, several parameters can be changed in expression, lysis, purification and storage. One simple thing that should be tested is the use of different salt concentrations in the buffers, especially in the storage buffer to prevent non-specific ionic interactions between the proteins. Proteins could also be stored with a higher glycerol concentration, up to 50 %, and dialyzed against proper buffer right before the interaction studies.

3.5 Size Exclusion Chromatography

SEC is a purification method where molecules are separated and purified based on size. SEC can also be used as an analytic method to determine the size of the proteins and protein complexes in solution, which it was used for after the protein interaction studies (section 3.4). The method was used for this purpose because of the suspicion of extensive multimerization or aggregation of the proteins used in the SPR experiment.

Aliquots of the protein samples used in the SPR experiments were loaded on the SEC column. As running buffer, the buffer used for the SPR experiments, 1x PBS-P+ or SPR-buffer, was used. Both GyrA S83L and GyrA WT were found in multimers, and the expected dimer-form was almost non-existent (Figure 30 and 31). It is possible that the highest peak at 14 mL is the

dimer-form, but according to a reference curve based on standard proteins of known sizes, both peaks for GyrA S83L and GyrA WT represents multimers of the proteins. For QnrS1 and QnrS2 most of the protein was in protein aggregates and only a low amount of the expected dimer-form was detected (Figure 32 and 32). For QnrB19 most of the protein is in the expected dimer-form, but some multimerization of the protein is visible (Figure 34).

In all the chromatograms there are a third peak, which is under 12.4 kDa according to the reference curve. The concentration of the fractions from these peaks was too low to measure on a spectrophotometer, and no band was visible on a Coomassie stained SDS-PAGE gel or an agarose gel (Figure 30-34).

It must be mentioned that the samples were stored at -20°C for 2 months after MST and 1 month after SPR, before SEC was performed. Multimerization and aggregation could have occurred during the storage and handling of the proteins.

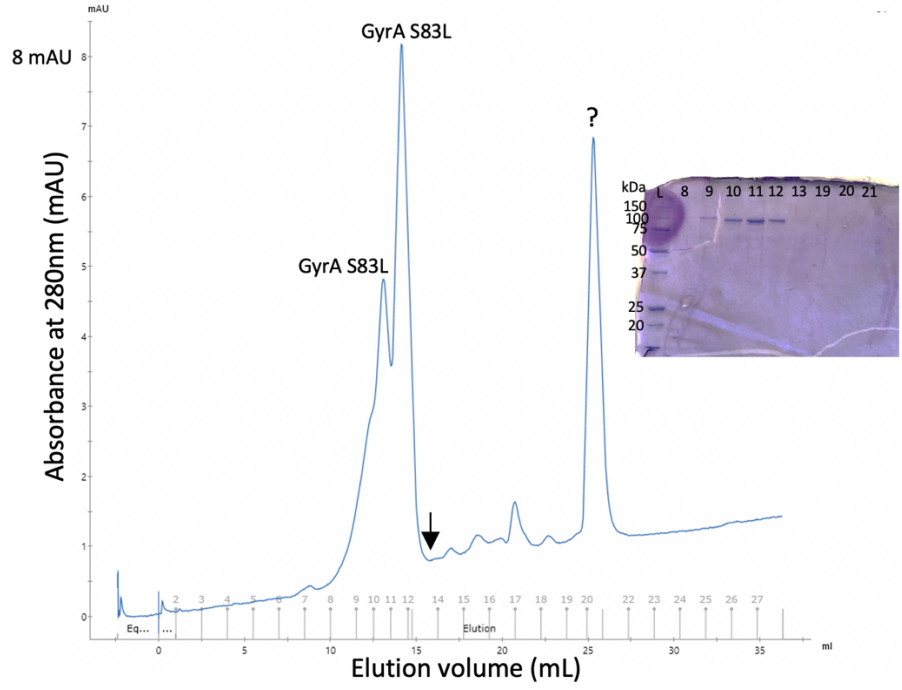

Figure 30. Analysis of GyrA S83L using SEC and SDS-PAGE followed by Coomassie staining. Chromatogram of GyrA S83L in SEC analysis with SPR-buffer as running buffer. Fractions corresponding to the peaks were separated on a 12 % SDS-gel. Arrow indicates expected elution of dimer-form of the protein. Protein was measured at absorbance 280 nm denoted in milli-absorbance units (mAU). **L** represents 4 µL Precision Plus Protein™ All Blue Prestained Protein Standard.

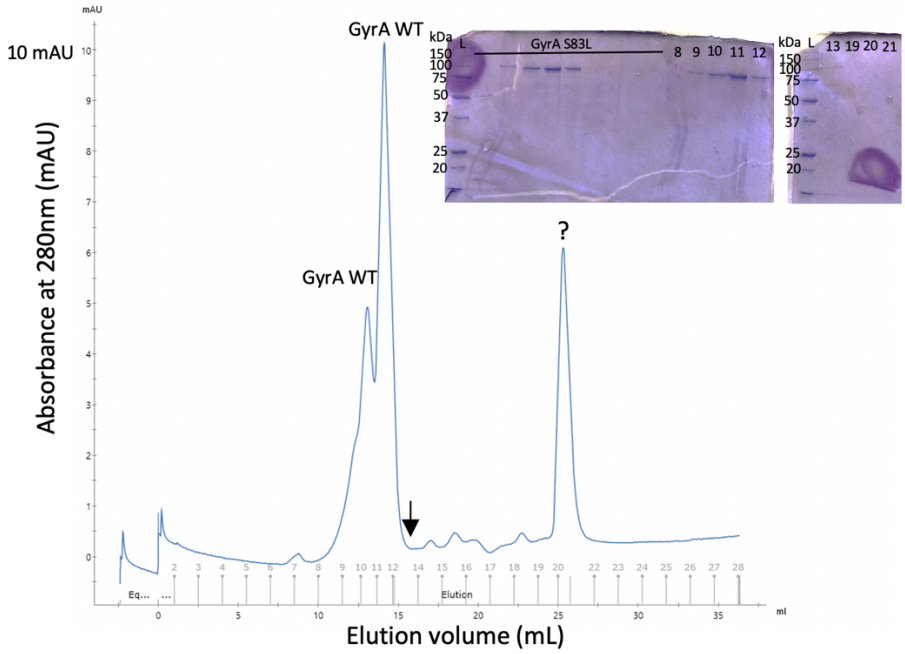

Figure 31. Analysis of GyrA WT using SEC and SDS-PAGE followed by Coomassie staining. Chromatogram of GyrA WT in SEC analysis with SPR-buffer as running buffer. Fractions corresponding to the peaks were separated on a 12 % SDS-gel. Arrow indicates expected elution of dimer-form of the protein. Protein was measured at absorbance 280 nm denoted in mAU. **L** represents 4 µL Precision Plus Protein™ All Blue Prestained Protein Standard.

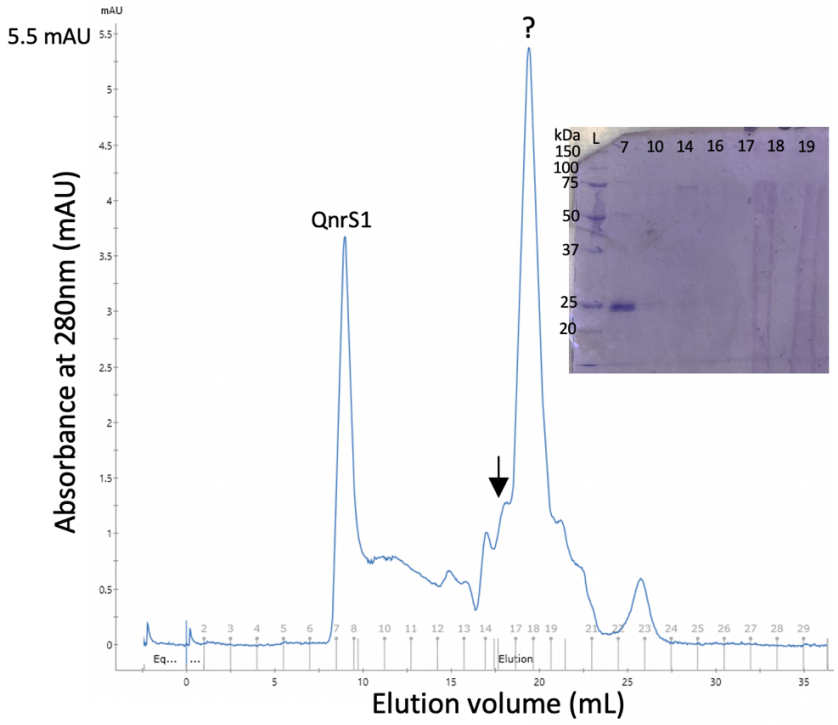

Figure 32. Analysis of QnrS1 using SEC and SDS-PAGE followed by Coomassie staining. Chromatogram of QnrS1 in SEC analysis with 1x PBS-P+ as running buffer. Fractions corresponding to the peaks were separated on a 12 % SDS-gel. Arrow indicates expected elution of dimer-form of the protein. Protein was measured at absorbance 280 nm denoted in mAU. **L** represents 4 µL Precision Plus Protein™ All Blue Prestained Protein Standard.

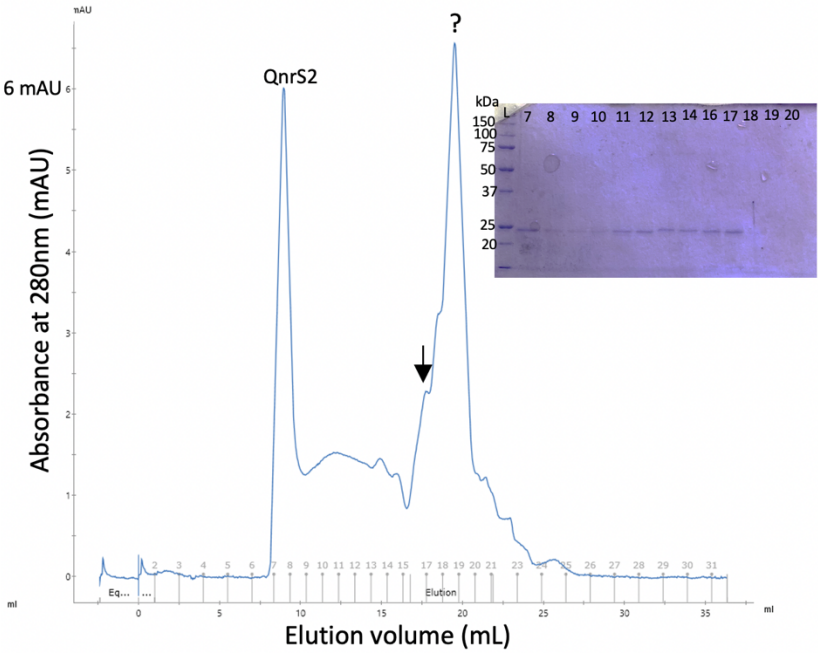

Figure 33. Analysis of QnrS2 using SEC and SDS-PAGE followed by Coomassie staining. Chromatogram of QnrS2 in SEC analysis with 1x PBS-P+ as running buffer. Fractions corresponding to the peaks were separated on a 12 % SDS-gel. Arrow indicates expected elution of dimer-form of the protein. Protein was measured at absorbance 280 nm denoted in mAU. **L** represents 4 µL Precision Plus Protein™ All Blue Prestained Protein Standard.

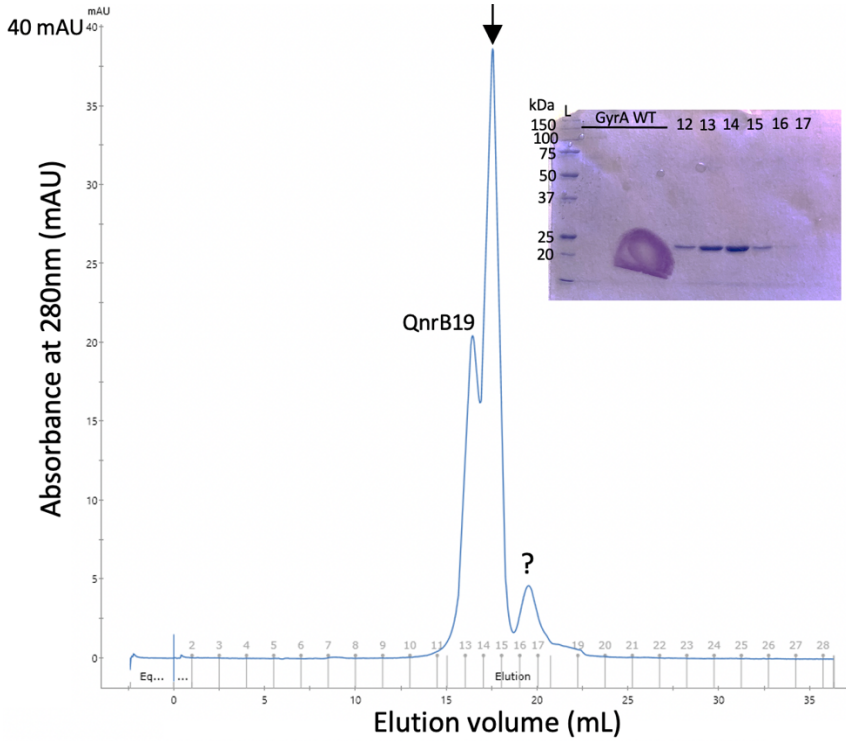

Figure 34. Analysis of QnrB19 using SEC and SDS-PAGE followed by Coomassie staining. Chromatogram of QnrB19 in SEC analysis with 1x PBS-P+ as running buffer. Fractions corresponding to the peaks were separated on a 12 % SDS-gel. Arrow indicates expected elution of dimer-form of the protein. Protein was measured at absorbance 280 nm denoted in mAU. **L** represents 4 µL Precision Plus Protein™ All Blue Prestained Protein Standard.

3.6 Broth microdilution assays

E.coli strains expressing different Qnr variants in the presence of GyrA WT or QRDR mutated GyrA was tested in broth microdilution assays, this was to determine if different Qnr protein can cause different susceptibility against ciprofloxacin and nalidixic acid.

3.6.1 Susceptibility against ciprofloxacin

Both DH5α and GyrA-S83L-5022 have a GyrA mutation and shows a decreased susceptibility to ciprofloxacin compared to BL21 and GyrA-WT-1085 harboring GyrA WT (Table 3). Strains carrying the S83L mutation (GyrA-S83L-5022) yielded a 4-fold increase in MIC compared to the strains with D87N mutation (DH5α, mutation confirmed with sequencing). Here only strains with S83L mutation have susceptibility above the ECOFF for ciprofloxacin (0.06 μg/mL). The S83L and D87N mutations are the most common chromosomal mutations in GyrA causing quinolone resistance, and have been shown to cause higher levels of resistance than other types of GyrA mutations (Hopkins et al., 2005; Yoshida et al., 1991). Both residues play an important role in the binding of quinolones through the water metal-ion bridge, and mutations in these two locations are therefore critical for quinolone activity. The higher MIC observed in this study for the strain with the S83L mutation agrees with earlier studies (Bagel et al., 1999; Johnning et al., 2015; Marcusson et al., 2009; Ozeki et al., 1997). This can indicate that the S83 residue is more important for quinolone binding than the D87 residue (Aldred, Schwanz, et al., 2013; Bax et al., 2010; Blower et al., 2016).

When Qnr proteins are expressed the susceptibility decreases for both mutant strains, leading to resistance in the DH5α strain as well (0.25 μg/mL) (Table 3). The GyrA-S83L-5022 strains expressing Qnr displays a MIC seen for clinical resistant strains against ciprofloxacin with a MIC over 0.5 μg/mL. This additive effect on resistance by expressing several resistance mechanisms is confirmed by earlier studies (Chen et al., 2012; Machuca et al., 2014). In DH5α, the expression in QnrS1 seems to give a fitness cost, since there is a decrease in MIC compared to DH5α without any Qnr expression. This should be confirmed in a future growth assay. When Qnr was expressed in the WT strains, BL21 and GyrA-WT-1085, a 32-fold and 64-fold decrease in susceptibility was observed respectively. However, only the GyrA-WT-1085 strains displays a MIC consistent with resistant strains (MIC over 0.06 μg/mL). BL21 has a MIC that is

consistent with a WT strain, even though it is expressing Qnr proteins. The big difference in MIC between the WT strains expressing Qnr has also been shown earlier, and does not seem to be uncommon (Briales et al., 2011; Garoff et al., 2018; Machuca et al., 2014, 2017; Tavío et al., 2014). Even though the strains expressing GyrA WT and Qnr do not cause clinical resistance (MIC over 0.5 μg/mL), they can still pose a threat in the clinic. This is because the plasmid encoded Qnr proteins can be acquired through HGT. If the plasmid is acquired by a strain expressing GyrA S83L, the strain can become clinical resistant, as observed for the strains expressing Qnr and GyrA S83L in this study.

Table 3. Ciprofloxacin MICs in different *E.coli* strains.

Strain	**Ciprofloxacin MICs (μg/mL)[1]**			
	Arabinose concentration			
	0%	**0.001%**	**0.01%**	**0.1%**
DH5α (pBAD30)	0.06	0.06	0.06	0.06
DH5α (pBAD30-QnrS1)	0.03	0.03	0.125	0.25
DH5α (pBAD30-QnrS2)	0.06	0.125	0.125	0.25
DH5α (pBAD30-QnrB19)	0.06	0.125	0.125	0.25
BL21 (pBAD30)	0.001	0.001	0.001	0.001
BL21 (pBAD30-QnrS1)	0.002	0.004	0.03	0.06
BL21 (pBAD30-QnrS2)	0.004	0.015	0.03	0.03
BL21 (pBAD30-QnrB19)	0.004	0.004-0.008	0.015	0.03
GyrA-S83L-5022 (pBAD30)	0.25	0.25	0.25	0.25
GyrA-S83L-5022 (pBAD30-QnrS1)	0.25	0.5	1	2
GyrA-S83L-5022 (pBAD30-QnrS2)	0.5	0.5	0.5	1
GyrA-S83L-5022 (pBAD30-QnrB19)	0.25	0.5	0.5	1
GyrA-WT-1085 (pBAD30)	0.008	0.008	0.008	0.008
GyrA-WT-1085 (pBAD30-QnrS1)	0.015	0.015	0.125	0.5
GyrA-WT-1085 (pBAD30-QnrS2)	0.015	0.015	0.125	0.25
GyrA-WT-1085 (pBAD30-QnrB19)	0.015	0.06	0.125	0.25

1)The MIC values were obtained from three broth microdilution assays. MICs shown are in μg/mL.

The increase in arabinose concentration induces Qnr expression, this likely explains the step-wise increase in MIC of ciprofloxacin. This increase in MIC caused by higher expression of Qnr has been reported earlier (Garoff et al., 2018; Tavío et al., 2014). In general, there seems to be a trend that at high expression levels, QnrS1 causes higher resistance to ciprofloxacin than

QnrS2 and QnrB19, with and without chromosomal mutations. The trend of QnrS1 causing higher resistance compared to other Qnr variants have been shown before, even though it has not previously been compared to QnrS2 and QnrB19 (Briales et al., 2011; Machuca et al., 2014; Strahilevitz et al., 2009). There can be several reasons for why some Qnr proteins are displaying a higher MIC compared to other variants. This can be the copy number of the plasmid, promoter strength, transcription levels and additional resistance mechanisms encoded on the plasmid (Martínez-Martínez et al., 2008). In our study, all three *qnr* genes were cloned into the same vector, which rules out differences in promoter strength and copy number. The constructs were transformed into the same strains so other quinolone resistance mechanisms should not affect the results for different Qnr variants within a strain, apart from possible mutations gained during the experiments. Transcription levels were controlled with the same concentration of arabinose in all strains. Therefore, the higher MIC may indicate that QnrS1 has a higher affinity against the GyrA WT and GyrA S83L than the other Qnr variants. The protein is therefore able to cause a higher level of resistance by interacting with more cleavage complexes. Other explanations could be that QnrS2 and QnrB19 are more toxic for the cells, reducing growth, but for GyrA-WT-1085 and GyrA-S83L-5022 strains this is not the case as observed in the growth assay (discussed later). Another explanation is a lower concentration of functional protein for QnrS2 and QnrB19 due to aggregation or degradation of these proteins.

3.6.2 Susceptibility against nalidixic acid

The strains with a chromosomal mutation in GyrA, DH5α and GyrA-S83L-5022, are both resistant against nalidixic acid according to the ECOFF of 16 μg/mL (Table 4). Here the strain with an S83L mutation has a 4x decreased susceptibility against nalidixic acid compared to the strain with an D87N mutation in GyrA, similar to what was observed for ciprofloxacin. This emphasizes the importance of residues S83 and D87, especially S83, in docking of quinolones. These two amino acids are especially important in the binding of nalidixic acid. While ciprofloxacin has fluorine at position C6 and a ring structure at C7 which also can interact with Gyrase, nalidixic acid is dependent on S83 and D87 residues for binding (Aldred, Schwanz, et al., 2013; Bax et al., 2010; Blower et al., 2016).

The additive effect of a chromosomal mutation in GyrA and the presence of Qnr seen for ciprofloxacin is not observed for nalidixic acid (Table 4), which is confirmed by previous studies (Martínez-Martínez et al., 1998; Strahilevitz et al., 2009). The effect of expressing Qnr

proteins in the WT strains on susceptibility to nalidixic acid is small, with only a 4-8x fold decrease in MIC. Both of the GyrA WT strains display MIC that is below the ECOFF for nalidixic acid (16 μg/mL), even when Qnr proteins are expressed. To understand why Qnr causes only low level of protection against nalidixic acid and why the additive effect is not observed, more information about the Gyrase-Qnr interaction is needed.

Table 4. **Nalidixic acid MICs in different *E.coli* strains.**

Strain	**Nalidixic acid MICs (μg/mL)[1]**			
	Arabinose concentration			
	0%	**0.001%**	**0.01%**	**0.1%**
DH5α (pBAD30)	64	64	64	64
DH5α (pBAD30-QnrS1)	64	64	64	64
DH5α (pBAD30-QnrS2)	64	64	64	64
DH5α (pBAD30-QnrB19)	64	64	64	64
BL21 (pBAD30)	1	1	1	1
BL21 (pBAD30-QnrS1)	1	2-4	8	8
BL21 (pBAD30-QnrS2)	1	2-4	4-8	8
BL21 (pBAD30-QnrB19)	1	2	4	4
GyrA-S83L-5022 (pBAD30)	256	256	256	256
GyrA-S83L-5022 (pBAD30-QnrS1)	256	256	256	256
GyrA-S83L-5022 (pBAD30-QnrS2)	256	256	256	256
GyrA-S83L-5022 (pBAD30-QnrB19)	256	256	256	256
GyrA-WT-1085 (pBAD30)	2	2	2	2
GyrA-WT-1085 (pBAD30-QnrS1)	2	2	8	16
GyrA-WT-1085 (pBAD30-QnrS2)	2	2-4	8	8
GyrA-WT-1085 (pBAD30-QnrB19)	2	4	8	8

1)The MIC values were obtained from three broth microdilution assays. MICs shown are in μg/mL.

What must be taken into consideration is that each of the strains used in the broth microdilution assays might have other resistance mechanisms that could decrease the susceptibility. This can be unknown mechanisms like reduced membrane permeability and/or mutations in the chromosome leading to higher expression of efflux pumps. As observed for the two WT strains, GyrA-WT-1085 displayed a MIC 8x higher than the BL21 cells, even though none of the strains express any known resistance mechanisms. This also applies to DH5α and GyrA-S83L-5022, where the GyrA-S83L-5022 with an S83L mutation in GyrA displays a 4x increase in MIC

compared to DH5α with a D87N mutation. This difference in MIC does not necessarily only depend on the difference in mutation and the role of the residues involved in quinolone binding.

A direct correlation was observed between the concentration of arabinose and the MIC-value of ciprofloxacin for all strains, but only the WT strains displayed a correlation between arabinose concentration and MIC of nalidixic acid. Hence, a western blot was performed on the bacterial suspension in the growth controls (no ciprofloxacin or nalidixic acid) of a broth microdilution assay (Figure 35). The cell lysates of DH5α and BL21 transformed with pBAD30-QnrS1, pBAD30-QnrS2, pBAD30-QnrB19 or pBAD30 were normalized according to OD_{600} in the experiment. In BL21 cells the concentration of QnrS1 and QnrS2 was similar, while the amount of protein was lower for QnrB19. This could indicate that the expression of QnrB19 is lower, or that it is degraded faster in the cells, maybe due to toxicity. The low concentration of QnrB19 was also observed for DH5α. Growth assays are necessary to confirm the hypothesis of QnrB19 toxicity. Even if there was a lower total amount of QnrB19 in both BL21 and DH5α compared to QnrS1 and QnrS2 the amount of soluble protein is not known. As observed from the overexpression experiments, a large proportion of the Qnr proteins can be insoluble, and then likely inactive. QnrB19 was more easily expressed as soluble protein, which can explain why QnrB19 displays a similar MIC as QnrS1 and QnrS2, even though the total amount of protein is lower. The proportion of soluble and functional protein would also explain why DH5α expressing QnrS1 displays a lower MIC of ciprofloxacin than DH5α carrying the vector control (Table 3, 0.001% arabinose). To be able to spot any potential difference in the expression level of Qnr in the BL21 cells, the samples should be diluted since the signal may be saturated and therefore not possible to quantify. The experiment should also be repeated to check for reproducibility of the results. Similar western blots should be done for the GyrA-S83L-5022 and GyrA-WT-1085.

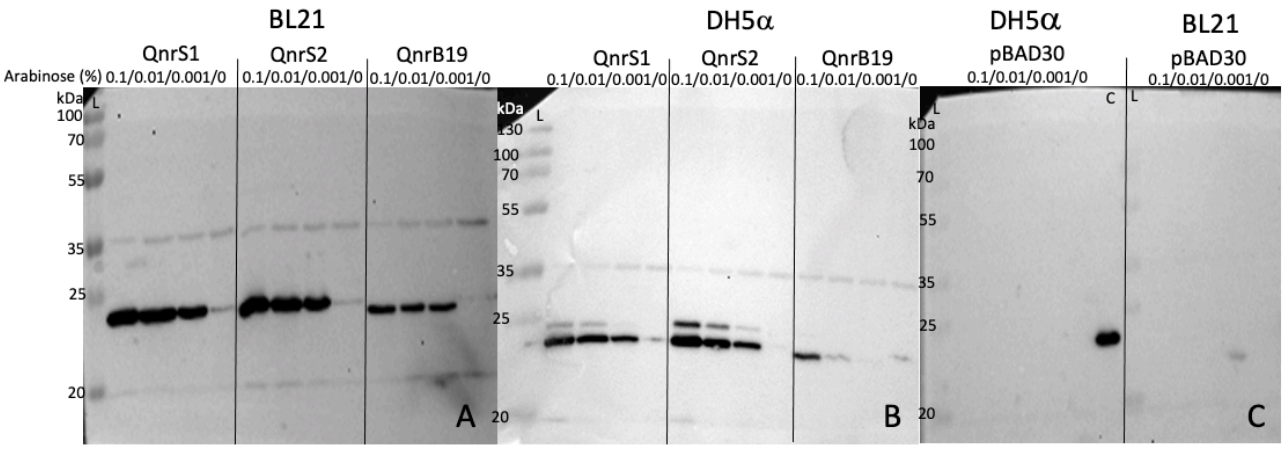

Figure 35. Western blot of growth controls from the broth microdilution assay. Whole cell lysates were run on an SDS-PAGE gel, transferred to a PVDF membrane and incubated with His-tag specific antibody overnight. **A)** BL21 cells transformed with pBAD30-QnrS1, pBAD30-QnrS2 or pBAD30-QnrB19 incubated for 22 h and 30 min at 37 °C in MHB supplemented with different arabinose concentrations **B)** DH5α cells transformed with pBAD30-QnrS1, pBAD30-QnrS2 or pBAD30-QnrB19 incubated for 22 h and 30 min at 37 °C in MHB supplemented with different arabinose concentrations. **C)** DH5α and BL21 transformed with empty vector (pBAD30). **L** refers to 3 μL PageRuler Plus Stained Protein Ladder (Thermo fisher). **C** in Figure 35C refers to purified QnrS2 used as control for binding of antibody to His-tag.

3.7 Growth assays

These experiments were performed to analyze the potential fitness costs associated with the expression of different Qnr-proteins. GyrA-S83L-5022 and GyrA-WT-1085 transformed with pBAD30-QnrS1, pBAD30-QnrS2, pBAD30-QnrB19 or pBAD30 were tested in single-strain growth assays in the presence of ampicillin with increasing concentration of arabinose. The generation time was calculated for each strain, but there was no significant difference between the generation times (Table 5). Ampicillin is the selective marker of the pBAD30 vector and was added to avoid contaminations, the assay was performed without ampicillin to determine if ampicillin would interfere with the bacterial fitness. The growth of the strains in the absence of ampicillin showed to be similar to the growth assay with ampicillin. GyrA-S83L-5022 transformed with pBAD30-QnrS1, pBAD30-QnrS2, pBAD30-QnrB19 or pBAD30 were also tested in the presence of nalidixic acid and ampicillin. It was performed with ampicillin since earlier assays confirmed that ampicillin did not interfere with the fitness. The presence of nalidixic acid did not show to cause any fitness cost in the strains either. However, this assay should be repeated several times to confirm the results.

Table 5 Generation time of *E.coli* strains.

Strain	Generation time (min) ± standard deviation (min)[1]			
	Arabinose concentration			
	0%	0.001%	0.01%.	0.1%
GyrA-S83L-5022 (pBAD30)	29.5 ± 4.5	33.6 ± 3.6	31.4 ± 3.6	30.6 ± 1.8
GyrA-S83L-5022 (pBAD30-QnrS1)	30.2 ± 2.4	35.9 ± 2.5	28.2 ± 3.9	29.7 ± 3.1
GyrA-S83L-5022 (pBAD30-QnrS2)	31.4 ± 3.1	34.4 ± 3.5	30.9 ± 4.7	33.2 ± 2.6
GyrA-S83L-5022 (pBAD30-QnrB19)	31.6 ± 3.5	30.2 ± 3.5	30.8 ± 4.1	30.2 ± 4.6
GyrA-WT-1085 (pBAD30)	34.1 ± 4.6	34.0 ± 2.0	35.4 ±1.3	34.7 ± 3.3
GyrA-WT-1085 (pBAD30-QnrS1)	33.2 ± 3.6	35.3 ± 1.1	29.8 ± 2.0	34.8 ± 2.0
GyrA-WT-1085 (pBAD30-QnrS2)	32.2 ± 5.1	32.8 ± 3.7	30.7 ± 3.5	33.5 ± 4.3
GyrA-WT-1085 (pBAD30-QnrB19)	31.6 ± 3.8	33.2 ± 3.7	31.2 ± 2.8	33.1 ± 2.6

1) Generation time (min) ± standard deviation (min) was calculated using the exponential phase of growth curves in Figures 36-39.

The maximum OD_{600} in the stationary phase was very similar for all the strains in most of the experiments, especially in the absence of arabinose and at 0.001 % arabinose (Figure 36 and 37). There seems to be a tendency towards a small increase in maximum OD_{600} at 0.01 % arabinose for all the strains, but the increase in OD_{600} is seems to be higher for GyrA-S83L-5022 expressing QnrS1 or QnrS2, compared to GyrA-S83L-5022 with vector control (Figure 38). However, the only significant increase in maximum OD_{600} was observed at the highest induction level (0.1 % arabinose) (Figure 39). The increase in OD_{600} observed for GyrA-S83L-5022 expressing QnrS1 or QnrS2 is significantly higher compared to the other strains (Figure 39D and E). There is also a tendency towards a minor increase in maximum OD_{600} for GyrA-WT-1085 expressing QnrS1 and QnrS2, compared to the GyrA-WT-1085 strain expressing QnrB19 and the vector control.

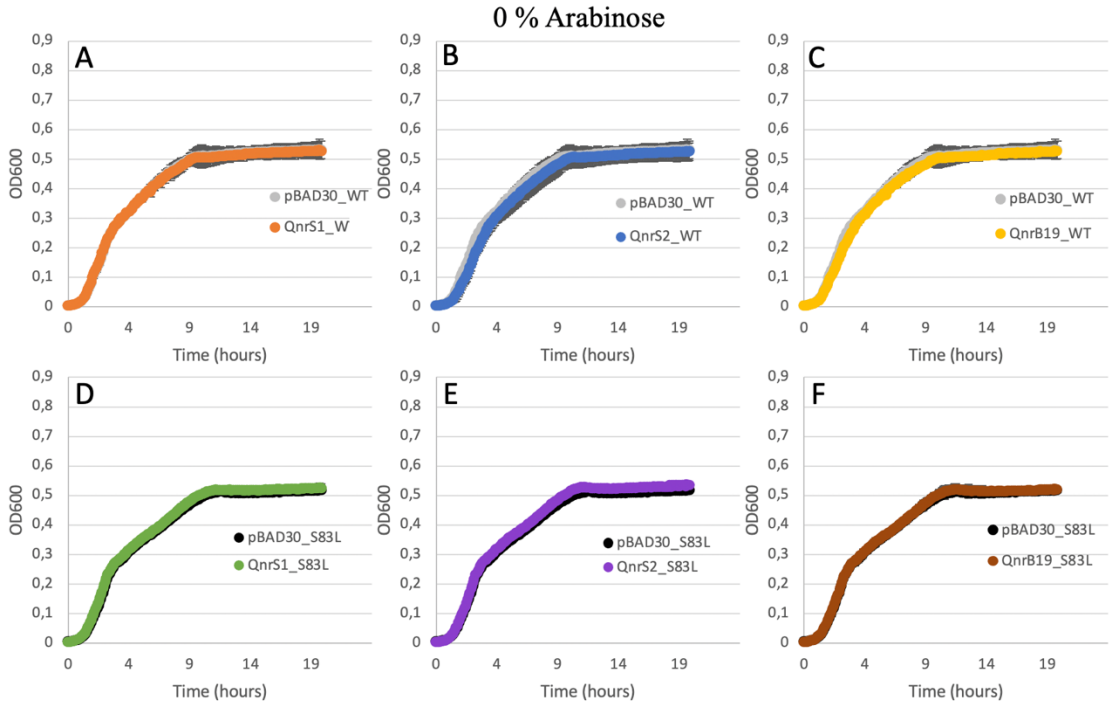

Figure 36. Growth curves of GyrA-WT-1085 transformed with pBAD30-QnrS1, pBAD30-QnrS2, pBAD30-QnrB19 or pBAD30 **(A-C)** and GyrA-S83L-5022 transformed with pBAD30-QnrS1, pBAD30-QnrS2, pBAD30-QnrB19 or pBAD30 **(D-F)** in LB medium supplied with ampicillin and 0 % arabinose. Cultures were incubated in a plate reader for 20 h at 37 °C with OD600 measurements every 5 min. Data is the mean of three experiments. Error bars represents 95 % confidence interval. The figures were made in Microsoft Excel.

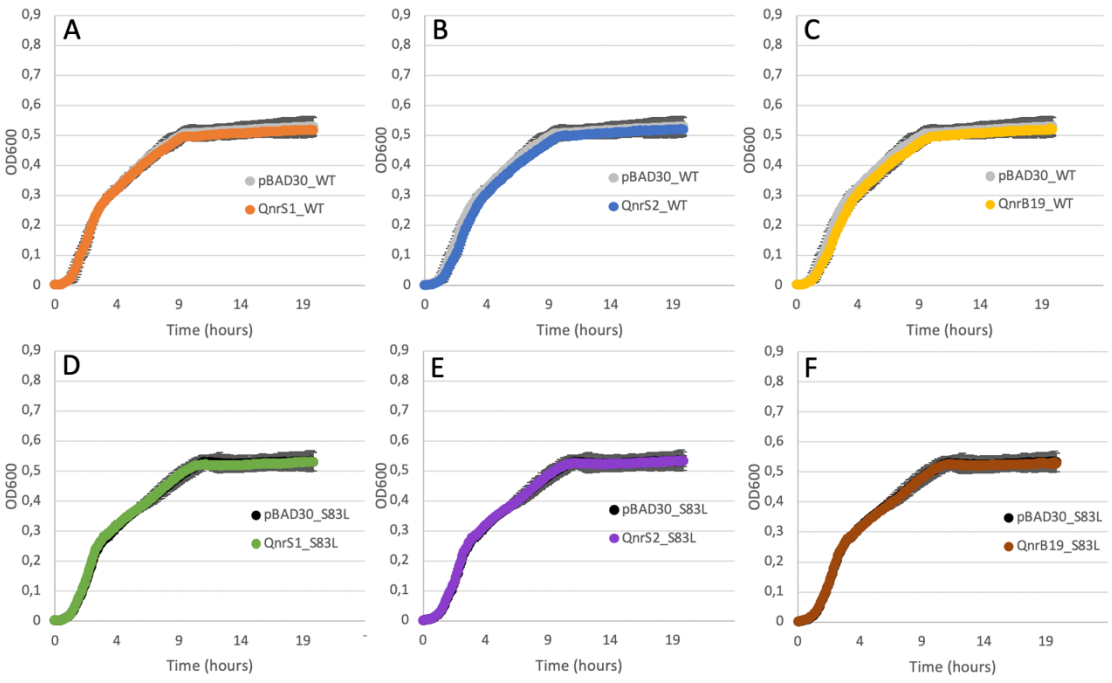

Figure 37. Growth curves of GyrA-WT-1085 transformed with pBAD30-QnrS1, pBAD30-QnrS2, pBAD30-QnrB19 or pBAD30 **(A-C)** and GyrA-S83L-5022 transformed with pBAD30-QnrS1, pBAD30-QnrS2, pBAD30-QnrB19 or pBAD30 **(D-F)** in LB medium supplied with ampicillin and 0.001 % arabinose. Cultures were incubated in a plate reader for 20 h at 37 °C with OD_{600} measurements every 5 min. Data is the mean of three experiments. Error bars represents 95 % confidence interval. The figures were made in Microsoft Excel.

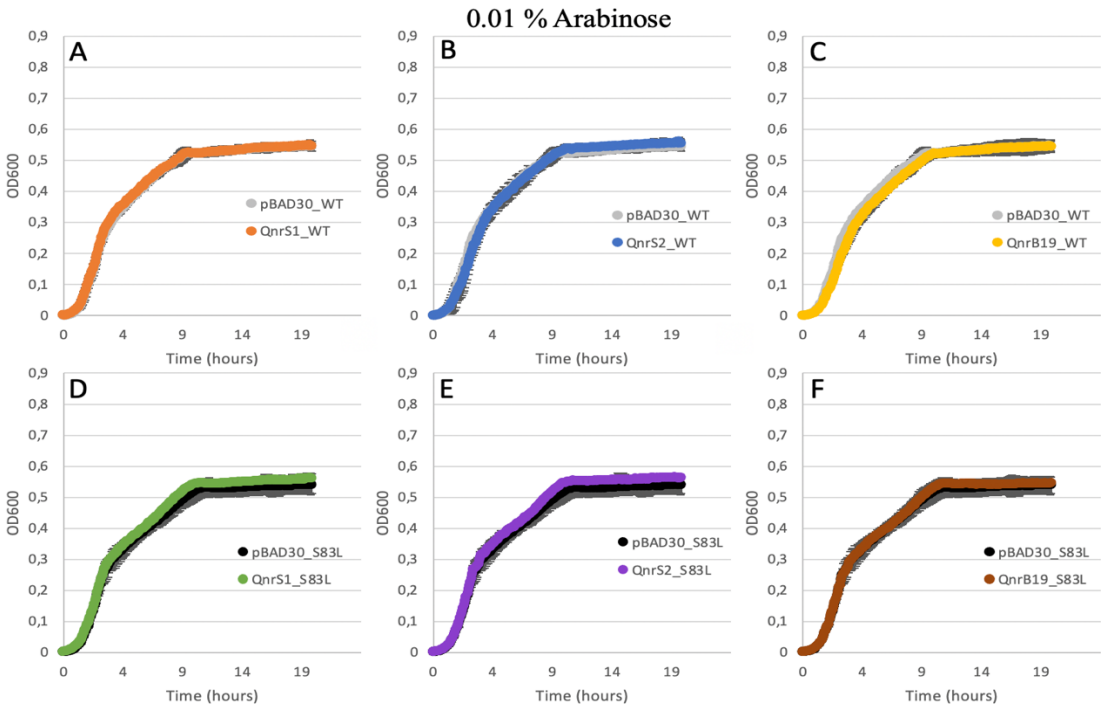

Figure 38. Growth curves of GyrA-WT-1085 transformed with pBAD30-QnrS1, pBAD30-QnrS2, pBAD30-QnrB19 or pBAD30 **(A-C)** and GyrA-S83L-5022 transformed with pBAD30-QnrS1, pBAD30-QnrS2, pBAD30-QnrB19 or pBAD30 **(D-F)** in LB medium supplied with ampicillin and 0.01 % arabinose. Cultures were incubated in a plate reader for 20 h at 37 °C with OD_{600} measurements every 5 min. Data is the mean of three experiments. Error bars represents 95 % confidence interval. The figures were made in Microsoft Excel.

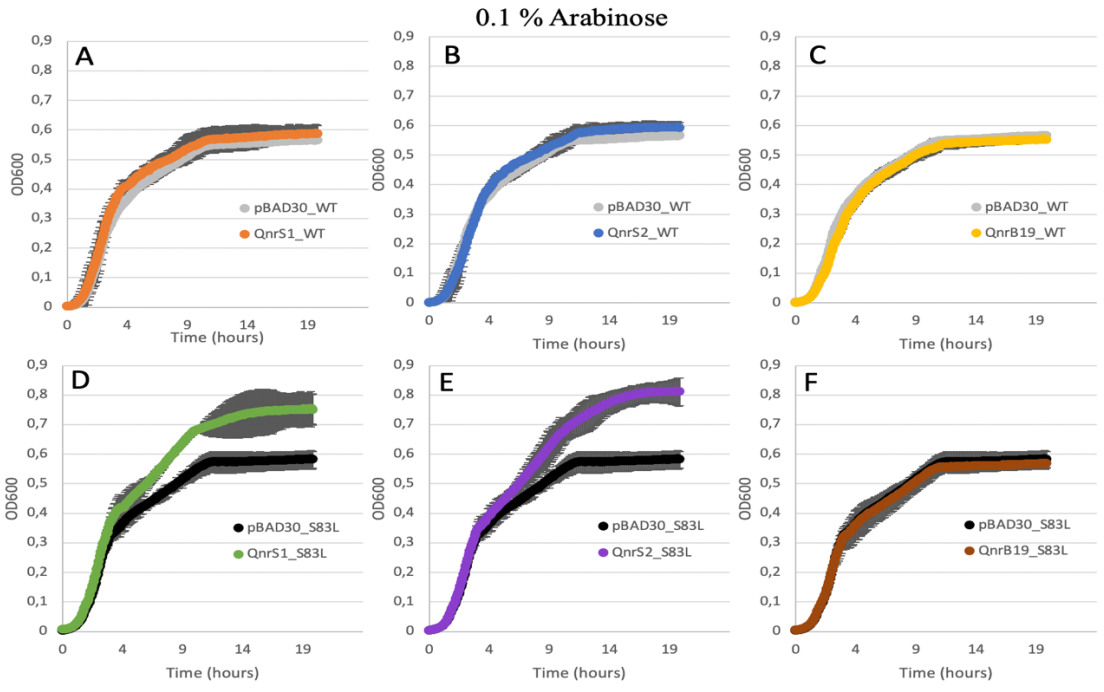

Figure 39. Growth curves of GyrA-WT-1085 transformed with pBAD30-QnrS1, pBAD30-QnrS2, pBAD30-QnrB19 or pBAD30 (A-C) and GyrA-S83L-5022 transformed with pBAD30-QnrS1, pBAD30-QnrS2, pBAD30-QnrB19 or pBAD30 (D-F) in LB medium supplied with ampicillin and 0.1 % arabinose. Cultures were incubated in a plate reader for 20 h at 37 °C with OD_{600} measurements every 5 min. Data is the mean of three experiments. Error bars represents 95 % confidence interval. The figures were made in Microsoft Excel.

Acquired quinolone resistance has previously been shown to affect fitness differently (Machuca et al., 2014, 2017; Marcusson et al., 2009). Our results suggest that expression of QnrS1 or QnrS2 in the GyrA S83L mutant background can give a fitness advantage compared to expression of these proteins in the GyrA WT, while expression of QnrB19 does not seem to be associated with an effect on fitness in either background. This result could explain the occurrence of quinolone resistant *E. coli* isolates carrying both the S83L mutation and plasmid mediated resistance mechanisms in the form of QnrS1 and QnrS2, but not QnrB19. These findings should be tested further to ensure that the increased fitness is caused by the expression of QnrS1 or QnrS2 in the GyrA S83L background. This is to ensure that mutations have not occurred in the stock bacteria that could cause a fitness advantages in the presence of arabinose. The bacterial suspension should also be streaked out on a plate after the assay to look for different colony morphotypes to test for possible contamination.

In this study it was tested if the expression of the Qnr protein could cause any growth advantage or disadvantage. But there are still other factors of acquiring Qnr as a resistance mechanism that can affect fitness. The Qnr proteins are usually found on relatively large plasmids, and acquisition of resistance plasmids has been linked to fitness costs due to the energy needed for replication of the plasmids and protein expression from the plasmids (Dahlberg & Chao, 2003). The extent of the fitness cost can depend on various factors such as the copy number of the plasmid, occurrence of genes encoding toxic products, the promoter strength, transcription levels of the Qnr proteins and other proteins encoded on the WT plasmids (Martínez-Martínez et al., 2008).

4 Conclusion and future perspective

4.1 Conclusion

In this thesis, the main aim was to increase the knowledge about the interplay between chromosomal- and plasmid-mediated quinolone resistance mechanisms.

Through this study, we managed to express all five proteins, GyrA S83L, GyrA WT, QnrS1, QnrS2 and QnrB19, in BL21 cells and to isolate soluble protein. We have also shown that the purification of the protein using a His-tag, yielded pure protein that could be used for interaction studies. However, the data obtained from the interaction studies were not reliable enough to conclude if there are any differences in the interaction between the two variants of GyrA and the three Qnr proteins. The SEC analysis revealed that most of the protein were not in the expected dimer-form, which could explain why the data from the interaction studies are unreliable.

From the susceptibility testing, we found that expression of QnrS1 in general resulted in a slightly higher MIC than expression of QnrS2 and QnrB19. Further, we found that expression of the Qnr variants leads to resistance to ciprofloxacin according to ECOFF (MIC over 0.06 μg/mL) and to clinical resistance against ciprofloxacin (MIC over 0.5 μg/mL) when expressed together with GyrA S83L. The growth assays showed that expressing the different Qnr proteins did not cause any fitness disadvantages in the presence of GyrA WT or GyrA S83L. However, we discovered that there was a fitness advantage in the clinically resistant strains expressing GyrA S83L and QnrS1 or QnrS2.

4.2 Future perspective

To be able to perform the interaction studies, the proteins need to be in a functional form. So, a solid expression, purification and storage protocol is needed for obtaining pure protein in the dimer-form. This thesis has provided important information for the expression and purification of both the GyrA variants and Qnr variants that will be useful for further optimization of the protocols. It is not known at which stage of the purification procedure that aggregation and multimerization occurred. This could easily be examined by taking samples of the proteins after

each stage of the purification procedure and analyzing them using SEC or a native SDS-PAGE gel. This way the native size of the proteins can be analyzed in each step. When the proteins are confirmed to be in the expected dimer-form, the interaction studies using MST and SPR can be performed.

The GyrB subunit was not included in this study since the main interest was to see how the S83L mutation in GyrA could affect the interaction with the Qnr proteins of interest. In future studies, GyrB could be included because it has been shown to be important for binding of Qnr (Kim et al., 2015; Mazurek et al., 2021; Tran et al., 2005a). It would also give a better representation of the interaction since Qnr are thought to interact with the whole complex and not just one subunit at the time. If GyrB is also included the activity of the proteins can be tested in a Gyrase supercoiling assay, where the ability of Gyrase to supercoil DNA is tested (Maxwell et al., 2006). To test the activity of the Qnr proteins, quinolones and one of the Qnr proteins are added to the assay to determine if Qnr can rescue Gyrase from quinolone activity. This way, the ability of Gyrase and Qnr to interact in a given buffer and temperature, can be confirmed before differences between the interactions are studied through MST and SPR.

As mentioned earlier, the Qnr proteins are usually encoded on different plasmids. This means that the actual expression level of the Qnr proteins and fitness of bearing the plasmids could be different based on which plasmid the Qnr protein is encoded on. To test if the WT plasmids encoding QnrS1, QnrS2 or QnrB19 are associated with different fitness costs, the original isolates should be used as donors in a conjugation experiment. The recipient of the plasmid would be a strain that either express GyrA WT or GyrA S83L, without any other differences. The transconjugants carrying one of the WT plasmids encoding QnrS1, QnrS2 or QnrB19 should be tested in broth microdilution assay and growth assay. Through the broth microdilution assay, the level of resistance achieved by each of the Qnr proteins expressed from their native promoters would be determined. For the growth assays, the fitness cost of bearing the WT plasmids would be tested. This was not tested in this thesis, but this can be one of the explanations why some *qnr* variants are more frequently observed with GyrA S83L than others.

The long-term goal will be to increase the knowledge about the interplay of chromosome-mediated and plasmid-mediated resistance mechanisms. This can facilitate the interpretation of different genotypes, which is important for correct diagnosis and treatment success.

5 References

Abraham, E. P., & Chain, E. (1940). An Enzyme from Bacteria able to Destroy Penicillin. *Nature*, *146*(3713), 837. https://doi.org/10.1038/146837a0

Aedo, S., & Tse-Dinh, Y.-C. (2013). SbcCD-Mediated Processing of Covalent Gyrase-DNA Complex in Escherichia coli *Antimicrobial Agents and Chemotherapy*, *57*(10), 5116. https://doi.org/10.1128/AAC.00130-13

Aldred, K. J., Kerns, R. J., & Osheroff, N. (2014). Mechanism of quinolone action and resistance. *Biochemistry*, *53*(10), 1565–1574. https://doi.org/10.1021/bi5000564

Aldred, K. J., McPherson, S. A., Turnbough Jr, C. L., Kerns, R. J., & Osheroff, N. (2013). Topoisomerase IV-quinolone interactions are mediated through a water-metal ion bridge: mechanistic basis of quinolone resistance. *Nucleic Acids Research*, *41*(8), 4628–4639. https://doi.org/10.1093/nar/gkt124

Aldred, K. J., Schwanz, H. A., Li, G., McPherson, S. A., Turnbough Jr, C. L., Kerns, R. J., & Osheroff, N. (2013). Overcoming target-mediated quinolone resistance in topoisomerase IV by introducing metal-ion-independent drug-enzyme interactions. *ACS Chemical Biology*, *8*(12), 2660–2668. https://doi.org/10.1021/cb400592n

Altschul, S. F., Gish, W., Miller, W., Myers, E. W., & Lipman, D. J. (1990). Basic local alignment search tool. *Journal of Molecular Biology*, *215*(3), 403–410. https://doi.org/https://doi.org/10.1016/S0022-2836(05)80360-2

Andersen, K. R., Leksa, N. C., & Schwartz, T. U. (2013). Optimized E. coli expression strain LOBSTR eliminates common contaminants from His-tag purification. *Proteins*, *81*(11), 1857–1861. https://doi.org/10.1002/prot.24364

Andersson, M. I. (2003). Development of the quinolones. *Journal of Antimicrobial Chemotherapy*, *51*(90001). https://doi.org/10.1093/jac/dkg212

Arya, R., Sabir, J. S. M., Bora, R. S., & Saini, K. S. (2015). Optimization of Culture Parameters and Novel Strategies to Improve Protein Solubility. In E. García-Fruitós (Ed.), *Insoluble Proteins: Methods and Protocols* (pp. 45–63). Springer New York. https://doi.org/10.1007/978-1-4939-2205-5_3

Bagel, S., Hüllen, V., Wiedemann, B., & Heisig, P. (1999). Impact of gyrA and parC mutations on quinolone resistance, doubling time, and supercoiling degree of Escherichia coli. *Antimicrobial Agents and Chemotherapy*, *43*(4), 868–875. https://doi.org/10.1128/AAC.43.4.868

Barnard, F. M., & Maxwell, A. (2001). Interaction between DNA gyrase and quinolones: effects of alanine mutations at GyrA subunit residues Ser(83) and Asp(87). *Antimicrobial Agents and Chemotherapy*, *45*(7), 1994–2000. https://doi.org/10.1128/AAC.45.7.1994-2000.2001

Bax, B. D., Chan, P. F., Eggleston, D. S., Fosberry, A., Gentry, D. R., Gorrec, F., Giordano, I., Hann, M. M., Hennessy, A., Hibbs, M., Huang, J., Jones, E., Jones, J., Brown, K. K., Lewis, C. J., May, E. W., Saunders, M. R., Singh, O., Spitzfaden, C. E., … Gwynn, M. N. (2010). Type IIA topoisomerase inhibition by a new class of antibacterial agents. *Nature*, *466*(7309), 935–940. https://doi.org/10.1038/nature09197

Bell, B. G., Schellevis, F., Stobberingh, E., Goossens, H., & Pringle, M. (2014). A systematic review and meta-analysis of the effects of antibiotic consumption on antibiotic resistance. *BMC Infectious Diseases*, *14*, 13. https://doi.org/10.1186/1471-2334-14-13

Berman, H. M., Westbrook, J., Feng, Z., Gilliland, G., Bhat, T. N., Weissig, H., Shindyalov, I. N., & Bourne, P. E. (2000). The Protein Data Bank. *Nucleic Acids Research*, *28*(1), 235–242. https://doi.org/10.1093/nar/28.1.235

Bernhofer, M., Dallago, C., Karl, T., Satagopam, V., Heinzinger, M., Littmann, M., Olenyi, T., Qiu, J., Schütze, K., Yachdav, G., Ashkenazy, H., Ben-Tal, N., Bromberg, Y., Goldberg, T., Kajan, L., O'Donoghue, S.,

Sander, C., Schafferhans, A., Schlessinger, A., … Rost, B. (2021). PredictProtein – Predicting Protein Structure and Function for 29 Years. *BioRxiv*, 2021.02.23.432527. https://doi.org/10.1101/2021.02.23.432527

Bhatnagar, K., & Wong, A. (2019). The mutational landscape of quinolone resistance in Escherichia coli. *PLOS ONE*, *14*(11), e0224650-. https://doi.org/10.1371/journal.pone.0224650

Blower, T. R., Williamson, B. H., Kerns, R. J., & Berger, J. M. (2016). Crystal structure and stability of gyrase–fluoroquinolone cleaved complexes from Mycobacterium tuberculosis *Proceedings of the National Academy of Sciences*, *113*(7), 1706. https://doi.org/10.1073/pnas.1525047113

Bornhorst, J. A., & Falke, J. J. (2000). Purification of proteins using polyhistidine affinity tags. *Methods in Enzymology*, *326*, 245–254. https://doi.org/10.1016/s0076-6879(00)26058-8

Briales, A., Rodríguez-Martínez, J. M., Velasco, C., Díaz de Alba, P., Domínguez-Herrera, J., Pachón, J., & Pascual, A. (2011). *In Vitro* Effect of *qnrA1* , *qnrB1* , and *qnrS1* Genes on Fluoroquinolone Activity against Isogenic *Escherichia coli* Isolates with Mutations in *gyrA* and *parC*. *Antimicrobial Agents and Chemotherapy*, *55*(3). https://doi.org/10.1128/AAC.00927-10

Bush, N. G., Diez-Santos, I., Abbott, L. R., & Maxwell, A. (2020). Quinolones: Mechanism, Lethality and Their Contributions to Antibiotic Resistance. *Molecules (Basel, Switzerland)*, *25*(23), 5662. https://doi.org/10.3390/molecules25235662

Calhoun, C., Wermuth, H. R., & Hall, G. A. (2020). *Antibiotics*. StatPearls Publishing LLC.

Cattoir, V., Nordmann, P., Silva-Sanchez, J., Espinal, P., & Poirel, L. (2008). ISEcp1-mediated transposition of qnrB-like gene in Escherichia coli. *Antimicrobial Agents and Chemotherapy*, *52*(8), 2929–2932. https://doi.org/10.1128/AAC.00349-08

Cebrián, J., Castán, A., Martínez, V., Kadomatsu-Hermosa, M. J., Parra, C., Fernández-Nestosa, M. J., Schaerer, C., Hernández, P., Krimer, D. B., & Schvartzman, J. B. (2015). Direct Evidence for the Formation of Precatenanes during DNA Replication*. *Journal of Biological Chemistry*, *290*(22), 13725–13735. https://doi.org/https://doi.org/10.1074/jbc.M115.642272

Cetinkaya, Y., Falk, P., & Mayhall, C. G. (2000). Vancomycin-resistant enterococci. *Clinical Microbiology Reviews*, *13*(4), 686–707. https://doi.org/10.1128/cmr.13.4.686-707.2000

Chen, X., Zhang, W., Pan, W., Yin, J., Pan, Z., Gao, S., & Jiao, X. (2012). Prevalence of qnr, aac(6')-Ib-cr, qepA, and oqxAB in Escherichia coli isolates from humans, animals, and the environment. *Antimicrobial Agents and Chemotherapy*, *56*(6), 3423–3427. https://doi.org/10.1128/AAC.06191-11

Chien, J.-Y., Chiu, W.-Y., Chien, S.-T., Chiang, C.-J., Yu, C.-J., & Hsueh, P.-R. (2016). Mutations in gyrA and gyrB among Fluoroquinolone- and Multidrug-Resistant Mycobacterium tuberculosis Isolates. *Antimicrobial Agents and Chemotherapy*, *60*(4), 2090. https://doi.org/10.1128/AAC.01049-15

Choi, U., & Lee, C.-R. (2019). Distinct Roles of Outer Membrane Porins in Antibiotic Resistance and Membrane Integrity in Escherichia coli. *Frontiers in Microbiology*, *10*, 953. https://www.frontiersin.org/article/10.3389/fmicb.2019.00953

Consortium, T. U. (2021). UniProt: the universal protein knowledgebase in 2021. *Nucleic Acids Research*, *49*(D1), D480–D489. https://doi.org/10.1093/nar/gkaa1100

Cox, M. M., & Nelson, D. L. (2013). *Lehninger principles of biochemistry* (6th ed.). W.H.Freeman & Co Ltd.

Crossman, L. C., Gould, V. C., Dow, J. M., Vernikos, G. S., Okazaki, A., Sebaihia, M., Saunders, D., Arrowsmith, C., Carver, T., Peters, N., Adlem, E., Kerhornou, A., Lord, A., Murphy, L., Seeger, K., Squares, R., Rutter, S., Quail, M. A., Rajandream, M.-A., … Avison, M. B. (2008). The complete genome, comparative and functional analysis of Stenotrophomonas maltophiliareveals an organism heavily shielded by drug resistance determinants. *Genome Biology*, *9*(4), R74. https://doi.org/10.1186/gb-2008-9-4-r74

D S Horowitz, & J C Wang. (1987). *Mapping the active site tyrosine of Escherichia coli DNA gyrase*. https://pubmed.ncbi.nlm.nih.gov/3031051/

Dahlberg, C., & Chao, L. (2003). Amelioration of the cost of conjugative plasmid carriage in Eschericha coli K12. *Genetics*, *165*(4), 1641–1649. https://pubmed.ncbi.nlm.nih.gov/14704155

de Lastours, V., Chau, F., Roy, C., Larroque, B., & Fantin, B. (2014). Emergence of quinolone resistance in the microbiota of hospitalized patients treated or not with a fluoroquinolone. *Journal of Antimicrobial Chemotherapy*, *69*(12), 3393–3400. https://doi.org/10.1093/jac/dku283

Dolgova, A. S., & Stukolova, O. A. (2017). High-fidelity PCR enzyme with DNA-binding domain facilitates de novo gene synthesis. *3 Biotech*, *7*(2), 128. https://doi.org/10.1007/s13205-017-0745-2

Dönhöfer, A., Franckenberg, S., Wickles, S., Berninghausen, O., Beckmann, R., & Wilson, D. N. (2012). Structural basis for TetM-mediated tetracycline resistance. *Proceedings of the National Academy of Sciences of the United States of America*, *109*(42), 16900–16905. https://doi.org/10.1073/pnas.1208037109

Douzi, B. (2017). Protein–Protein Interactions: Surface Plasmon Resonance. In L. Journet & E. Cascales (Eds.), *Bacterial Protein Secretion Systems: Methods and Protocols* (pp. 257–275). Springer New York. https://doi.org/10.1007/978-1-4939-7033-9_21

Drlica, K., Hiasa, H., Kerns, R., Malik, M., Mustaev, A., & Zhao, X. (2009). Quinolones: action and resistance updated. *Current Topics in Medicinal Chemistry*, *9*(11), 981–998. https://doi.org/10.2174/156802609789630947

Dubendorf, J. W., & Studier, F. W. (1991). Controlling basal expression in an inducible T7 expression system by blocking the target T7 promoter with lac repressor. *Journal of Molecular Biology*, *219*(1), 45–59. https://doi.org/https://doi.org/10.1016/0022-2836(91)90856-2

Dwyer, D. J., Collins, J. J., & Walker, G. C. (2015). Unraveling the Physiological Complexities of Antibiotic Lethality. *Annual Review of Pharmacology and Toxicology*, *55*(1), 313–332. https://doi.org/10.1146/annurev-pharmtox-010814-124712

Dwyer, D. J., Kohanski, M. A., Hayete, B., & Collins, J. J. (2007). Gyrase inhibitors induce an oxidative damage cellular death pathway in Escherichia coli. *Molecular Systems Biology*, *3*, 91. https://doi.org/10.1038/msb4100135

Edgar, R. C. (2004). MUSCLE: multiple sequence alignment with high accuracy and high throughput. *Nucleic Acids Research*, *32*(5), 1792–1797. https://doi.org/10.1093/nar/gkh340

Eliopoulos, G. M., & Huovinen, P. (2001). Resistance to Trimethoprim-Sulfamethoxazole. *Clinical Infectious Diseases*, *32*(11), 1608–1614. https://doi.org/10.1086/320532

European Centre for Disease Prevention and Control. (2017). *Summary of the latest data on antibiotic resistance in the European Union*. https://www.ecdc.europa.eu/en/publications-data/summary-latest-data-antibiotic-resistance-european-union

Feng, L., Mundy, J. E. A., Stevenson, C. E. M., Mitchenall, L. A., Lawson, D. M., Mi, K., & Maxwell, A. (2021). The pentapeptide-repeat protein, MfpA, interacts with mycobacterial DNA gyrase as a DNA T-segment mimic. *Proceedings of the National Academy of Sciences*, *118*(11), e2016705118. https://doi.org/10.1073/pnas.2016705118

Fernández, L., & Hancock, R. E. W. (2012). Adaptive and Mutational Resistance: Role of Porins and Efflux Pumps in Drug Resistance. *Clinical Microbiology Reviews*, *25*(4), 661. https://doi.org/10.1128/CMR.00043-12

Folkehelseinstituttet. (2017). *Antibiotikaresistens*. https://www.fhi.no/nettpub/hin/smitte/resistens/

Francis, D. M., & Page, R. (2010). Strategies to optimize protein expression in E. coli. *Current Protocols in Protein Science*, *Chapter 5*(1), 5241-5.24.29. https://doi.org/10.1002/0471140864.ps0524s61

Fu, Y., Zhang, W., Wang, H., Zhao, S., Chen, Y., Meng, F., Zhang, Y., Xu, H., Chen, X., & Zhang, F. (2013).

Specific patterns of gyr A mutations determine the resistance difference to ciprofloxacin and levofloxacin in Klebsiella pneumoniae and Escherichia coli. *BMC Infectious Diseases*, *13*(1), 8. https://doi.org/10.1186/1471-2334-13-8

Garoff, L., Yadav, K., & Hughes, D. (2018). Increased expression of Qnr is sufficient to confer clinical resistance to ciprofloxacin in Escherichia coli. *Journal of Antimicrobial Chemotherapy*, *73*(2), 348–352. https://doi.org/10.1093/jac/dkx375

Gasteiger, E., Hoogland, C., Gattiker, A., Duvaud, S., Wilkins, M. R., Appel, R. D., & Bairoch, A. (2005). Protein Identification and Analysis Tools on the ExPASy Server. In J. M. Walker (Ed.), *The Proteomics Protocols Handbook* (pp. 571–607). Humana Press. https://doi.org/10.1385/1-59259-890-0:571

Gay, K., Robicsek, A., Strahilevitz, J., Park, C. H., Jacoby, G., Barrett, T. J., Medalla, F., Chiller, T. M., & Hooper, D. C. (2006). Plasmid-Mediated Quinolone Resistance in Non-Typhi Serotypes of Salmonella enterica. *Clinical Infectious Diseases*, *43*(3), 297–304. https://doi.org/10.1086/505397

Gould, K. (2016). Antibiotics: from prehistory to the present day. *Journal of Antimicrobial Chemotherapy*, *71*(3), 572–575. https://doi.org/10.1093/jac/dkv484

Gubaev, A., & Klostermeier, D. (2014). Reprint of "The mechanism of negative DNA supercoiling: A cascade of DNA-induced conformational changes prepares gyrase for strand passage." *DNA Repair*, *20*, 130–141. https://doi.org/https://doi.org/10.1016/j.dnarep.2014.06.006

Guex, N., & Peitsch, M. C. (1997). SWISS-MODEL and the Swiss-Pdb Viewer: An environment for comparative protein modeling. *Electrophoresis*, *18*(15). https://doi.org/10.1002/elps.1150181505

Guzman, L. M., Belin, D., Carson, M. J., & Beckwith, J. (1995). Tight regulation, modulation, and high-level expression by vectors containing the arabinose PBAD promoter. *Journal of Bacteriology*, *177*(14), 4121–4130. https://doi.org/10.1128/jb.177.14.4121-4130.1995

Hansen, L. H., Jensen, L. B., Sørensen, H. I., & Sørensen, S. J. (2007). Substrate specificity of the OqxAB multidrug resistance pump in Escherichia coli and selected enteric bacteria. *Journal of Antimicrobial Chemotherapy*, *60*(1), 145–147. https://doi.org/10.1093/jac/dkm167

Hartmann, S., Gubaev, A., & Klostermeier, D. (2017). Binding and Hydrolysis of a Single ATP Is Sufficient for N-Gate Closure and DNA Supercoiling by Gyrase. *Journal of Molecular Biology*, *429*(23), 3717–3729. https://doi.org/https://doi.org/10.1016/j.jmb.2017.10.005

Hata, M., Suzuki, M., Matsumoto, M., Takahashi, M., Sato, K., Ibe, S., & Sakae, K. (2005). Cloning of a novel gene for quinolone resistance from a transferable plasmid in Shigella flexneri 2b. *Antimicrobial Agents and Chemotherapy*, *49*(2), 801–803. https://doi.org/10.1128/AAC.49.2.801-803.2005

Heep, M., Rieger, U., Beck, D., & Lehn, N. (2000). Mutations in the Beginning of the rpoBGene Can Induce Resistance to Rifamycins in both Helicobacter pylori and Mycobacterium tuberculosis *Antimicrobial Agents and Chemotherapy*, *44*(4), 1075. https://doi.org/10.1128/AAC.44.4.1075-1077.2000

Hegde, S. S., Vetting, M. W., Mitchenall, L. A., Maxwell, A., & Blanchard, J. S. (2011). Structural and Biochemical Analysis of the Pentapeptide Repeat Protein EfsQnr, a Potent DNA Gyrase Inhibitor. *Antimicrobial Agents and Chemotherapy*, *55*(1), 110. https://doi.org/10.1128/AAC.01158-10

Hegde, S. S., Vetting, M. W., Roderick, S. L., Mitchenall, L. A., Maxwell, A., Takiff, H. E., & Blanchard, J. S. (2005). A Fluoroquinolone Resistance Protein from Mycobacterium tuberculosis That Mimics DNA. *Science*, *308*(5727), 1480. https://doi.org/10.1126/science.1110699

Hong, Y., Li, Q., Gao, Q., Xie, J., Huang, H., Drlica, K., & Zhao, X. (2020). Reactive oxygen species play a dominant role in all pathways of rapid quinolone-mediated killing. *Journal of Antimicrobial Chemotherapy*, *75*(3), 576–585. https://doi.org/10.1093/jac/dkz485

Hooper, D. C., & Jacoby, G. A. (2016). Topoisomerase Inhibitors: Fluoroquinolone Mechanisms of Action and Resistance. *Cold Spring Harbor Perspectives in Medicine*, *6*(9), a025320.

https://doi.org/10.1101/cshperspect.a025320

Hooper, D. C., & Strahilevitz, J. (2015). 34 - Quinolones. In J. E. Bennett, R. Dolin, & M. J. Blaser (Eds.), *Mandell, Douglas, and Bennett's Principles and Practice of Infectious Diseases (Eighth Edition)* (pp. 419-439.e8). W.B. Saunders. https://doi.org/https://doi.org/10.1016/B978-1-4557-4801-3.00034-5

Hopkins, K. L., Davies, R. H., & Threlfall, E. J. (2005). Mechanisms of quinolone resistance in Escherichia coli and Salmonella: Recent developments. *International Journal of Antimicrobial Agents*, *25*(5), 358–373. https://doi.org/https://doi.org/10.1016/j.ijantimicag.2005.02.006

Hoseini, S. S., & Sauer, M. G. (2015). Molecular cloning using polymerase chain reaction, an educational guide for cellular engineering. *Journal of Biological Engineering*, *9*(1), 2. https://doi.org/10.1186/1754-1611-9-2

Humphries, R. M., Abbott, A. N., & Hindler, J. A. (2019). Understanding and Addressing CLSI Breakpoint Revisions: a Primer for Clinical Laboratories. *Journal of Clinical Microbiology*, *57*(6), e00203-19. https://doi.org/10.1128/JCM.00203-19

Hutchings, M. I., Truman, A. W., & Wilkinson, B. (2019). Antibiotics: past, present and future. *Current Opinion in Microbiology*, *51*, 72–80. https://doi.org/https://doi.org/10.1016/j.mib.2019.10.008

Jacoby, G. A., Corcoran, M. A., Mills, D. M., Griffin, C. M., & Hooper, D. C. (2013). Mutational analysis of quinolone resistance protein QnrB1. *Antimicrobial Agents and Chemotherapy*, *57*(11), 5733–5736. https://doi.org/10.1128/AAC.01533-13

Jacoby, G. A., Strahilevitz, J., & Hooper, D. C. (2014). Plasmid-mediated quinolone resistance. *Microbiology Spectrum*, *2*(5), 10.1128/microbiolspec.PLAS-0006–2013. https://doi.org/10.1128/microbiolspec.PLAS-0006-2013

Jacoby, G. A., Walsh, K. E., Mills, D. M., Walker, V. J., Oh, H., Robicsek, A., & Hooper, D. C. (2006). qnrB, another plasmid-mediated gene for quinolone resistance. *Antimicrobial Agents and Chemotherapy*, *50*(4), 1178–1182. https://doi.org/10.1128/AAC.50.4.1178-1182.2006

Jacoby, G., Cattoir, V., Hooper, D., Martínez-Martínez, L., Nordmann, P., Pascual, A., Poirel, L., & Wang, M. (2008). qnr Gene nomenclature. *Antimicrobial Agents and Chemotherapy*, *52*(7), 2297–2299. https://doi.org/10.1128/AAC.00147-08

Jerabek-Willemsen, M., André, T., Wanner, R., Roth, H. M., Duhr, S., Baaske, P., & Breitsprecher, D. (2014). MicroScale Thermophoresis: Interaction analysis and beyond. *Journal of Molecular Structure*, *1077*, 101–113. https://doi.org/https://doi.org/10.1016/j.molstruc.2014.03.009

Jerabek-Willemsen, M., Wienken, C. J., Braun, D., Baaske, P., & Duhr, S. (2011). Molecular interaction studies using microscale thermophoresis. *Assay and Drug Development Technologies*, *9*(4), 342–353. https://doi.org/10.1089/adt.2011.0380

Jim O'Neill. (2016). *TACKLING DRUG-RESISTANT INFECTIONS GLOBALLY: FINAL REPORT AND RECOMMENDATIONS*. https://amr-review.org/sites/default/files/160518_Final paper_with cover.pdf

Johnning, A., Kristiansson, E., Fick, J., Weijdegård, B., & Larsson, D. G. J. (2015). Resistance Mutations in gyrA and parC are Common in Escherichia Communities of both Fluoroquinolone-Polluted and Uncontaminated Aquatic Environments. *Frontiers in Microbiology*, *6*. https://doi.org/10.3389/fmicb.2015.01355

Kaspersen, H., Sekse, C., Zeyl Fiskebeck, E., Slettemeås, J. S., Simm, R., Norström, M., Urdahl, A. M., & Lagesen, K. (2020). Dissemination of Quinolone-Resistant Escherichia coli in the Norwegian Broiler and Pig Production Chains and Possible Persistence in the Broiler Production Environment. *Applied and Environmental Microbiology*, *86*(7), e02769-19. https://doi.org/10.1128/AEM.02769-19

Kelley, L. A., Mezulis, S., Yates, C. M., Wass, M. N., & Sternberg, M. J. E. (2015). The Phyre2 web portal for protein modeling, prediction and analysis. *Nature Protocols*, *10*(6), 845–858. https://doi.org/10.1038/nprot.2015.053

Kiffer, C. R. V, Camargo, E. C. G., Shimakura, S. E., Ribeiro, P. J., Bailey, T. C., Pignatari, A. C. C., &

Monteiro, A. M. V. (2011). A spatial approach for the epidemiology of antibiotic use and resistance in community-based studies: the emergence of urban clusters of Escherichia coli quinolone resistance in Sao Paulo, Brasil. *International Journal of Health Geographics*, *10*(1), 17. https://doi.org/10.1186/1476-072X-10-17

Kim, E. S., Chen, C., Braun, M., Kim, H. Y., Okumura, R., Wang, Y., Jacoby, G. A., & Hooper, D. C. (2015). Interactions between QnrB, QnrB Mutants, and DNA Gyrase. *Antimicrobial Agents and Chemotherapy*, *59*(9), 5413. https://doi.org/10.1128/AAC.00771-15

Kohanski, M. A., DePristo, M. A., & Collins, J. J. (2010a). Sublethal Antibiotic Treatment Leads to Multidrug Resistance via Radical-Induced Mutagenesis. *Molecular Cell*, *37*(3). https://doi.org/10.1016/j.molcel.2010.01.003

Kohanski, M. A., DePristo, M. A., & Collins, J. J. (2010b). Sublethal antibiotic treatment leads to multidrug resistance via radical-induced mutagenesis. *Molecular Cell*, *37*(3), 311–320. https://doi.org/10.1016/j.molcel.2010.01.003

Krause, K. M., Serio, A. W., Kane, T. R., & Connolly, L. E. (2016). Aminoglycosides: An Overview. *Cold Spring Harbor Perspectives in Medicine*, *6*(6), a027029. https://doi.org/10.1101/cshperspect.a027029

Kreuzer, K. N. (2013). DNA damage responses in prokaryotes: regulating gene expression, modulating growth patterns, and manipulating replication forks. *Cold Spring Harbor Perspectives in Biology*, *5*(11), a012674–a012674. https://doi.org/10.1101/cshperspect.a012674

Lanz, M. A., Farhat, M., & Klostermeier, D. (2014). The acidic C-terminal tail of the GyrA subunit moderates the DNA supercoiling activity of Bacillus subtilis gyrase. *The Journal of Biological Chemistry*, *289*(18), 12275–12285. https://doi.org/10.1074/jbc.M114.547745

Laponogov, I., Sohi, M. K., Veselkov, D. A., Pan, X.-S., Sawhney, R., Thompson, A. W., McAuley, K. E., Fisher, L. M., & Sanderson, M. R. (2009). Structural insight into the quinolone–DNA cleavage complex of type IIA topoisomerases. *Nature Structural & Molecular Biology*, *16*(6), 667–669. https://doi.org/10.1038/nsmb.1604

Leclercq, R., Cantón, R., Brown, D. F. J., Giske, C. G., Heisig, P., MacGowan, A. P., Mouton, J. W., Nordmann, P., Rodloff, A. C., Rossolini, G. M., Soussy, C.-J., Steinbakk, M., Winstanley, T. G., & Kahlmeter, G. (2013). EUCAST expert rules in antimicrobial susceptibility testing. *Clinical Microbiology and Infection*, *19*(2). https://doi.org/10.1111/j.1469-0691.2011.03703.x

Lee, P. Y., Costumbrado, J., Hsu, C.-Y., & Kim, Y. H. (2012). Agarose gel electrophoresis for the separation of DNA fragments. *Journal of Visualized Experiments : JoVE*, *62*, 3923. https://doi.org/10.3791/3923

Leekha, S., Terrell, C. L., & Edson, R. S. (2011). General principles of antimicrobial therapy. *Mayo Clinic Proceedings*, *86*(2), 156–167. https://doi.org/10.4065/mcp.2010.0639

Leibly, D. J., Nguyen, T. N., Kao, L. T., Hewitt, S. N., Barrett, L. K., & Van Voorhis, W. C. (2012). Stabilizing Additives Added during Cell Lysis Aid in the Solubilization of Recombinant Proteins. *PLOS ONE*, *7*(12), e52482-. https://doi.org/10.1371/journal.pone.0052482

Lesher, G. Y., Froelich, E. J., Gruett, M. D., Bailey, J. H., & Brundage, R. P. (1962). 1,8-Naphthyridine Derivatives. A New Class of Chemotherapeutic Agents. *Journal of Medicinal and Pharmaceutical Chemistry*, *5*(5), 1063–1065. https://doi.org/10.1021/jm01240a021

Li, X.-Z., & Nikaido, H. (2009). Efflux-mediated drug resistance in bacteria: an update. *Drugs*, *69*(12), 1555–1623. https://doi.org/10.2165/11317030-000000000-00000

Lodish, U. H. (2016). *Molecular Cell Biology.* W.H. Freeman.

López, E., & Blázquez, J. (2009). Effect of subinhibitory concentrations of antibiotics on intrachromosomal homologous recombination in Escherichia coli. *Antimicrobial Agents and Chemotherapy*, *53*(8), 3411–3415. https://doi.org/10.1128/AAC.00358-09

López, E., Elez, M., Matic, I., & Blázquez, J. (2007). Antibiotic-mediated recombination: ciprofloxacin

stimulates SOS-independent recombination of divergent sequences in Escherichia coli. *Molecular Microbiology*, *64*(1). https://doi.org/10.1111/j.1365-2958.2007.05642.x

Machuca, J., Briales, A., Labrador, G., Díaz-de-Alba, P., López-Rojas, R., Docobo-Pérez, F., Martínez-Martínez, L., Rodríguez-Baño, J., Pachón, M. E., Pascual, Á., & Rodríguez-Martínez, J.-M. (2014). Interplay between plasmid-mediated and chromosomal-mediated fluoroquinolone resistance and bacterial fitness in Escherichia coli. *Journal of Antimicrobial Chemotherapy*, *69*(12), 3203–3215. https://doi.org/10.1093/jac/dku308

Machuca, J., Diaz de Alba, P., Recacha, E., Pascual, Á., & Rodriguez-Martinez, J. M. (2017). Cytotoxic Effect Associated with Overexpression of QNR Proteins in *Escherichia coli*. *Microbial Drug Resistance*, *23*(7). https://doi.org/10.1089/mdr.2016.0245

MacLean, R. C., Hall, A. R., Perron, G. G., & Buckling, A. (2010). The population genetics of antibiotic resistance: integrating molecular mechanisms and treatment contexts. *Nature Reviews Genetics*, *11*(6), 405–414. https://doi.org/10.1038/nrg2778

Madigan, M. T., Martinko, J. M., Bender, K. S., Buckley, D. H. (Daniel H., & Stahl, D. A. (2015). Brock biology of microorganisms / Michael T. Madigan, Southern Illinois University Carbondale ; John M. Martinko, Southern Illinois University Carbondale ; Kelly S. Bender Southern Illinois University Carbondale ; Daniel H. Buckley, Cornell University ; David A. Stahl, University of Washington Seattle. In *Biology of microorganisms* (Fourteenth edition.). Pearson.

Malik, M., Zhao, X., & Drlica, K. (2006). Lethal fragmentation of bacterial chromosomes mediated by DNA gyrase and quinolones. *Molecular Microbiology*, *61*(3). https://doi.org/10.1111/j.1365-2958.2006.05275.x

Marcusson, L. L., Frimodt-Møller, N., & Hughes, D. (2009). Interplay in the Selection of Fluoroquinolone Resistance and Bacterial Fitness. *PLOS Pathogens*, *5*(8), e1000541-. https://doi.org/10.1371/journal.ppat.1000541

Martínez-Martínez, L., Eliecer Cano, M., Manuel Rodríguez-Martínez, J., Calvo, J., & Pascual, Á. (2008). Plasmid-mediated quinolone resistance. *Expert Review of Anti-Infective Therapy*, *6*(5), 685–711. https://doi.org/10.1586/14787210.6.5.685

Martínez-Martínez, L., Pascual, A., & Jacoby, G. A. (1998). Quinolone resistance from a transferable plasmid. *The Lancet*, *351*(9105). https://doi.org/10.1016/S0140-6736(97)07322-4

Matrat, S., Petrella, S., Cambau, E., Sougakoff, W., Jarlier, V., & Aubry, A. (2007). Expression and Purification of an Active Form of the Mycobacterium leprae DNA Gyrase and Its Inhibition by Quinolones. *Antimicrobial Agents and Chemotherapy*, *51*(5), 1643. https://doi.org/10.1128/AAC.01282-06

Maxwell, A., Burton, N. P., & O'Hagan, N. (2006). High-throughput assays for DNA gyrase and other topoisomerases. *Nucleic Acids Research*, *34*(15), e104–e104. https://doi.org/10.1093/nar/gkl504

Mazurek, Ł., Ghilarov, D., Michalczyk, E., Pakosz, Z., Metelev, M., Czyszczoń, W., Wawro, K., Behroz, I., Dubiley, S., Süssmuth, R. D., & Heddle, J. G. (2021). Pentapeptide repeat protein QnrB1 requires ATP hydrolysis to rejuvenate poisoned gyrase complexes. *Nucleic Acids Research*, *49*(3), 1581–1596. https://doi.org/10.1093/nar/gkaa1266

Melnyk, A. H., Wong, A., & Kassen, R. (2015). The fitness costs of antibiotic resistance mutations. *Evolutionary Applications*, *8*(3), 273–283. https://doi.org/10.1111/eva.12196

Mérens, A., Matrat, S., Aubry, A., Lascols, C., Jarlier, V., Soussy, C.-J., Cavallo, J.-D., & Cambau, E. (2009). The Pentapeptide Repeat Proteins MfpA_{Mt} and QnrB4 Exhibit Opposite Effects on DNA Gyrase Catalytic Reactions and on the Ternary Gyrase-DNA-Quinolone Complex. *Journal of Bacteriology*, *191*(5), 1587. https://doi.org/10.1128/JB.01205-08

Mirzaii, M., Jamshidi, S., Zamanzadeh, M., Marashifard, M., Malek Hosseini, S. A. A., Haeili, M., Jahanbin, F., Mansouri, F., Darban-Sarokhalil, D., & Khoramrooz, S. S. (2018). Determination of gyrA and parC mutations and prevalence of plasmid-mediated quinolone resistance genes in Escherichia coli and Klebsiella pneumoniae isolated from patients with urinary tract infection in Iran. *Journal of Global*

Antimicrobial Resistance, *13*, 197–200. https://doi.org/https://doi.org/10.1016/j.jgar.2018.04.017

Monochamus Sutor. (2018). *DNA gyrase catalytic cycle*. Https://En.Wikipedia.Org/Wiki/DNA_gyrase#/Media/File:Gyrase_catalytic_cycle_eng_Sutormin_eng.Png .

Morales, E. S., Parcerisa, I. L., & Ceccarelli, E. A. (2019). A novel method for removing contaminant Hsp70 molecular chaperones from recombinant proteins. *Protein Science : A Publication of the Protein Society*, *28*(4), 800–807. https://doi.org/10.1002/pro.3574

Munita, J. M., & Arias, C. A. (2016). Mechanisms of Antibiotic Resistance. *Microbiology Spectrum*, *4*(2), 10.1128/microbiolspec.VMBF-0016–2015. https://doi.org/10.1128/microbiolspec.VMBF-0016-2015

NanoTemper Technologies. (2021, March). *User Manual Monolith® NT.115*. Https://Www2.Helsinki.Fi/Sites/Default/Files/Atoms/Files/Manual_nt115.Pdf.

Neuman, K. C., Charvin, G., Bensimon, D., & Croquette, V. (2009). Mechanisms of chiral discrimination by topoisomerase IV. *Proceedings of the National Academy of Sciences*, *106*(17), 6986. https://doi.org/10.1073/pnas.0900574106

Norsk overvåkningssystem for antibiotika resistens hos mikrober & Norsk overvåkningssystem for antibiotika resistens hos mikrober fra fôr og dyr og næringsmidler. (2019). *Usage of Antimicrobial Agents and Occurrence of Antimicrobial Resistance in Norway*. https://www.fhi.no/globalassets/dokumenterfiler/rapporter/2020/norm-norm-vet-rapport/norm-norm-vet-2019_komplett.pdf

Oteo, J., Navarro, C., Cercenado, E., Delgado-Iribarren, A., Wilhelmi, I., Orden, B., García, C., Miguelañez, S., Pérez-Vázquez, M., García-Cobos, S., Aracil, B., Bautista, V., & Campos, J. (2006). Spread of Escherichia coli Strains with High-Level Cefotaxime and Ceftazidime Resistance between the Community, Long-Term Care Facilities, and Hospital Institutions. *Journal of Clinical Microbiology*, *44*(7), 2359. https://doi.org/10.1128/JCM.00447-06

Ozeki, S., Deguchi, T., Yasuda, M., Nakano, M., Kawamura, T., Nishino, Y., & Kawada, Y. (1997). Development of a rapid assay for detecting gyrA mutations in Escherichia coli and determination of incidence of gyrA mutations in clinical strains isolated from patients with complicated urinary tract infections. *Journal of Clinical Microbiology*, *35*(9), 2315–2319. https://doi.org/10.1128/JCM.35.9.2315-2319.1997

Pagès, J.-M., James, C. E., & Winterhalter, M. (2008). The porin and the permeating antibiotic: a selective diffusion barrier in Gram-negative bacteria. *Nature Reviews Microbiology*, *6*(12), 893–903. https://doi.org/10.1038/nrmicro1994

Pan, X.-S., & Fisher, L. M. (1999). Streptococcus pneumoniae DNA Gyrase and Topoisomerase IV: Overexpression, Purification, and Differential Inhibition by Fluoroquinolones. *Antimicrobial Agents and Chemotherapy*, *43*(5). https://doi.org/10.1128/AAC.43.5.1129

Pankey, G. A., & Sabath, L. D. (2004). Clinical Relevance of Bacteriostatic versus Bactericidal Mechanisms of Action in the Treatment of Gram-Positive Bacterial Infections. *Clinical Infectious Diseases*, *38*(6), 864–870. https://doi.org/10.1086/381972

Patching, S. G. (2014). Surface plasmon resonance spectroscopy for characterisation of membrane protein–ligand interactions and its potential for drug discovery. *Biochimica et Biophysica Acta (BBA) - Biomembranes*, *1838*(1, Part A), 43–55. https://doi.org/https://doi.org/10.1016/j.bbamem.2013.04.028

Périchon, B., Courvalin, P., & Galimand, M. (2007). Transferable resistance to aminoglycosides by methylation of G1405 in 16S rRNA and to hydrophilic fluoroquinolones by QepA-mediated efflux in Escherichia coli. *Antimicrobial Agents and Chemotherapy*, *51*(7), 2464–2469. https://doi.org/10.1128/AAC.00143-07

Peter, B. J., Ullsperger, C., Hiasa, H., Marians, K. J., & Cozzarelli, N. R. (1998). The Structure of Supercoiled Intermediates in DNA Replication. *Cell*, *94*(6), 819–827. https://doi.org/https://doi.org/10.1016/S0092-8674(00)81740-7

Pham, T. D. M., Ziora, Z. M., & Blaskovich, M. A. T. (2019). Quinolone antibiotics. *MedChemComm*, *10*(10), 1719–1739. https://doi.org/10.1039/c9md00120d

Piddock, L. J., Walters, R. N., & Diver, J. M. (1990). Correlation of quinolone MIC and inhibition of DNA, RNA, and protein synthesis and induction of the SOS response in Escherichia coli. *Antimicrobial Agents and Chemotherapy*, *34*(12), 2331. https://doi.org/10.1128/AAC.34.12.2331

Pinho, M. G., de Lencastre, H., & Tomasz, A. (2001). An acquired and a native penicillin-binding protein cooperate in building the cell wall of drug-resistant staphylococci. *Proceedings of the National Academy of Sciences of the United States of America*, *98*(19), 10886–10891. https://doi.org/10.1073/pnas.191260798

Poirel, L., Liard, A., Rodriguez-Martinez, J.-M., & Nordmann, P. (2005). Vibrionaceae as a possible source of Qnr-like quinolone resistance determinants. *Journal of Antimicrobial Chemotherapy*, *56*(6), 1118–1121. https://doi.org/10.1093/jac/dki371

Poirel, L., Rodriguez-Martinez, J.-M., Mammeri, H., Liard, A., & Nordmann, P. (2005). Origin of Plasmid-Mediated Quinolone Resistance Determinant QnrA. *Antimicrobial Agents and Chemotherapy*, *49*(8), 3523. https://doi.org/10.1128/AAC.49.8.3523-3525.2005

Poole, K. (2005). Efflux-mediated antimicrobial resistance. *Journal of Antimicrobial Chemotherapy*, *56*(1), 20–51. https://doi.org/10.1093/jac/dki171

Postow, L., Crisona, N. J., Peter, B. J., Hardy, C. D., & Cozzarelli, N. R. (2001). Topological challenges to DNA replication: Conformations at the fork. *Proceedings of the National Academy of Sciences*, *98*(15), 8219. https://doi.org/10.1073/pnas.111006998

Pourahmad Jaktaji, R., & Mohiti, E. (2010). Study of Mutations in the DNA gyrase gyrA Gene of Escherichia coli. *Iranian Journal of Pharmaceutical Research : IJPR*, *9*(1), 43–48. https://pubmed.ncbi.nlm.nih.gov/24363705

Ratelade, J., Miot, M.-C., Johnson, E., Betton, J.-M., Mazodier, P., & Benaroudj, N. (2009). Production of Recombinant Proteins in the lon-Deficient BL21(DE3) Strain of Escherichia coli in the Absence of the DnaK Chaperone. *Applied and Environmental Microbiology*, *75*(11), 3803. https://doi.org/10.1128/AEM.00255-09

Reyes-Domínguez, Y., Contreras-Ferrat, G., Ramírez-Santos, J., Membrillo-Hernández, J., & Gómez-Eichelmann, M. C. (2003). Plasmid DNA supercoiling and gyrase activity in Escherichia coli wild-type and rpoS stationary-phase cells. *Journal of Bacteriology*, *185*(3), 1097–1100. https://doi.org/10.1128/jb.185.3.1097-1100.2003

Reygaert, W. C. (2018). An overview of the antimicrobial resistance mechanisms of bacteria. *AIMS Microbiology*, *4*(3), 482–501. https://doi.org/10.3934/microbiol.2018.3.482

Rial, D. V, & Ceccarelli, E. A. (2002). Removal of DnaK contamination during fusion protein purifications. *Protein Expression and Purification*, *25*(3), 503–507. https://doi.org/https://doi.org/10.1016/S1046-5928(02)00024-4

Rizkia, P. R., Silaban, S., Hasan, K., Kamara, D. S., Subroto, T., Soemitro, S., & Maksum, I. P. (2015). Effect of Isopropyl-β-D-thiogalactopyranoside Concentration on Prethrombin-2 Recombinan Gene Expression in Escherichia Coli ER2566. *Procedia Chemistry*, *17*, 118–124. https://doi.org/https://doi.org/10.1016/j.proche.2015.12.121

Robicsek, A., Strahilevitz, J., Jacoby, G. A., Macielag, M., Abbanat, D., Hye Park, C., Bush, K., & Hooper, D. C. (2006). Fluoroquinolone-modifying enzyme: a new adaptation of a common aminoglycoside acetyltransferase. *Nature Medicine*, *12*(1), 83–88. https://doi.org/10.1038/nm1347

Roca, J., & Wang, J. C. (1992). The capture of a DNA double helix by an ATP-dependent protein clamp: A key step in DNA transport by type II DNA topoisomerases. *Cell*, *71*(5). https://doi.org/10.1016/0092-8674(92)90558-T

Rodríguez-Martínez, J. M., Pascual, A., García, I., & Martínez-Martínez, L. (2003). Detection of the plasmid-mediated quinolone resistance determinant qnr among clinical isolates of Klebsiella pneumoniae

producing AmpC-type β-lactamase. *Journal of Antimicrobial Chemotherapy*, *52*(4), 703–706. https://doi.org/10.1093/jac/dkg388

Rodríguez-Martínez, J. M., Velasco, C., Briales, A., García, I., Conejo, M. C., & Pascual, A. (2008). Qnr-like pentapeptide repeat proteins in Gram-positive bacteria. *Journal of Antimicrobial Chemotherapy*, *61*(6), 1240–1243. https://doi.org/10.1093/jac/dkn115

Rubinstein, E., & Lagacé-Wiens, P. (2017). 144 - Quinolones. In J. Cohen, W. G. Powderly, & S. M. Opal (Eds.), *Infectious Diseases (Fourth Edition)* (pp. 1239-1248.e2). Elsevier. https://doi.org/https://doi.org/10.1016/B978-0-7020-6285-8.00144-1

Sanz-García, F., Anoz-Carbonell, E., Pérez-Herrán, E., Martín, C., Lucía, A., Rodrigues, L., & Aínsa, J. A. (2019). Mycobacterial Aminoglycoside Acetyltransferases: A Little of Drug Resistance, and a Lot of Other Roles. *Frontiers in Microbiology*, *10*. https://doi.org/10.3389/fmicb.2019.00046

Schleif, R. (2010). AraC protein, regulation of the l-arabinose operon in Escherichia coli, and the light switch mechanism of AraC action. *FEMS Microbiology Reviews*, *34*(5), 779–796. https://doi.org/10.1111/j.1574-6976.2010.00226.x

Schrödinger LLC. (2015). *The PyMOL Molecular Graphics System, Version~1.8*.

Shah, S., & Heddle, J. G. (2014). Squaring up to DNA: pentapeptide repeat proteins and DNA mimicry. *Applied Microbiology and Biotechnology*, *98*(23), 9545–9560. https://doi.org/10.1007/s00253-014-6151-3

Shea, M. E., & Hiasa, H. (2003). The RuvAB Branch Migration Complex Can Displace Topoisomerase IV·Quinolone·DNA Ternary Complexes*. *Journal of Biological Chemistry*, *278*(48), 48485–48490. https://doi.org/https://doi.org/10.1074/jbc.M304217200

Sigma Aldrich. (n.d.). *Amino Acids Reference Charts*. Https://Www.Sigmaaldrich.Com/Life-Science/Metabolomics/Learning-Center/Amino-Acid-Reference-Chart.Html.

Singh, P., Jain, A., Dixit, P., Prakash, S., Jaiswal, I., Venkatesh, V., & Singh, M. (2015). Prevalence of gyrA and B gene mutations in fluoroquinolone-resistant and -sensitive clinical isolates of Mycobacterium tuberculosis and their relationship with MIC of ofloxacin. *The Journal of Antibiotics*, *68*(1), 63–66. https://doi.org/10.1038/ja.2014.95

Soczek, K. M., Grant, T., Rosenthal, P. B., & Mondragón, A. (2018). CryoEM structures of open dimers of gyrase A in complex with DNA illuminate mechanism of strand passage. *ELife*, *7*. https://doi.org/10.7554/eLife.41215

Spriestersbach, A., Kubicek, J., Schäfer, F., Block, H., & Maertens, B. (2015). Chapter One - Purification of His-Tagged Proteins. In J. R. Lorsch (Ed.), *Methods in Enzymology* (Vol. 559, pp. 1–15). Academic Press. https://doi.org/https://doi.org/10.1016/bs.mie.2014.11.003

Stamey, T. A. (1976). Resistance to Nalidixic Acid: A Misconception Due to Underdosage. *JAMA*, *236*(16), 1857–1860. https://doi.org/10.1001/jama.1976.03270170023019

Stein, G. E. (1988). The 4-Quinolone Antibiotics: Past, Present, and Future. *Pharmacotherapy: The Journal of Human Pharmacology and Drug Therapy*, *8*(6). https://doi.org/10.1002/j.1875-9114.1988.tb04088.x

Stelljes, J. T., Weidlich, D., Gubaev, A., & Klostermeier, D. (2018). Gyrase containing a single C-terminal domain catalyzes negative supercoiling of DNA by decreasing the linking number in steps of two. *Nucleic Acids Research*, *46*(13), 6773–6784. https://doi.org/10.1093/nar/gky470

Strahilevitz, J., Jacoby, G. A., Hooper, D. C., & Robicsek, A. (2009). Plasmid-mediated quinolone resistance: a multifaceted threat. *Clinical Microbiology Reviews*, *22*(4), 664–689. https://doi.org/10.1128/CMR.00016-09

Tamayo, M., Santiso, R., Gosalvez, J., Bou, G., & Fernández, J. L. (2009). Rapid assessment of the effect of ciprofloxacin on chromosomal DNA from Escherichia coli using an in situ DNA fragmentation assay. *BMC Microbiology*, *9*(1), 69. https://doi.org/10.1186/1471-2180-9-69

Tavío, M. M., Jacoby, G. A., & Hooper, D. C. (2014). QnrS1 structure-activity relationships. *The Journal of Antimicrobial Chemotherapy*, *69*(8), 2102–2109. https://doi.org/10.1093/jac/dku102

Terahara, F., & Nishiura, H. (2019). Fluoroquinolone consumption and Escherichia coli resistance in Japan: an ecological study. *BMC Public Health*, *19*(1), 426. https://doi.org/10.1186/s12889-019-6804-3

The European Committee on Antimicrobial Susceptibility Testing. (2021a). *MIC and Inhibition zone diameter distributions of microorganisms without and with phenotypically evident resistance mechanisms*. Https://Mic.Eucast.Org/.

The European Committee on Antimicrobial Susceptibility Testing. (2021b). *The European Committee on Antimicrobial Susceptibility Testing*. Https://Www.Eucast.Org/.

The European Committee on Antimicrobial Susceptibility Testing. (2021c, January). *EUCAST reading guide for broth microdilution*. Https://Www.Eucast.Org/Ast_of_bacteria/Mic_determination/?No_cache=1.

Toh, S.-M., Xiong, L., Arias, C. A., Villegas, M. V, Lolans, K., Quinn, J., & Mankin, A. S. (2007). Acquisition of a natural resistance gene renders a clinical strain of methicillin-resistant Staphylococcus aureus resistant to the synthetic antibiotic linezolid. *Molecular Microbiology*, *64*(6), 1506–1514. https://doi.org/10.1111/j.1365-2958.2007.05744.x

Tran, J. H., & Jacoby, G. A. (2002). Mechanism of plasmid-mediated quinolone resistance. *Proceedings of the National Academy of Sciences of the United States of America*, *99*(8), 5638–5642. https://doi.org/10.1073/pnas.082092899

Tran, J. H., Jacoby, G. A., & Hooper, D. C. (2005a). Interaction of the plasmid-encoded quinolone resistance protein Qnr with Escherichia coli DNA gyrase. *Antimicrobial Agents and Chemotherapy*, *49*(1), 118–125. https://doi.org/10.1128/AAC.49.1.118-125.2005

Tran, J. H., Jacoby, G. A., & Hooper, D. C. (2005b). Interaction of the plasmid-encoded quinolone resistance protein QnrA with Escherichia coli topoisomerase IV. *Antimicrobial Agents and Chemotherapy*, *49*(7), 3050–3052. https://doi.org/10.1128/AAC.49.7.3050-3052.2005

Vagenende, V., Yap, M. G. S., & Trout, B. L. (2009). Mechanisms of Protein Stabilization and Prevention of Protein Aggregation by Glycerol. *Biochemistry*, *48*(46), 11084–11096. https://doi.org/10.1021/bi900649t

Vanden Broeck, A., Lotz, C., Ortiz, J., & Lamour, V. (2019). Cryo-EM structure of the complete E. coli DNA gyrase nucleoprotein complex. *Nature Communications*, *10*(1), 4935. https://doi.org/10.1038/s41467-019-12914-y

Vedantam, G., Guay, G. G., Austria, N. E., Doktor, S. Z., & Nichols, B. P. (1998). Characterization of mutations contributing to sulfathiazole resistance in Escherichia coli. *Antimicrobial Agents and Chemotherapy*, *42*(1), 88–93. https://doi.org/10.1128/AAC.42.1.88

Velasco, C., Rodríguez-Martínez, J. M., Briales, A., Díaz de Alba, P., Calvo, J., & Pascual, A. (2010). Smaqnr, a new chromosome-encoded quinolone resistance determinant in Serratia marcescens. *Journal of Antimicrobial Chemotherapy*, *65*(2), 239–242. https://doi.org/10.1093/jac/dkp424

Ventola, C. L. (2015). The antibiotic resistance crisis: part 1: causes and threats. *P & T : A Peer-Reviewed Journal for Formulary Management*, *40*(4), 277–283. https://pubmed.ncbi.nlm.nih.gov/25859123

Veterinærinsituttet. (2016). *QREC-MaP - Quinolone resistance despite low antimicrobial usage – mechanisms and possible preventive measures*. Https://Www.Vetinst.No/Forskning-Innovasjon/Pagaende-Forskningsprosjekter/Quinolone-Resistance-despite-Low-Antimicrobial-Usage--Mechanisms-and-Possible-Preventive-Measures-Qrec-Map.

Vetting, M. W., Hegde, S. S., Wang, M., Jacoby, G. A., Hooper, D. C., & Blanchard, J. S. (2011). Structure of QnrB1, a Plasmid-mediated Fluoroquinolone Resistance Factor*. *Journal of Biological Chemistry*, *286*(28), 25265–25273. https://doi.org/https://doi.org/10.1074/jbc.M111.226936

Vos, S. M., Tretter, E. M., Schmidt, B. H., & Berger, J. M. (2011). All tangled up: how cells direct, manage and exploit topoisomerase function. *Nature Reviews Molecular Cell Biology*, *12*(12), 827–841.

https://doi.org/10.1038/nrm3228

Walch, G., Knapp, M., Rainer, G., & Peintner, U. (2016). Colony-PCR Is a Rapid Method for DNA Amplification of Hyphomycetes. *Journal of Fungi (Basel, Switzerland)*, *2*(2), 12. https://doi.org/10.3390/jof2020012

Wang, J. C. (1998). Moving one DNA double helix through another by a type II DNA topoisomerase: the story of a simple molecular machine. *Quarterly Reviews of Biophysics*, *31*(2), 107–144. https://doi.org/DOI: 10.1017/S0033583598003424

Wang, M., Sahm, D. F., Jacoby, G. A., & Hooper, D. C. (2004). Emerging plasmid-mediated quinolone resistance associated with the qnr gene in Klebsiella pneumoniae clinical isolates in the United States. *Antimicrobial Agents and Chemotherapy*, *48*(4), 1295–1299. https://doi.org/10.1128/aac.48.4.1295-1299.2004

Wang, M., Tran, J. H., Jacoby, G. A., Zhang, Y., Wang, F., & Hooper, D. C. (2003). Plasmid-mediated quinolone resistance in clinical isolates of Escherichia coli from Shanghai, China. *Antimicrobial Agents and Chemotherapy*, *47*(7), 2242–2248. https://doi.org/10.1128/aac.47.7.2242-2248.2003

Waterhouse, A. M., Procter, J. B., Martin, D. M. A., Clamp, M., & Barton, G. J. (2009). Jalview Version 2--a multiple sequence alignment editor and analysis workbench. *Bioinformatics (Oxford, England)*, *25*(9), 1189–1191. https://doi.org/10.1093/bioinformatics/btp033

William Studier, F., Rosenberg, A. H., Dunn, J. J., & Dubendorff, J. W. (1990). [6] Use of T7 RNA polymerase to direct expression of cloned genes. In *Methods in Enzymology* (Vol. 185, pp. 60–89). Academic Press. https://doi.org/https://doi.org/10.1016/0076-6879(90)85008-C

Wohlkonig, A., Chan, P. F., Fosberry, A. P., Homes, P., Huang, J., Kranz, M., Leydon, V. R., Miles, T. J., Pearson, N. D., Perera, R. L., Shillings, A. J., Gwynn, M. N., & Bax, B. D. (2010). Structural basis of quinolone inhibition of type IIA topoisomerases and target-mediated resistance. *Nature Structural & Molecular Biology*, *17*(9), 1152–1153. https://doi.org/10.1038/nsmb.1892

World Health Organization. (2019). *Highest Priority Critically Important Antimicrobials*. Https://Www.Who.Int/Foodsafety/Cia/En/.

World Health Organization. (2021). *Antibiotic resistance*. Https://Www.Who.Int/News-Room/Fact-Sheets/Detail/Antibiotic-Resistance.

Wright, G. D. (2010). Q&A: Antibiotic resistance: where does it come from and what can we do about it? *BMC Biology*, *8*(1), 123. https://doi.org/10.1186/1741-7007-8-123

Xiong, X., Bromley, E. H. C., Oelschlaeger, P., Woolfson, D. N., & Spencer, J. (2011). Structural insights into quinolone antibiotic resistance mediated by pentapeptide repeat proteins: conserved surface loops direct the activity of a Qnr protein from a gram-negative bacterium. *Nucleic Acids Research*, *39*(9), 3917–3927. https://doi.org/10.1093/nar/gkq1296

Yamane, K., Wachino, J.-I., Suzuki, S., Kimura, K., Shibata, N., Kato, H., Shibayama, K., Konda, T., & Arakawa, Y. (2007). New plasmid-mediated fluoroquinolone efflux pump, QepA, found in an Escherichia coli clinical isolate. *Antimicrobial Agents and Chemotherapy*, *51*(9), 3354–3360. https://doi.org/10.1128/AAC.00339-07

Yigit, H., Queenan, A. M., Anderson, G. J., Domenech-Sanchez, A., Biddle, J. W., Steward, C. D., Alberti, S., Bush, K., & Tenover, F. C. (2001). Novel carbapenem-hydrolyzing beta-lactamase, KPC-1, from a carbapenem-resistant strain of Klebsiella pneumoniae. *Antimicrobial Agents and Chemotherapy*, *45*(4), 1151–1161. https://doi.org/10.1128/AAC.45.4.1151-1161.2001

Yoo, J.-H., Huh, D.-H., Choi, J.-H., Shin, W.-S., Kang, M.-W., Kim, C.-C., & Kim, D.-J. (1997). Molecular Epidemiological Analysis of Quinolone-Resistant Escherichia coli Causing Bacteremia in Neutropenic Patients with Leukemia in Korea. *Clinical Infectious Diseases*, *25*(6), 1385–1391. https://doi.org/10.1086/516132

Yoshida, H., Bogaki, M., Nakamura, M., & Nakamura, S. (1990). Quinolone resistance-determining region in

the DNA gyrase gyrA gene of Escherichia coli. *Antimicrobial Agents and Chemotherapy*, *34*(6), 1271. https://doi.org/10.1128/AAC.34.6.1271

Yoshida, H., Bogaki, M., Nakamura, M., Yamanaka, L. M., & Nakamura, S. (1991). Quinolone resistance-determining region in the DNA gyrase gyrB gene of Escherichia coli. *Antimicrobial Agents and Chemotherapy*, *35*(8), 1647. https://doi.org/10.1128/AAC.35.8.1647

Zhang, R., Ni, S., & Kennedy, M. A. (2019). Type I beta turns make a new twist in pentapeptide repeat proteins: Crystal structure of Alr5209 from Nostoc sp. PCC 7120 determined at 1.7 angström resolution. *Journal of Structural Biology: X*, *3*, 100010. https://doi.org/https://doi.org/10.1016/j.yjsbx.2019.100010

Zhu, D.-M., Li, Q.-H., Shen, Y., & Zhang, Q. (2020). Risk factors for quinolone-resistant Escherichia coli infection: a systematic review and meta-analysis. *Antimicrobial Resistance & Infection Control*, *9*(1), 11. https://doi.org/10.1186/s13756-019-0675-3

Zhu, D., Zheng, M., Xu, J., Wang, M., Jia, R., Chen, S., Liu, M., Zhao, X., Yang, Q., Wu, Y., Zhang, S., Huang, J., Liu, Y., Zhang, L., Yu, Y., Pan, L., Chen, X., & Cheng, A. (2019). Prevalence of fluoroquinolone resistance and mutations in the gyrA, parC and parE genes of Riemerella anatipestifer isolated from ducks in China. *BMC Microbiology*, *19*(1), 271. https://doi.org/10.1186/s12866-019-1659-4

Zimmermann, L., Stephens, A., Nam, S.-Z., Rau, D., Kübler, J., Lozajic, M., Gabler, F., Söding, J., Lupas, A. N., & Alva, V. (2018). A Completely Reimplemented MPI Bioinformatics Toolkit with a New HHpred Server at its Core. *Journal of Molecular Biology*, *430*(15), 2237–2243. https://doi.org/https://doi.org/10.1016/j.jmb.2017.12.007

Appendix

Appendix A: Bacteria and primers

Table S1. Strains used in this work. This includes the name of strain and name used in the thesis, the gene of interest, purpose and the origin.

Bacterial strain	DNA sequence of interest	Purpose	Name used	Origin
E.coli DHα; AH285	-	Cloning, broth microdilution assays	DHα	Thermo Fisher Scientific
E.coli BL21 (DE3); AH1498	-	Protein Expression, broth microdilution assays	BL21	Thermo Fisher Scientific
E.coli; 2015-01-5022	GyrA-S83L	Genomic DNA extraction, broth microdilution assays, growth assays	GyrA-S83L-5022	NVI
E.coli; 2014-01-1891	GyrA-WT	Genomic DNA extraction	GyrA-WT-1891	NVI
E.coli; 2006-01-1085	GyrA-WT	Broth microdilution assay, growth assay	GyrA-WT-1085	NVI
E.coli; 2016-17-292	QnrS1	Genomic DNA extraction	QnrS1-292	NVI
E.coli; 2016-01-725-2	QnrS2	Genomic DNA extraction	QnrS2-725	NVI

E.coli; 2015-01-1826	QnrB19	Genomic DNA extraction	QnrB19-1826	NVI

Table S2. Primer used in this study listed with sequence, name, annealing temperature and its purpose.

Primer sequence	**Name**	**Annealing temperature**	**Purpose**
5′-ATATATTCTAGAAAGGAGATATACCATGAGCGACCTTGCGAGAG-3′	GyrA-For	60 °C	Cloning primer for GyrA-S83L and GyrA-WT
5′-ATATATGGATCCTTAGTGGTGATGATGGTGGTGTTCTTCTTCTGGCTCGTCGT-3′	GyrA-Rev	60 °C	Cloning primer GyrA-S83L and GyrA-WT
5′-ATATATCCATGGAAACCTACAATCATACAT-3′	QnrS1-For	58 °C	Cloning primer for QnrS1
5′-ATATATGGATCCTTAGTGGTGATGATGGTGGTGGTCAGGATAAACAACAATACC-3′	QnrS1-Rev	58 °C	Cloning primer for QnrS1
5′-ATATATCCATGGAAACCTACCGTCACAC-3′	QnrS2-For	60 °C	Cloning primer for QnrS2
5′-ATATATGGATCCCTAGTGGTGATGATGGTGGTGGTCAGGAAAAACAACAATACC-3′	QnrS2-Rev	58 °C	Cloning primer for QnrS2
5′-ATATATTCTAGAAAGGAGATATACCATGACTCTGGCATTAGTTGG-3′	QnrB19-For	58 °C	Cloning primer for QnrB19

5′-ATATATGGATCCCTAGTGGTGATGATGGTGGTGACCAATCACAGCGATGCCA-3′	QnrB19-Rev	58 °C	Cloning primer for QnrB19
5- ACCTGTGGCGCCGGTGA-3	pET28-For	58 °C	Colony PCR and sequencing of pET28a(+) constructs
5-TCAGCGGTGGCAGCAGC-3	pET28-Rev	58 °C	Colony PCR and sequencing of pET28a(+) constructs
5′-GATGGCCGATCTCGAAAAA-3′	GyrA-1	56 °C	Sequencing of GyrA
5′-TGCGCATCGTGATTGAAGT-3′	GyrA-2	56 °C	Sequencing of GyrA
5′-GGTCTTGAGCACGAAAAAC-3′	GyrA-3	56 °C	Sequencing of GyrA
5’-TATGCCATAGCATTTTTATCC-3’	pBAD30-For	56 °C	Colony PCR and sequencing of pBAD30 contructs
5’-TCTGATTTAATCTGTATCAGG-3’	pBAD30-Rev	56 °C	Colony PCR and sequencing of pBAD30 contructs

Table S3. List of stock bacteria prepared in this study. Listed with name describing bacteria, insert of interest, vector type and cell type.

Name	Insert	Vector	Cells
DHα (pET28a- GyrA S83L)	GyrA S83L	pET28a	*E.coli;* DHα
BL21 (pET28a- GyrA S83L)	GyrA S83L	pET28a	*E.coli;* BL21 (DE3)
DHα (pET28a- GyrA WT)	GyrA WT	pET28a	*E.coli;* DHα
BL21 (pET28a- GyrA WT)	GyrA WT	pET28a	*E.coli;* BL21 (DE3)
DHα (pET28a- QnrS1)	QnrS1	pET28a	*E.coli;* DHα
BL21 (pET28a- QnrS1)	QnrS1	pET28a	*E.coli;* BL21 (DE3)
DHα (pBAD30- QnrS1)	QnrS1	pBAD30	*E.coli;* DHα
BL21 (pBAD30- QnrS1)	QnrS1	pBAD30	*E.coli;* BL21 (DE3)
GyrA-S83L-5022 (pBAD30- QnrS1)	QnrS1	pBAD30	*E.coli*; 2015-01-5022
GyrA-WT-1085 (pBAD30- QnrS1)	QnrS1	pBAD30	*E.coli*; 2006-01-1085
DHα (pET28a- QnrS2)	QnrS2	pET28a	*E.coli;* DHα
BL21 (pET28a- QnrS2)	QnrS2	pET28a	*E.coli;* BL21 (DE3)
DHα (pBAD30- QnrS2)	QnrS2	pBAD30	*E.coli;* DHα
BL21 (pBAD30- QnrS2)	QnrS2	pBAD30	*E.coli;* BL21 (DE3)
GyrA-S83L-5022 (pBAD30- QnrS2)	QnrS2	pBAD30	*E.coli*; 2015-01-5022
GyrA-WT-1085 (pBAD30- QnrS2)	QnrS2	pBAD30	*E.coli*; 2006-01-1085
DHα (pET28a- QnrB19)	QnrB19	pET28a	*E.coli;* DHα
BL21 (pET28a- QnrB19)	QnrB19	pET28a	*E.coli;* BL21 (DE3)
DHα (pBAD30- QnrB19)	QnrB19	pBAD30	*E.coli;* DHα
BL21 (pBAD30- QnrB19)	QnrB19	pBAD30	*E.coli;* BL21 (DE3)
GyrA-S83L-5022 (pBAD30- QnrB19)	QnrB19	pBAD30	*E.coli*; 2015-01-5022
GyrA-WT-1085 (pBAD30- QnrB19)	QnrB19	pBAD30	*E.coli*; 2006-01-1085

Appendix B: Polymerase chain reaction

Table S4. Phusion DNA polymerase protocol (NEB)

Component	50 µL reaction	Final concentration	Manufacturer
Nuclease-free water	32,5 µL	-	-
5x Phusion HF Buffer	10 µL	1x	Thermo scientific
10 mM dNTPs	1 µL	200 µM	Invitrogen
10 µM Forward primer	2,5 µL	0.5 µM	Sigma
10 µM Revers primer	2,5 µL	0.5 µM	Sigma
Template DNA	1 µL	-	-
Phution DNA polymerase	0,5 µL	1.0 units/50 µL PCR	Thermo scientific

Table S5. Phusion DNA polymerase protocol (NEB) thermo cycling program.

Step	Temperature	Time
Initial denaturation	98 °C	30 s
34 cycles	98 °C 58°C-60 °C 72 °C	10 s 10 s 90 s
Final extension	72 °C	300 s
Hold	4 °C	∞

Table S6. Colony PCR Protocol with DreamTaq DNA polymerase (NEB)

Component	20 µL reaction	Final concentration	Manufacturer
50x dNTP mix (10 mM)	0,4 µL	200 µM	Invitrogen
10x Thermo Pol Buffer	2 µL	1x	Thermo scientific
Primer 1 (10 µM)	2 µL	1 µM	Sigma
Primer 2 (10 µM)	2 µL	1 µM	Sigma
Nuclease-free water	13,4 µL	-	-
Taq DNA Polymerase	0,2 µL	1,25 units/50 µL PCR	Thermo scientific

Table S7. Colony PCR Protocol with DreamTaq DNA polymerase (NEB) thermo cycling program

Step	Temperature	Time
Initial denaturation	95 °C	180 s
32 cycles	94 °C 58 °C/56 °C 72 °C	30 s 30 s 1 min/kb PCR Product
Final extension	72 °C	300 s
Hold	4 °C	∞

Appendix C: Supplementary figures

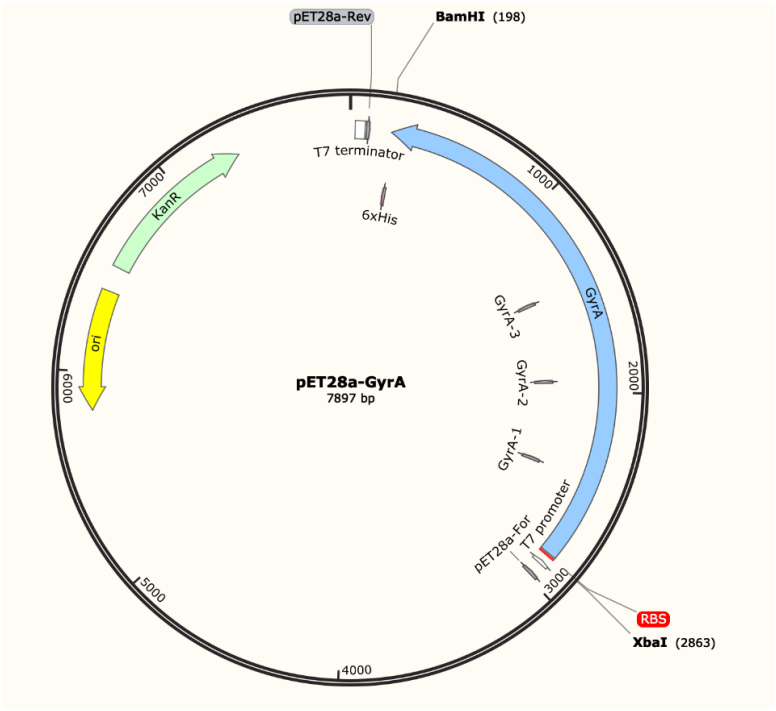

Figure S1. pET28a-GyrA construct used for protein expression. GyrA-S83L and GyrA WT are the same expect 1 point mutation at position 83. Placement of insert, restriction enzymes used in cloning, RBS, His-tag and annealing sites for primers are visualized. The figure was made in Snapgene.

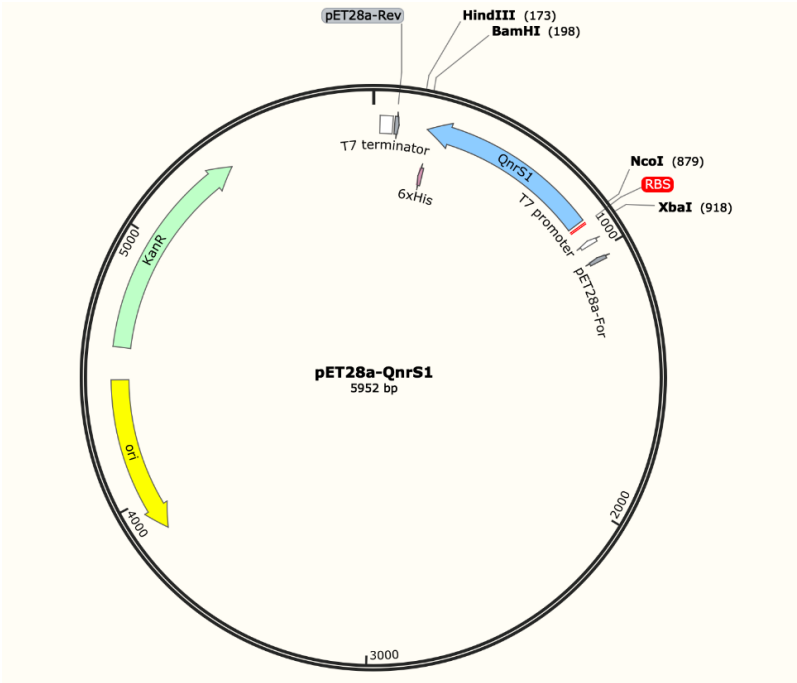

Figure S2. pET28a-QnrS1 construct used for protein expression. Placement of insert, restriction enzymes used in cloning and subcloning, RBS, His-tag and annealing sites for primers are visualized. The figure was made in Snapgene.

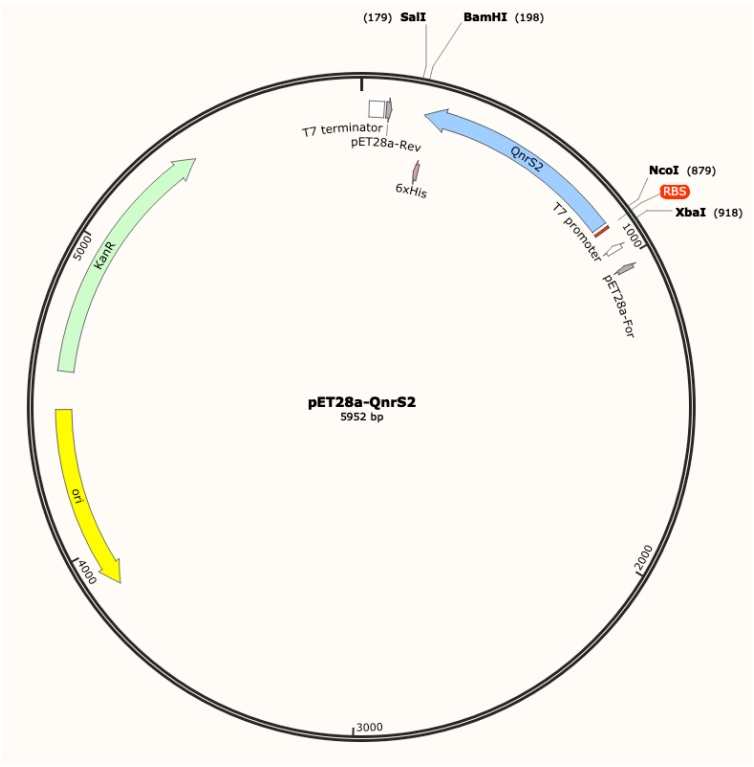

Figure S3. pET28a-QnrS2 construct used for protein expression. Placement of insert, restriction enzymes used in cloning and subcloning, RBS, His-tag and annealing sites for primers are visualized. The figure was made in Snapgene.

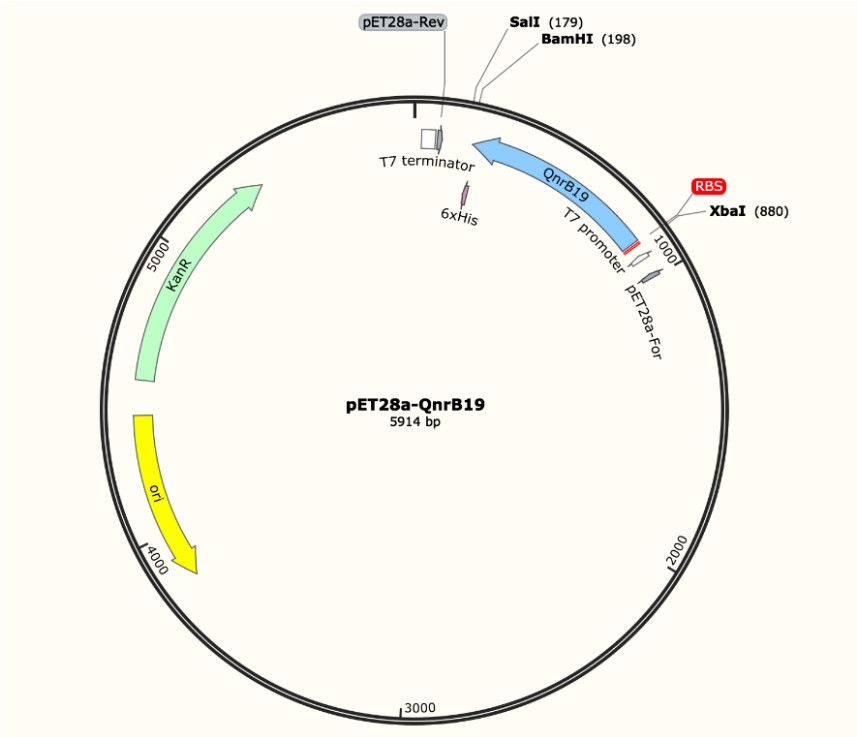

Figure S4. pET28a-QnrB19 construct used for protein expression. Placement of insert, restriction enzymes used in cloning and subcloning, RBS, His-tag and annealing sites for primers are visualized. Figure was made in Snapgene.

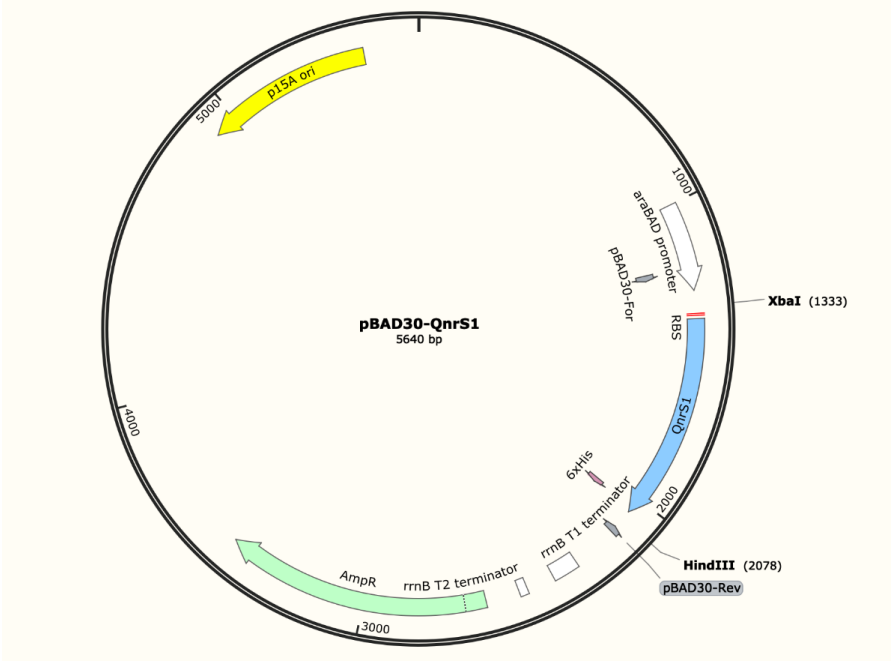

Figure S5. pBAD30-QnrS1 construct used for microbroth dilution and growth assays. Placement of insert, restriction enzymes used in subcloning, RBS, his-tag and annealing sites for primers are visualized. Figure was made in Snapgene.

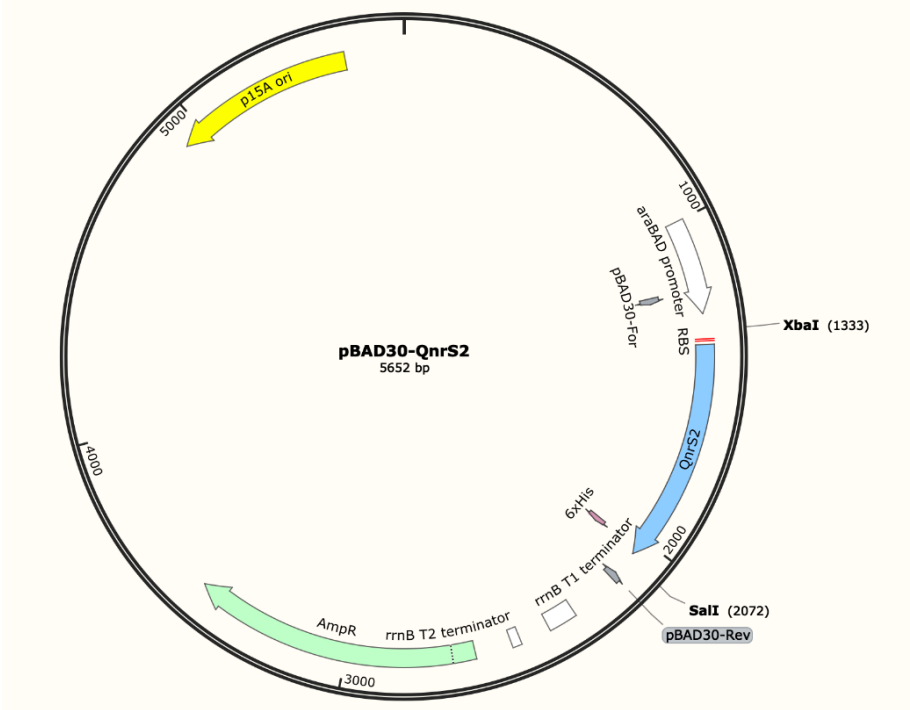

Figure S6. pBAD30-QnrS2 construct used for microbroth dilution and growth assays. Placement of insert, restriction enzymes used in subcloning, RBS, his-tag and annealing sites for primers are visualized. Figure was made in Snapgene.

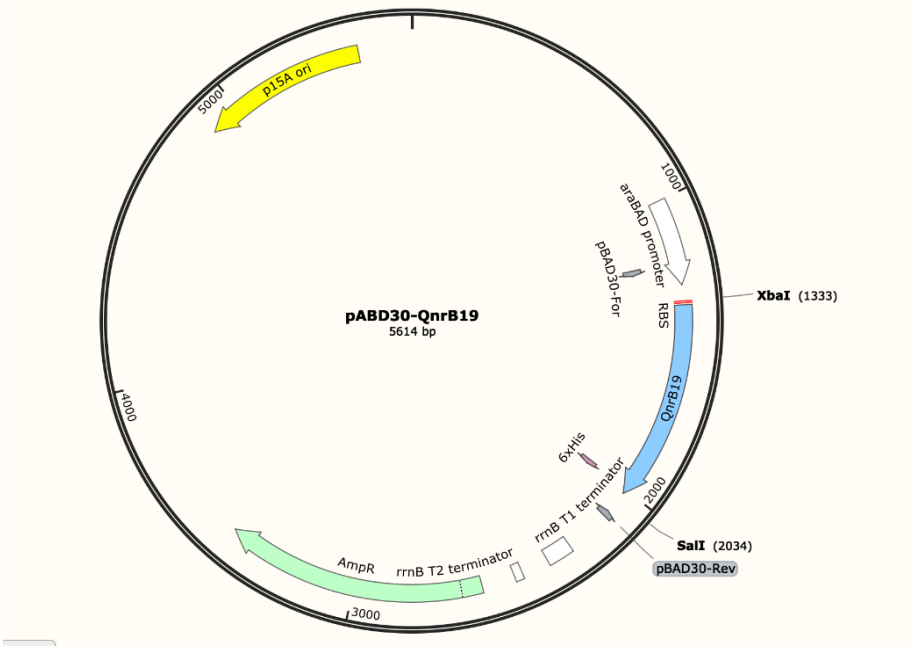

Figure S7. pBAD30-QnrB19 construct used for microbroth dilution and growth assays. Placement of insert, restriction enzymes used in subcloning, RBS, his-tag and annealing sites for primers are visualized. Figure was made in Snapgene.

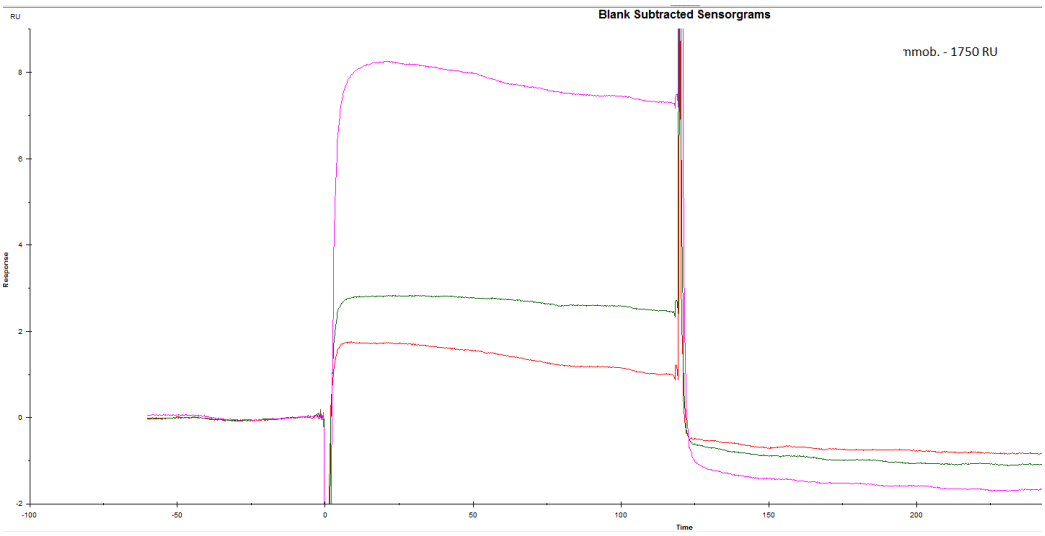

Figure S8. Blank subtracted curves of QnrS1 (125 nM- 1000 nM) interacting with GyrA WT (1750 RU immobilized) in channel 2, flowrate 30 µL/min. Both samples with 500 nM is removed.

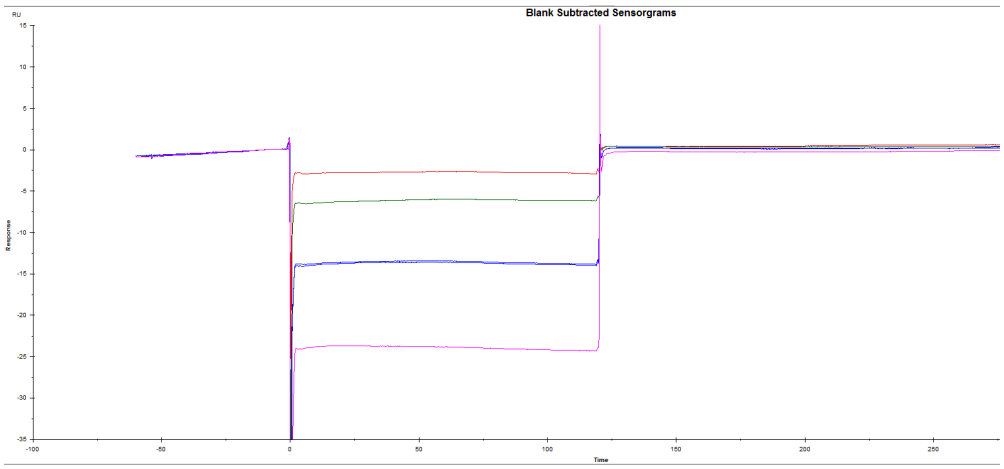

Figure S9. Blank subtracted curves of QnrS1 (125 nM- 1000 nM) interacting with GyrA S83L (1850 RU immobilized) in channel 4, flowrate 30 µL/min.

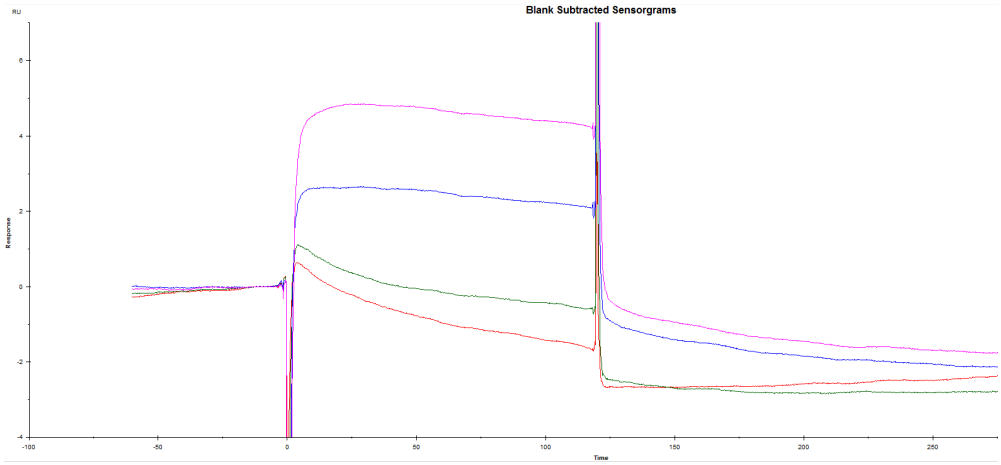

Figure S10. Blank subtracted curves of QnrS2 (125 nM- 1000 nM) interacting with GyrA WT (1750 RU immobilized) in channel 2, flowrate 30µL/min. One sample with 500 nM is removed.

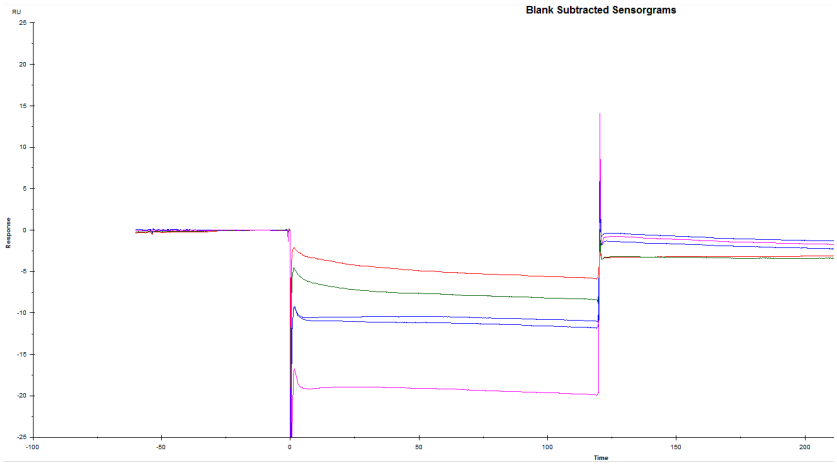

Figure S11. Blank subtracted curves of QnrS2 (125 nM- 1000 nM) interacting with GyrA S83L (1850 RU immobilized) in channel 4, flowrate 30 µL/min.

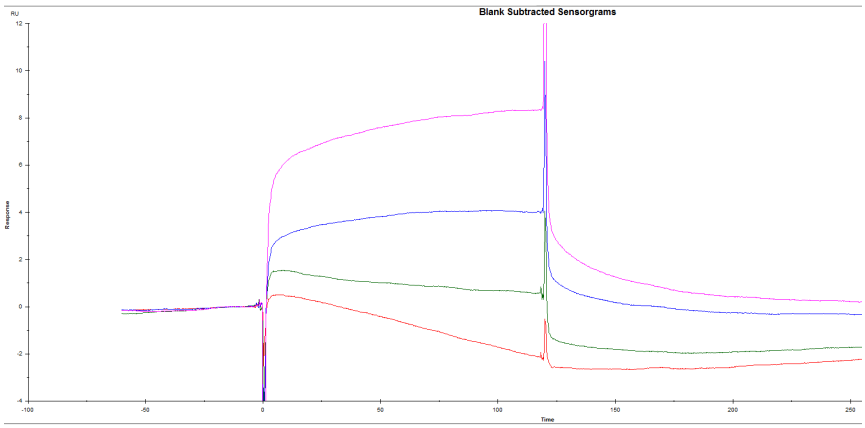

Figure S12. Black subtracted curves of QnrB19 (125 nM- 1000 nM) interacting with GyrA WT (1750 RU immobilized) in channel 2, flowrate 30 µL/min. One sample with 500 nM is removed.

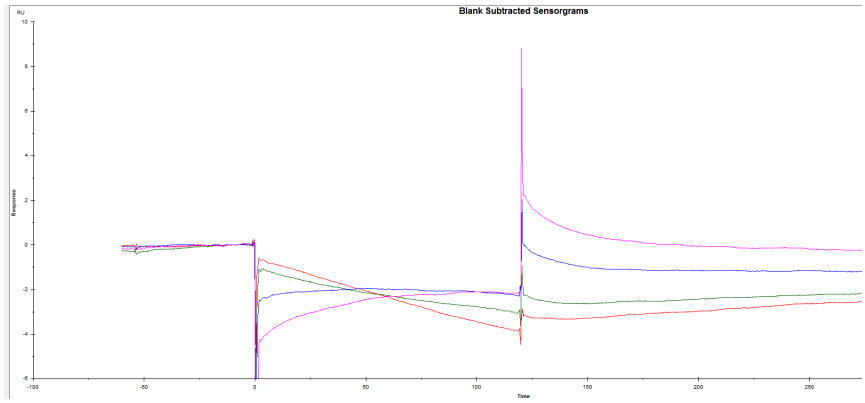

Figure S13. Black subtracted curves of QnrB19 (125 nM- 1000 nM) interacting with GyrA WT (1850 RU immobilized) in channel 4, flowrate 30 µL/min. One sample with 500 nM is removed.

Appendix D Reagents and solutions

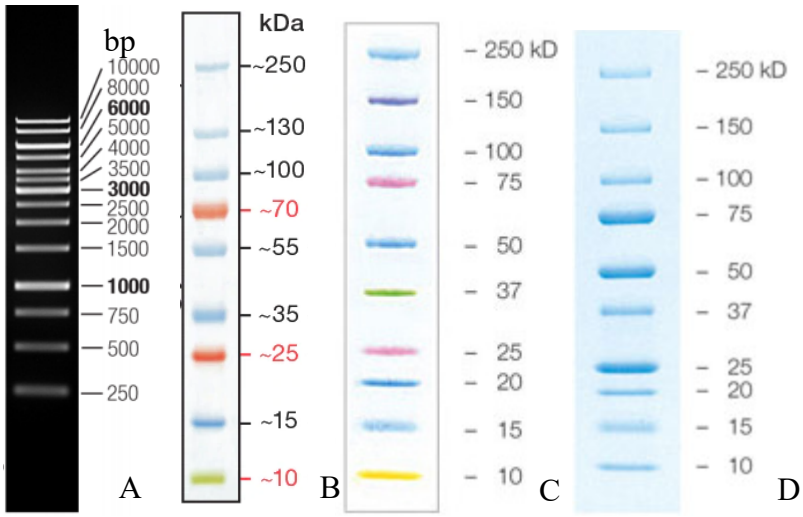

Figure S14. **A)** DNA Thermo scientific gene ruler 1kb DNA ladder **B)** PageRuler Plus Stained Protein Ladder (Thermo fisher) **C)** Precision Plus Protein™ Kaleidoscope™ Prestained Protein Standard (Bio-rad) **D)** Precision Plus Protein™ All Blue Prestained Protein Standard (Bio-rad)

Table S8. Antibodies used in the study.

Antibody	**Product number**	**Dilution**		**Orgin**
6x His Tag antibody	MA1-21315-BTIN	1:4000	Bind to His-tag	Invitrogen
Donkey anti-Mouse IgG (H+L) Cross-Adsorbed Secondary Antibody, HRP	SA1-100	1:10000	Bind to light and heavy chain of a mouse antibody.	Invitrogen

LB medium

10 g/L Bacto Tryptone (OXOID)

5 g/L Bacto Yeast Extract (OXOID)

10 g/L NaCl (Merck)

Dissolved in ddH_2O and autoclaved Stored at 4 °C

Agar plates

LB medium

15 g/L Bacteriological agar (VWR)

Dissolved in ddH_2O and autoclaved. Cooled down to 50 °C before adding antibiotic. Stored at 4 °C

Enzymatic lysis buffer

100 µL Trizma hydrocloride 1 M pH 8.00 (Sigma)

50 µL EDTA (2 mM) (Sigma)

2 µL TritonX-100 (1.2 %) (Sigma)

50 µL Lysozome (20 mg/mL) (Sigma)

Mueller-Hinton broth

21 g/L Mueller-Hinton broth (Sigma)

Dissolved in ddH_2O and autoclaved. Stored at 4 °C

Transformation and storage solution

10 % (w/v) polyethylene glycol

5 % (v/v) dimethyl sulfoxide

50 mM Mg^{2+}

Dissolved in LB medium, pH 6.5. Filter sterilized and stored at 4 °C

1x TAE buffer

40 mM Tris-Acetate, 1mM EDTA, pH 8.3 (Fisher bioregents)

50x diluted to 1x in ddH_2O and stored in RT

1 % agarose gel

1 % (v/w) Agarose (Lonza)

Dissolved in 1x TAE buffer and heated to dissolve agarose

1x PBS

10x PBS (1 M phosphate buffer, 15.4M NaCl, pH 7.4) (Sigma)

10x diluted to 1x in ddH_2O. Autoclaved or filter sterilized and stored at RT.

Tris buffer stock solution

50 mM Tris (Sigma)

200 mM NaCl (Merck)

30 % (v/v) glycerol (Sigma/Omnipure, Merck)

Dissolved in ddH_2O, pH adjusted to 8.0, filter sterilized and stored at 4 °C

Equilibrium buffer- PBS

1x PBS

10 mM Imidazole (Sigma)

Filter sterilized and stored at 4 °C

Equilibrium buffer- Tris

Tris buffer stock solution

10 mM Imidazole (Sigma)

pH adjusted to 8.0, filter sterilized and stored at 4 °C

Wash buffer- PBS

1x PBS

25 mM Imidazole (wash buffer 1) / 50 mM imidazole (wash buffer 2) (Sigma)

pH adjusted to 7.4, filter sterilized and stored at 4 °C

Wash buffer- Tris

Tris buffer stock solution

25 mM Imidazole (wash buffer 1) / 50 mM imidazole (wash buffer 2) / 100 mM imidazole (wash buffer 3) (Sigma)

pH adjusted to 8.0, filter sterilized and stored at 4 °C

Elution buffer- PBS

1x PBS

250 mM Imidazole (Sigma)

pH adjusted to 7.4, filter sterilized and stored at 4 °

Elution- Tris

Tris buffer stock solution

250 mM Imidazole (Sigma)

pH adjusted to 8.0, filter sterilized and stored at 4 °C

Storage buffer –PBS

1x PBS

0.05 % (v/v) Tween-20 (Sigma)

10 % (v/v) glycerol (Sigma or Omnipur, Merck)

pH adjusted to 7.4, filter sterilized and stored at 4 °C

Storage buffer –Tris

20 mM Tris (Sigma)

50 mM Arginine (Sigma)

10 % glycerol (v/v) (Sigma or Omnipur, Merck)

pH adjusted to 8.0, filter sterilized and stored at 4 °C

Storage buffer2 –Tris

50 mM Tris (Sigma)

200 mM NaCl (Merck)

10 % glycerol (v/v) (Sigma or Omnipur, Merck)

pH adjusted to 8.0, filter sterilized and stored at 4 °C

1x PBS-P+

10x PBS-P+ (0.2 mM phosphate buffer, 27 mM KCl, 137 mM NaCl, 0.5 % Tween 20, pH 7.4) (GE healthcare)

Dissolved to 1x in ddH_2O and stored at RT

SPR-buffer

35 mM Tris, pH 7.5

25 mM KCl

4 mM $MgCl_2$

1 mM DTT

Dissolved in ddH_2O and stored at 4 °C

1x SDS-PAGE running buffer

25 mM Tris (Sigma)

192 mM Glycine (Sigma)

0.1 % (w/v) SDS (Sigma)

Dissolved in ddH_2O and stored at RT.

2x SDS-PAGE sample buffer

0.346 mM SDS (Sigma)

0.1 M Tris, pH 6.8 (Sigma)

20 % (v/v) glycerol (Sigma)

1 mM EDTA (Sigma)

0.175 g/L Coomassie Brilliant Blue R-250 (Bio-rad)

50 mM DTT

Dissolved in ddH_2O, aliquoted and stored at -20°C.

One 12 % SDS SDS-PAGE gel

1.7 mL ddH_2O

2.0 mL 30 % acrylamide (37.5:1) (Bio-rad)

1.3 mL 1.5 M Tris, pH 8.8 (Sigma)

50 µL 10 % (w/v) SDS (Sigma)

50 µL 10 % (w/v) APS (Sigma)

2 µL Tetramethylethylenediamine (TEMED) (Bio-rad)

One 4 % stacking gel

680 µL ddH_2O

170 µL 30 % acrylamide (37.5:1) (Bio-rad)

130 µL 1.0 M Tris, pH 6.8 (Sigma)

10 µL 10 % (w/v) SDS (Sigma)

10 µL 10 % (w/v) APS (Sigma)

1 µL Tetramethylethylenediamine (TEMED) (Bio-rad)

Coomassie Blue staining solution

40 % (v/v) ddH_2O

50 % (v/v) Methanol (VWR)

10 % (v/v) Acetic acid (VWR)

0.5 g/L Coomassie Blue R-250 (Bio-rad)

Stirred to Coomassie is dissolved. Stored at RT.

Destaining solution

88 % (v/v) ddH_2O

5 % (v/v) Methanol (VWR)

7 % (v/v) Acetic acid (VWR)

Stored at RT

Stripping buffer

20 mM Sodium monophosphate (Sigma)

0.5 M NaCl (Merck)

50 mM EDTA (Sigma)

Dissolved in ddH_2O and stored at 4°C

Nickel loading buffer

1 M $NiCl_2xH_2O$ (Sigma)

Dissolved in ddH_2O and stored at 4 °C

1x TBS-T

10 mM Tris-HCl, pH 7.4

0.9 % NaCl

0.1 % Tween-20

Dissolved in ddH_2O and stored in RT

1x Transfer buffer

25 mM Tris (Sigma)

192 mM Glycine (Sigma)

10 % / 20 % (v/v) Methanol (VWR)

Dissolved in ddH_2O and stored in RT. Methanol added right before use.

Blocking buffer

1X TBS-T

5 % (w/v) Bovine serum albumin (Sigma)

Stored at 4 °C for maximum one day.

Ampicillin stock solution

100 mg/mL Ampicillin sodium salt (Sigma)

Dissolved in ddH_2O, filter sterilized and stored at -20 °C.

Kanamycin stock solution

50 mg/mL Kanamycin sulfate (Sigma)

Dissolved in ddH_2O, filter sterilized and stored at -20 °C.

Ciprofloxacin stock solution

10 mg/mL Ciprofloxacin (Sigma)

Dissolved in 0.1 M HCl, filter sterilized and stored at -20 °C

Nalidixic acid stock solution

100 mg/mL Nalidixic acid sodium salt (Sigma)

Dissolved in ddH_2O, filter sterilized and stored at -20 °C

Dithiothreitol (DTT) stock solution

154.3 g/L Dithiothreitol (1 M) (Sigma)

Dissolved in ddH_2O, filter sterilized and stored at -20 °C

DNase stock solution

10 mg/mL DNase (Sigma)

Dissolved in ddH_2O, filter sterilized and stored at -20 °C

Lysozyme stock solution

50 mg/mL Lysozyme (Sigma)

Dissolved in ddH_2O, filter sterilized and stored at -20 °C

IPTG stock solution

238.1 g/L IPTG (1 M) (Sigma)

Dissolved in ddH_2O, filter sterilized and stored at -20 °C

Arabinose stock solution

15% (w/v) Arabinose

Dissolved in ddH_2O, filter sterilized and stored at 4 °C

Appendix E DNA sequences

>GyrA_S83L

ATGAGCGACCTTGCGAGAGAAATTACACCGGTCAACATTGAGGAAGAGCTGAAG
AGCTCCTATCTGGATTATGCGATGTCGGTCATTGTTGGCCGTGCGCTGCCAGATGT
CCGAGATGGCCTGAAGCCGGTACACCGTCGCGTACTTTACGCCATGAACGTACTA
GGCAATGACTGGAACAAAGCCTATAAAAAATCTGCCCGTGTCGTTGGTGACGTAA
TCGGTAAATACCATCCCCATGGTGACTTGGCGGTCTATGACACGATCGTCCGCAT
GGCGCAGCCATTCTCGCTGCGTTATATGCTGGTAGACGGTCAGGGTAACTTCGGT
TCTATCGACGGCGACTCTGCGGCGGCAATGCGTTATACGGAAATCCGTCTGGCGA
AAATTGCCCATGAACTGATGGCCGATCTCGAAAAAGAGACGGTCGATTTCGTTGA
TAACTATGACGGCACGGAAAAAATTCCGGACGTCATGCCAACCAAAATTCCTAAC
CTGCTGGTGAACGGTTCTTCCGGTATCGCCGTAGGTATGGCAACCAACATCCCGC
CGCACAACCTGACGGAAGTCATCAACGGTTGTCTGGCGTATATTGATGATGAAGA
CATCAGCATTGAAGGGCTGATGGAACACATCCCGGGGCCGGACTTCCCGACGGC
GGCAATCATTAACGGTCGTCGCGGTATTGAAGAAGCTTACCGTACCGGTCGCGGC
AAGGTGTATATCCGCGCTCGCGCAGAAGTGGAAGTTGACGCCAAAACCGGTCGT
GAAACCATTATCGTCCACGAAATTCCGTATCAGGTAAACAAAGCGCGCCTGATCG
AGAAGATTGCGGAACTGGTAAAAGAAAAACGCGTGGAAGGCATCAGCGCGCTGC
GTGACGAGTCTGACAAAGACGGTATGCGCATCGTGATTGAAGTGAAACGCGATG
CGGTCGGTGAAGTTGTGCTCAACAACCTCTACTCCCAGACCCAGTTGCAGGTTTC
TTTCGGTATCAACATGGTGGCATTGCACCATGGTCAGCCGAAGATCATGAACCTG
AAAGACATCATCGCGGCGTTTGTTCGTCACCGCCGTGAAGTGGTGACCCGTCGTA
CTATTTTCGAACTGCGTAAAGCTCGCGATCGTGCTCATATCCTTGAAGCATTAGCC
GTGGCGCTGGCGAACATCGACCCGATCATCGAACTGATCCGTCATGCGCCGACGC
CTGCAGAAGCGAAAACTGCGCTGGTTGCTAATCCGTGGCAGCTGGGCAACGTTGC
CGCGATGCTCGAACGTGCTGGCGACGATGCTGCGCGTCCGGAATGGCTGGAGCC
AGAGTTCGGCGTGCGTGATGGTCTGTACTACCTGACCGAACAGCAAGCTCAGGCG
ATTCTGGATCTGCGTTTGCAGAAACTGACCGGTCTTGAGCACGAAAAACTGCTCG
ACGAATACAAAGAGCTGCTGGATCAGATCGCGGAACTGTTGCGTATTCTTGGTAG
CGCCGATCGTCTGATGGAAGTGATCCGTGAAGAGCTGGAGCTGGTTCGTGAACAG
TTCGGTGACAAACGTCGTACTGAAATCACCGCCAACAGCGCAGACATCAACCTGG
AAGATCTGATCACCCAGGAAGATGTGGTCGTGACGCTCTCTCACCAGGGCTACGT
TAAGTATCAGCCGCTTTCTGAATACGAAGCGCAGCGTCGTGGCGGGAAAGGTAA
ATCTGCCGCACGTATTAAAGAAGAAGACTTTATCGACCGACTGCTGGTGGCGAAC
ACTCACGACCATATTCTGTGCTTCTCCAGCCGTGGTCGCGTCTATTCGATGAAAGT
TTATCAGTTGCCGGAAGCCACTCGTGGCGCGCGCGGTCGTCCGATCGTCAACCTG
CTGCCGCTGGAGCAGGACGAACGTATCACTGCGATCCTGCCAGTGACCGAGTTTG
AAGAAGGCGTGAAAGTCTTCATGGCGACCGCTAACGGTACCGTGAAGAAAACTG
TCCTCACCGAGTTCAACCGTCTGCGTACCGCCGGTAAAGTGGCGATCAAACTGGT
TGACGGCGATGAGCTGATCGGCGTTGACCTGACCAGCGGCGAAGACGAAGTAAT
GCTGTTCTCCGCTGAAGGTAAAGTGGTGCGCTTTAAAGAGTCTTCTGTCCGTGCG

ATGGGCTGCAACACCACCGGTGTTCGCGGTATTCGCTTAGGTGAAGGCGATAAAG
TCGTCTCTCTGATCGTGCCTCGTGGCGATGGCGCAATCCTCACCGCAACGCAAAA
CGGTTACGGTAAACGTACCGCAGTGGCGGAATACCCAACCAAGTCGCGTGCGAC
GAAAGGGGTTATCTCCATCAAGGTTACCGAACGTAACGGTTTAGTTGTTGGCGCG
GTACAGGTAGATGACTGCGACCAGATCATGATGATCACCGATGCCGGTACGCTGG
TACGTACTCGCGTTTCGGAAATCAGCATCGTGGGCCGTAACACCCAGGGCGTGAT
CCTCATCCGTACTGCGGAAGATGAAAACGTAGTGGGTCTGCAACGTGTTGCTGAA
CCGGTTGACGAGGAAGATCTGGATACCATCGACGGCAGTGCCGCGGAAGGGGAC
GATGAAATCGCTCCGGAAGTGGACGTTGACGACGAGCCAGAAGAAGAATAA

>GyrA_WT

ATGAGCGACCTTGCGAGAGAAATTACACCGGTCAACATTGAGGAAGAGCTGAAG
AGCTCCTATCTGGATTATGCGATGTCGGTCATTGTTGGCCGTGCGCTGCCAGATGT
CCGAGATGGCCTGAAGCCGGTACACCGTCGCGTACTTTACGCCATGAACGTACTA
GGCAATGACTGGAACAAAGCCTATAAAAAATCTGCCCGTGTCGTTGGTGACGTAA
TCGGTAAATACCATCCCCATGGTGACTCGGCGGTCTATGACACGATCGTCCGCAT
GGCGCAGCCATTCTCGCTGCGTTATATGCTGGTAGACGGTCAGGGTAACTTCGGT
TCTATCGACGGCGACTCTGCGGCGGCAATGCGTTATACGGAAATCCGTCTGGCGA
AAATTGCCCATGAACTGATGGCCGATCTCGAAAAAGAGACGGTCGATTTCGTTGA
TAACTATGACGGCACGGAAAAAATTCCGGACGTCATGCCAACCAAAATTCCTAAC
CTGCTGGTGAACGGTTCTTCCGGTATCGCCGTAGGTATGGCAACCAACATCCCGC
CGCACAACCTGACGGAAGTCATCAACGGTTGTCTGGCGTATATTGATGATGAAGA
CATCAGCATTGAAGGGCTGATGGAACACATCCCGGGGCCGGACTTCCCGACGGC
GGCAATCATTAACGGTCGTCGCGGTATTGAAGAAGCTTACCGTACCGGTCGCGGC
AAGGTGTATATCCGCGCTCGCGCAGAAGTGGAAGTTGACGCCAAAACCGGTCGT
GAAACCATTATCGTCCACGAAATTCCGTATCAGGTAAACAAAGCGCGCCTGATCG
AGAAGATTGCGGAACTGGTAAAAGAAAAACGCGTGGAAGGCATCAGCGCGCTGC
GTGACGAGTCTGACAAAGACGGTATGCGCATCGTGATTGAAGTGAAACGCGATG
CGGTCGGTGAAGTTGTGCTCAACAACCTCTACTCCCAGACCCAGTTGCAGGTTTC
TTTCGGTATCAACATGGTGGCATTGCACCATGGTCAGCCGAAGATCATGAACCTG
AAAGACATCATCGCGGCGTTTGTTCGTCACCGCCGTGAAGTGGTGACCCGTCGTA
CTATTTTCGAACTGCGTAAAGCTCGCGATCGTGCTCATATCCTTGAAGCATTAGCC
GTGGCGCTGGCGAACATCGACCCGATCATCGAACTGATCCGTCATGCGCCGACGC
CTGCAGAAGCGAAAACTGCGCTGGTTGCTAATCCGTGGCAGCTGGGCAACGTTGC
CGCGATGCTCGAACGTGCTGGCGACGATGCTGCGCGTCCGGAATGGCTGGAGCC
AGAGTTCGGCGTGCGTGATGGTCTGTACTACCTGACCGAACAGCAAGCTCAGGCG
ATTCTGGATCTGCGTTTGCAGAAACTGACCGGTCTTGAGCACGAAAAACTGCTCG
ACGAATACAAAGAGCTGCTGGATCAGATCGCGGAACTGTTGCGTATTCTTGGTAG
CGCCGATCGTCTGATGGAAGTGATCCGTGAAGAGCTGGAGCTGGTTCGTGAACAG
TTCGGTGACAAACGTCGTACTGAAATCACCGCCAACAGCGCAGACATCAACCTGG
AAGATCTGATCACCCAGGAAGATGTGGTCGTGACGCTCTCTCACCAGGGCTACGT
TAAGTATCAGCCGCTTTCTGAATACGAAGCGCAGCGTCGTGGCGGGAAAGGTAA
ATCTGCCGCACGTATTAAAGAAGAAGACTTTATCGACCGACTGCTGGTGGCGAAC

ACTCACGACCATATTCTGTGCTTCTCCAGCCGTGGTCGCGTCTATTCGATGAAAGT
TTATCAGTTGCCGGAAGCCACTCGTGGCGCGCGCGGTCGTCCGATCGTCAACCTG
CTGCCGCTGGAGCAGGACGAACGTATCACTGCGATCCTGCCAGTGACCGAGTTTG
AAGAAGGCGTGAAAGTCTTCATGGCGACCGCTAACGGTACCGTGAAGAAAACTG
TCCTCACCGAGTTCAACCGTCTGCGTACCGCCGGTAAAGTGGCGATCAAACTGGT
TGACGGCGATGAGCTGATCGGCGTTGACCTGACCAGCGGCGAAGACGAAGTAAT
GCTGTTCTCCGCTGAAGGTAAAGTGGTGCGCTTTAAAGAGTCTTCTGTCCGTGCG
ATGGGCTGCAACACCACCGGTGTTCGCGGTATTCGCTTAGGTGAAGGCGATAAAG
TCGTCTCTCTGATCGTGCCTCGTGGCGATGGCGCAATCCTCACCGCAACGCAAAA
CGGTTACGGTAAACGTACCGCAGTGGCGGAATACCCAACCAAGTCGCGTGCGAC
GAAAGGGGTTATCTCCATCAAGGTTACCGAACGTAACGGTTTAGTTGTTGGCGCG
GTACAGGTAGATGACTGCGACCAGATCATGATGATCACCGATGCCGGTACGCTGG
TACGTACTCGCGTTTCGGAAATCAGCATCGTGGGCCGTAACACCCAGGGCGTGAT
CCTCATCCGTACTGCGGAAGATGAAAACGTAGTGGGTCTGCAACGTGTTGCTGAA
CCGGTTGACGAGGAAGATCTGGATACCATCGACGGCAGTGCCGCGGAAGGGGAC
GATGAAATCGCTCCGGAAGTGGACGTTGACGACGAGCCAGAAGAAGAATAA

>QnrS1

ATGGAAACCTACAATCATACATATCGGCACCACAACTTTTCACATAAAGACTTAA
GTGATCTCACCTTCACCGCTTGCACATTCATTCGCAGCGACTTTCGACGTGCTAAC
TTGCGTGATACGACATTCGTCAACTGCAAGTTCATTGAACAGGGTGATATCGAAG
GCTGCCACTTTGATGTCGCAGATCTTCGTGATGCAAGTTTCCAACAATGCCAACTT
GCGATGGCAAACTTCAGTAATGCCAATTGCTACGGTATAGAGTTCCGTGCGTGTG
ATTTAAAAGGTGCCAACTTTTCCCGAACAAACTTTGCCCATCAAGTGAGTAATCG
TATGTACTTTTGCTCAGCATTTATTTCTGGATGTAATCTTTCCTATGCCAATATGG
AGAGGGTTTGTTTAGAAAAATGTGAGTTGTTTGAAAATCGCTGGATAGGAACGAA
CCTAGCGGGTGCATCACTGAAAGAGTCAGACTTAAGTCGAGGTGTTTTTTCCGAA
GATGTCTGGGGGCAATTTAGCCTACAGGGTGCCAATTTATGCCACGCCGAACTCG
ACGGTTTAGATCCCCGCAAAGTCGATACATCAGGTATCAAAATTGCAGCCTGGCA
GCAAGAACTGATTCTCGAAGCACTGGGTATTGTTGTTTATCCTGACTAA

>QnrS2

ATGGAAACCTACCGTCACACATATCGACACCACAGTTTTTCACATCAAGATCTAA
GTGATATTACTTTCACTGCTTGCACCTTTATCCGATGCGATTTTCGACGTGCTAAC
TTGCGTGATGCGACATTTATTAACTGCAAGTTCATTGAACAGGGTGATATCGAAG
GTTGCCATTTTGATGTCGCAGACCTTCGCGATGCAAGTTTCCAACAATGCCAGCTT
GCGATGGCAAACTTTAGTAACGCCAATTGCTACGGTATTGAGTTACGTGAGTGTG
ATTTAAAAGGGGCCAACTTTTCCCGAGCAAACTTTGCCAATCAAGTGAGTAATCG
TATGTACTTTTGCTCAGCCTTTATTACTGGATGTAACCTGTCTTATGCCAATATGG
AGCGGGTCTGTTTAGAAAAATGTGAGCTGTTTGAAAATCGCTGGATAGGGACTCA
CCTCGCGGGCGCATCACTGAAAGAGTCAGACTTAAGTCGAGGTGTTTTTTCTGAA
GATGTCTGGGGACAGTTTAGCCTACAGGGTGCTAATTTATGTCACGCCGAACTCG

ACGGTTTAGATCCTCGAAAAGTCGATACATCAGGTATCAAAATTGCCAGCTGGCA
ACAAGAACAGCTTCTCGAAGCGTTGGGTATTGTTGTTTTTCCTGACTAG

>QnrB19

ATGACTCTGGCATTAGTTGGCGAAAAAATTGACAGAAATCGCTTCACCGGTGAGA
AAGTTGAAAATAGTACATTTTTTAACTGCGATTTTTCAGGTGCCGACCTGAGCGG
CACTGAATTTATCGGCTGCCAGTTCTATGATCGCGAAAGTCAGAAAGGGTGCAAT
TTTAGTCGCGCAATGCTGAAAGATGCCATTTTCAAAAGCTGTGATTTATCAATGG
CAGATTTCCGCAACGTCAGTGCCTTGGGCATTGAAATTCGCCACTGCCGCGCACA
AGGCGCAGATTTCCGCGGTGCAAGCTTTATGAATATGATCACCACGCGCACCTGG
TTTTGCAGCGCATATATCACTAATACTAATCTAAGCTACGCCAATTTTTCGAAAGT
CGTGTTGGAAAAGTGTGAGCTGTGGGAAAACCGCTGGATGGGGACTCAGGTACT
GGGTGCGACGTTCAGTGGTTCAGATCTCTCCGGCGGCGAGTTTTCGACTTTCGACT
GGCGAGCAGCAAACTTCACACATTGCGATCTGACCAATTCGGAGTTAGGTGACTT
AGATATTCGGGGTGTTGATTTACAAGGCGTTAAGTTAGACAGCTACCAGGCATCG
TTGCTCATGGAGCGGCTTGGCATCGCTGTGATTGGTTAG